PETROLEUM RESEARCH JOURNAL

TECHNICAL PAPERS

ENGINEERING

New experimental approach of saturation exponent measurements by continuous injection technique .....
O.B. Al-Mahtot, W.E. Mason and M.S. Nasar 1

EXPLORATION

Petrography and palaeoenvironment of the Sidi as Sid Formation in Northwest Libya .....
M.T. El-Bakai 9

Planktonic foraminiferal zonation of the Oligocene–Miocene succession of well H1–NC41, NW offshore Libya .....
I.I.M. Kassab, A. K. Abusrewil and F. E. Abuhmida 27

Petrography of the Triassic phosphorites in Gharyan area, NW Libya .....
S. Lagha 45

CHEMISTRY

Preparation of activated carbon from carbonaceous industrial wastes .....
L. H. Ali and A. B. Shebli 51

Isolation and characterization of two thermotolerant methylotrophic bacterial strains .....
I. Misurati, Hend I. Ben Hussein, A.M. Suliman and K. Baruni 61

Determination of trace amount of lead in potable water by flow injection flame atomic absorption spectrometry aided by a pre-concentration micro column ....
I.S. Bushina, H.M. Kut and Seham S. Elmahmudi 67

VOLUME 9 - (1426) / (1997)

Petroleum Research Centre
P. O. Box 6431 Tripoli
Great Socialist People's Libyan Arab Jamahiriya

Petroleum Res.J. Vol. 9 (1997); P. 1–7, 6 FIGS.

New Experimental Approach of Saturation Exponent Measurements by Continuous Injection Technique

O.B. Al-Mahtot*, W.E. Mason* and M.S. Nasar**

طريقة معمليّة جديدة لتحديد معامل التشبّع المائي بأسلوب الحقن المستمر

عمران المحتوت، و. ي. ميسن و محمد نصر

إن تحديد التشبع المائي في الصخور بواسطة معدات سرود المقاومة السلكية يعتمد أساساً على قيمة معامل المقاومة والذي يتم قياسه معملياً لنماذج العينات الصخرية باستخدام العلاقة المعروفة باسم (Archie) وهي ($I_R=R/R_0=Sw^{-n}$).

إن الأخطاء المحتملة في إيجاد معامل التشبع (n) يؤدي بلا شك إلى حدوث أخطاء جدية في تقدير التشبعات الهيدروكربونية في الصخور.. تعتبر طريقة الحقن المستمر من الطرق المعملية الشائعة في الصناعة النفطية لإيجاد معامل التشبع وذلك بحقن أحد الأطوار (الماء المالح) لإزاحة الطور الأخير (الزيت) عند معدل حقن ثابت.

في هذه الدراسة تم التحقق من استخدام أسلوب معملي جديد لإيجاد معامل التشبع المائي لعدد من نماذج الصخور بطريقة الحقن المستمر تحت معدلات حقن متغيرة. كما تم اختيار أربعة نماذج صخرية جيرية ذات خواص بتروفيزيائية مختلفة في النفاذية والمسامية لدراسة تأثير معدلات الحقن المتغيرة على قيم معامل التشبع، وشكل العلاقة بين معامل المقاومة والتشبع المائي في الصخور، وتبين بشكل واضح أن استخدام أسلوب الحقن المستمر بمعدلات متعددة وخاصة في الصخور ذات التبلل المائي (Water wet) ولمدى واسع من قيم التشبع المائي يضمن الحصول على علاقة منتظمة لمعامل التشبع المائي وخاصة عند الحقن بمعدلات منخفضة. وبذلك يمكن الاستنتاج أن معدل الحقن له دور مهم في تحديد شكل العلاقة التي تربط معامل المقاومة الصخرية (I_R) مع التشبع المائي (S_W) والذي سيؤدي بلا شك للتوصل إلى قيمة مناسبة ودقيقة لمعامل التشبع المائي (n) والذي بالإمكان استخدامه بثقة عالية في حسابات التشبع الهيدروكربوني بطريقة السرود الكهربائية.

Abstract *Water saturation determination from wireline resistivity log depends on the measurements of resistivity index on core samples. Resistivity index measurements are carried out in laboratory using Archie's equation; $I_R = R_t/R_0 = S_W^{-n}$. Errors in the saturation exponent n, can give rise to serious errors in the estimation of hydrocarbon saturations. One of the major sources of uncertainty is the method of measurements. The continuous injection technique is used routinely in the oil industry. In this technique one fluid phase (brine) is continuously displaced by another phase (oil) at a constant injection rate. In this paper, a new experimental approach is proposed in which repeated resistivity index measurements are carried out on the same samples at various injection rates. The effect of injection rate on saturation exponent for core samples can be investigated. Four carbonate core samples with a wide range of porosity and permeability were tested to demonstrate resistivity index measurements at low and high injection rates. Use of continuous injection technique at different rates has illustrated that for the water-wet samples a uniform I_R/S_W correlation was established over wide range of S_W when low rate is used. It is concluded that the injection rate selection has an important role on the I_R/S_W relation.*

*Robert Gordon University, Aberdeen, U.K.

**Petroleum Eng. Dept, Al-Fateh University, Tripoli, Libya

It is recommended as a result of this work that for resistivity index measurements, various injection rates should be used to obtain the best I_R/S_W relation and consequently the proper saturation exponent could be obtained.

INTRODUCTION

Water saturation is commonly determined from electric well logs based on an empirical Archie's equation [1]; $I_R = S_W^{-n} = R_t/R_0$. The Archie's parameters are frequently obtained from laboratory measurements on core samples. An assumption in laboratory measurements is that the sample saturation is distributed uniformly. It is assumed also that saturation exponent n, is constant over S_W range. Many cases are being encountered where resistivity index (I_R) versus brine saturation (S_W) gives non-linear relationship. Wettability, micro-porosity, capillary end effects, and some other factors which cause this non-linearity.

The experimental procedure design, and especially selection of injection rate in continuous injection technique could have an important influence on the non-linearity of I_R/S_W curves. The inaccurate evaluation of saturation exponent can result in large errors in hydrocarbon calculation as described by de Waal [2]. In order to use Archie's equation, the uniform water distribution should be maintained along the core sample, and I_R/S_W should have a linear relation (i.e. constant n). If improper desaturation procedure is used in resistivity index measurements, a non-uniform saturation distribution may prevail and invalid I_R/S_W curves will be produced, and hence erroneous value of saturation exponent may be obtained. The influence of injection rate on I_R/S_W relationships has received much less attention in the past, probably on account of the time and cost involved in such experiments. Generally, the fluid distribution in porous media is function of rock pore structure characteristics, wettability, fluid properties, stresses, and experimental conditions, rate of injection of displacing fluid, desaturation history. The pore structure also affects the shape of displacing front which in turn modifies the fluid distribution behind it and hence the resistivity values [3].

SATURATION EXPONENT TECHNIQUES

Numerous number of techniques have been devised to measure the electrical resistivity of rocks partially saturated with brine. Porous plate method, and continuous injection technique are the recent techniques used in the oil industry with wider use of the continuous technique. Lyle and Mills [4] showed theoretically that the laboratory-derived Archie saturation exponent may be different from the actual value, and concluded that whenever the core is other than uniformly saturated, the I_R versus S_W log-log plot will exhibit curvature. However, the most recent developed technique to measure the resistivity index is continuous injection which believed to be powerful, accurate and rapid, as well as it provides continuous I_R/S_W curve rather than a limited number of points [2]. It is reliable where experimental error can be minimized by automation of measurements procedure and performed at an equivalent reservoir stress. In this technique oil is injected at a constant rate to displace brine. The porous plate method has been used to obtain uniform desaturation and uniform I_R/S_W relation as described by Maerefat *et al.* [5]. They concluded that sufficient desaturation time should be allowed to obtain homogeneous saturation. It is believed that at capillary and electrical equilibrium, the uniform saturation distribution can be achieved, but small scale permeability heterogeneity seems to cause non-linearity even after this equilibrium [6]. Lewis *et al.* [7], used low injection rate to minimize fingering which may occurred during high injection process, then they used simultaneously high rate to compress the length of capillary end effect. They recommended that four-electrodes system which is not affected by contact resistance to be used. In their experiments they tested high porosity and permeability samples, and concluded that the capillary end effect and viscous fingering cause the non-linearity of I_R/S_W relationship [7]. Spurt [8] used X-ray CT scan to monitor saturation distribution along the core samples. He changed capillary pressure (not injection rate) and encountered problem in achieving homogenous saturation during resistivity index tests for the two high porosity and permeability grainstone samples desaturated at constant oil/brine capillary pressure. Gray *et al.*, [9] measured I_R for sandstone samples at low constant injection rate (0.02 cc/hr), they selected this rate so that an insignificant pressure drop existed across the sample through the desaturation processes. However, the uniform I_R/S_W plot had not been achieved except for S_W less than 45%. Elashahab *et al.*, [10] used multiple potential electrodes system in I_R measurement to enable assessment of saturation distribution and end effect.

The injection rate chosen for I_R measurements by

continuous injection technique, theoretically should be

(1) not so high, as to introduce fingering or channeling through the core sample,

(2) low to prevent significant saturation change at a given time along the sample.

This criteria was applied in this investigation. Four carbonate samples, 1.5" diameter, 3" length with wide range of porosity and permeability were collected to study the effect of injection rate on I_R/S_W relationship. The samples properties are listed in Table 1.

Table 1. The physical properties of the samples

Sample No.	ϕ (%)	*k (mD)*	*G.D. (gm/cc)*
1	15.1	3.74	2.859
2	34.5	29.09	2.853
3	33.0	26.14	2.834
4	17.7	9.5	2.850

Repeated resistivity index measurements by continuous injection technique on these samples were performed at alternating injection rate.

EXPERIMENTAL PROCEDURE

Low and high oil injection rate experiments were carried out on these samples and the rates chosen were (0.03 and 0.15) cc/hr. Fig. 1 shows the apparatus of I_R measurements and Fig. 2 illustrate the core sleeve with multiple elcetrodes system. The fully brine-saturated samples were mounted in a multiple core holder made of aluminum and subjected to confining pressure of 400 psi, which was increased to 3000 psi. The sample pore volume was calculated based on the brine volume collected in pipettes which is attached to the outlet of each sample after the system was being maintained in equilibrium. Oil was injected at one end of the samples, brine (100 g/l, Na Cl) was expelled at the other ends, through a semi-permeable membrane. The semi-permeable membrane was supported on a brine saturated high porosity glass disc. Both voltage, phase angle and temperature were monitored continuously during the oil injection process. All samples were made preferentially water-wet, and firstly cleaned with methanol, then fired to 600°C for one day in a high temperature furnace to make them water-wet [11].

Before the desaturation processes began, and samples loaded, the resistivity of fully saturated samples (R_0) was measured. The samples loaded to the core holder, then oil/brine desaturation process started and I_R measured when capillary and electrical equilibrium were reached. This equilibrium was indicated when there was no further change in resistance (i.e. no further fluid redistributed along the core length). Two different rates of 0.03 cc/hr and 0.15 cc/hr were used for the displacement of brine

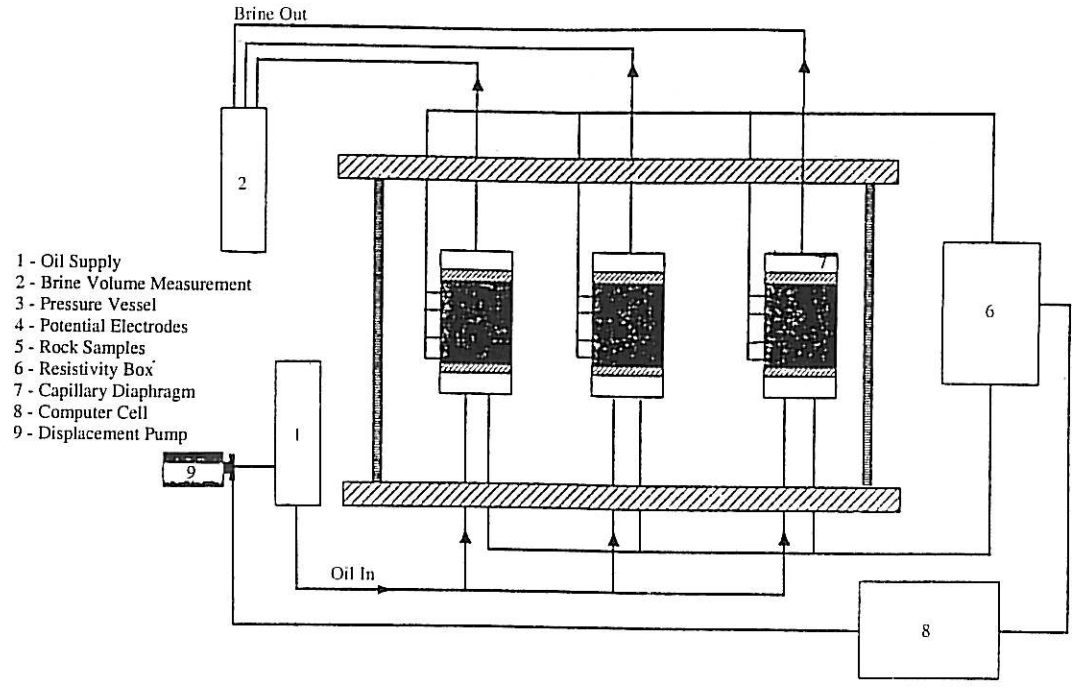
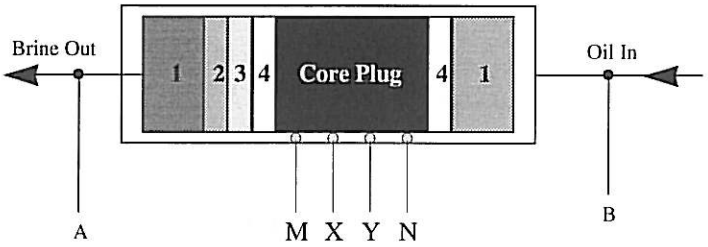


Fig. 1. Schematic diagram of core holder and resistivity index measurement apparatus



1 - Core Holder End
2 - Semi-permeable Membrane
3 - Ceramic Disk
4 - Filter Papers
A. B - Current Electrodes
M.X.N.Y - Potential Electrodes

Fig. 2. Schematic diagram of core sleeve with multi electrodes system

water by oil from the core samples. The amount of displaced fluid was measured by a calibrated potentiometer connected to the pump piston. The pump is regularly calibrated at experiments conditions. The samples were subjected to re-cleaning process to remove oil contamination and the cleaning method used kept them in water-wet condition and remain as that throughout the experiment. The resistance of samples measured at 1 kHz, to avoid polarization effect [11]. Resistivity was corrected to slight temperature variations by using Arp's equation [12].

On the second part of this experimental investigation, the resistivity index measurements were carried out using porous plate method, in order to compare it with continuous injection technique results. In this method the resistivity measurements and desaturation process take place separately. The samples were desaturated simultaneously by placing them on a porous plate in pressure cell, and gas pressure was applied. The gas (nitrogen) enters the samples from all directions except from end face. The gas pressure was maintained until no more brine produced. After the capillary equilibrium (samples held 4–5 days in plate) at each pressure point is reached, the gas is then released, and the samples removed from the pressure cell and weight measurements were taken as well as resistivity readings. The procedure was repeated by increasing gas pressure at various desaturation points.

RESULTS AND DISCUSSION

The continuous injection technique results in an accurate and precise determination of I_R versus S_W relationship of core samples [2]. The advantage of this technique is providing a continuous I_R/S_W curve rather than, a limited number of data points, this is of particular importance in the case of curved I_R/S_W relationship. In this technique, the non-wetting phase (oil) is injected into the sample at a constant rate. A uniform saturation distribution along the length of core sample is required to measure saturation exponent accurately which leads to proper hydrocarbon evaluation. It is believed that by using this technique with very low injection rate might achieve the homogenous saturation distribution and uniform I_R/S_W relation may be obtained.

To begin the continuous injection process, the displacement pump starts to inject the oil core holder. Initially this was performed at low rate (0.03 cc/hr) for displacing brine from the flowlines. This low rate has been selected such that an amount of oil corresponding to samples 1, 2, 3 and 4 pore volumes will be injected approximately in (26, 25, 13 and 12) days respectively, and for high rate (0.15 cc/hr) the samples pore volumes will be injected at (8, 8, 4 and 4) days respectively. The continuous injection of oil was stopped for each sample individually after that given time or when no more brine expelled from the sample. The samples then were cleaned and resaturated. After several resistivity readings were taken, S_W was determined. Figures 3, 4, 5 and 6 show the measured resistivity index versus average brine saturation for all the samples at low and high rates. The Archie's relation of $I_R = S_W^{-n}$ assumes that a straight-line relationship of log (I_R) versus log (S_W) exists (a constant saturation exponent over the entire saturation range). This assumption has been considered by many previous investigators [13, 14, 15, 16] as "invalid". In this experimental investigation this assumption may be proven as "valid".

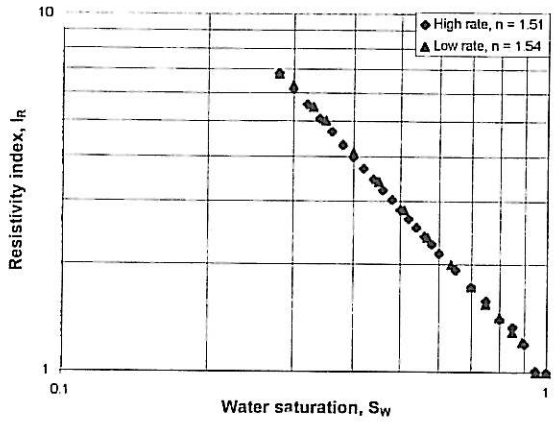


Fig. 3. Resistivity index, I_R vs. water saturation, S_W for core sample No. 1 at low and high injection rate

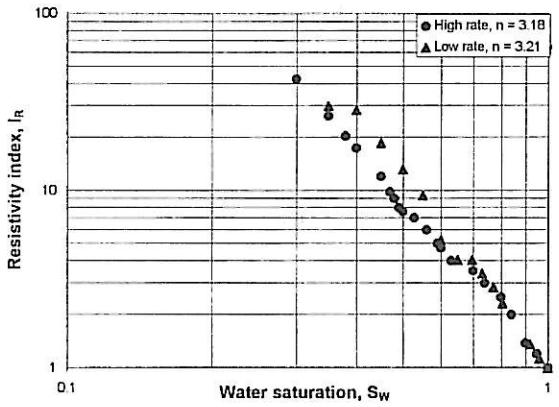


Fig. 4. Resistivity index, I_R vs. water saturation, S_W for core sample No 2 at low and high injection rate

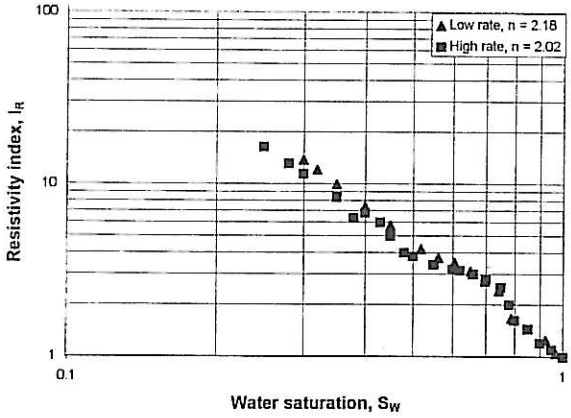


Fig. 5. Resistivity index, I_R vs. water saturation, S_W for core sample No. 3 at low and high injection rate

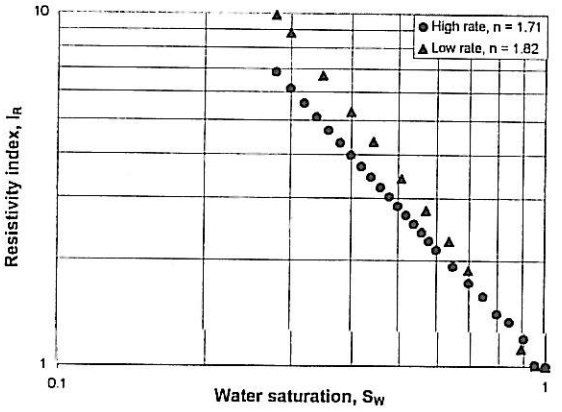


Fig. 6. Resistivity index, I_R vs. water saturation, S_W for core sample No 4 at low and high injection rate

However by comparing the plots of I_R/S_W for these tested samples with each other and with porous plate measurements, it has been found that a straight I_R/S_W correlation can be established over much wider range of S_W as shown in Figs. 3, 4, 5 and 6.

Basically, when non-wetting phase injected into the samples to displace wetting phase, the large pores will be penetrated firstly because they represent less resistance. As desaturation progresses a saturation heterogeneity through the core sample may persists and yield nonlinearity of I_R/S_W, but this may depends on the non-wetting injection rate and the heterogeneity of the core samples themselves. A rate of 0.03 cc/hr in sample 3 (Fig. 5), can be considered as the optimum because linear I_R/S_W relation was obtained. Also for sample 2 (Fig. 4), a constant n obtained over a good range of S_W by using the same injection rate. In contrast the I_R/S_W relationship becomes linear at brine saturation below (65–75%) when a low rate is chosen, as it is shown in Figs. 3, 4, 5 and 6. In this wide range of S_W,

Table 2. Saturation exponent values by two techniques

	Continuous Injection Technique		*Porous Plate Method*
Sample No.	*Low Rate*	*High Rate*	
1	1.54	1.51	1.55
2	2.18	2.02	2.15
3	3.21	3.18	3.18
4	1.82	1.71	1.83

the Archie's assumption has been proven its validity, and n from linear part of I_R/S_W curves should be used, provided that the desaturation process should be achieved at least to the reservoir S_W level in laboratory, to avoid improper extrapolation. On the other hand, high injection rate can create significant pressure drop through the desaturation process which results in an invalid I_R/S_W relations. Although the carbonate samples tested here have bimodal pore size distribution which believed to be the main cause

of the non-linearity of I_R/S_W, the selection of injection rate has an important role to overcome this problem. Also another interesting feature was observed, that low permeability sample (sample 1) shows clear linear I_R/S_W relation at S_W below 75%, (Fig. 3). In sample 3 (Fig. 5), the resistivity measurements for $S_W > 65$ and $< 100\%$ are useless in determining n, when low rate is used, but this range of S_W is much less when a high rate is used The saturation exponent values were found to be 1.55, 2.15, 3.18 and 1.83 by using the porous plate method. Very interesting feature was found where these n values are close to those measured by continuous injection technique at low rates. Again this confirms the importance of injection rate for establishment of proper I_R/S_W correlations. Table (2) presents the n values by the two methods.

CONCLUSIONS

Performing resistivity index by continuous injection technique at a fixed-rate may produce inaccurate (n) values, and subsequently an error in S_W determinations. The influence of injection rate on the resistivity index/brine saturation relationship has an important role to be considered. These measurements should be repeated at various injection rates to select an optimum rate for each core sample (proper n value).

This has shown that the low injection rate method is prefered on the high rate method, due to insignificant saturation changes taking place through the core sample at a given time. Furthermore, the low rate would produce linear relationship of I_R versus S_W over much wider range of S_W. This new experimental approach has illustrated that for water-wet samples a uniform I_R/S_W relation can be established. Therefore the usage of larger number of homogeneous and heterogeneous samples with various injection rates (high, moderate and low) is required for further investigation.

ACKNOWLEDGEMENTS

The authors wish to thank Robert Gordon University for permission to publish this work. Special thanks go to Core Laboratories (Aberdeen) for their permission to use the laboratory facilities. The Libyan Secretary of Higher Education People Committee is gratefully acknowledged for sponsoring Al-Mahtot during his postgraduate studies.

REFERENCES

[1] Archie G.E., 1942. The Electrical Resistivity Log as an Aid in Determining Some of Reservoir Characteristics, Trans. AIME, **146**, p. 54.

[2] de Wall J.A., Smits R.M., de Graaf J.D., and Schipper B.A., 1991. Measurements and Evaluation of Resistivity Index Curves The Log Analysts, (Sep–Oct), 583–595.

[3] Grattoni C.A., 1994. 'Influence of Pore Scale Structure on Electrical Resistivity of Reservoir Rocks", Ph. D. Thesis, Imperial College of Science Technology and Medicine, London, UK.

[4] Lyle W.D. and Mills W.R., 1989. "Effect of Nonuniform core Saturation on Laboratory Determination of the Archie Saturation Exponent", SPE, Formation Evaluation, (March), 49–52.

[5] Maerefat N.L., Baldwin B.A., Chaves A.A., La Torraca G.A., and Swanson B.F., 1990. "SCA Guidelines for Samples Preparation and Porosity Measurements of Electrical Resistivity Samples", *The Log Analysts*, (March–April), 68–75.

[6] Jing X.D., Alisdair G., and Trewin B.M., 1993. "Resistivity Index from non-equilibrium Measurements Using Detailed In-Situ Saturation Monitoring" *SPE* 26798, Offshore Conference Held in Aberdeen, 7–10 Sep.

[7] Lewis M.G., Sharma M.M., Dunlap H.F. and Dorfman M.H., 1988. "Techniques for Measuring the Electrical Properties of Sandstone Cores", SPE 18178, 63rd Annual Tech. Conf. and Exh. of the SPE held in Houston, TX, Oct. 2–5.

[8] Sprunt E.S., Desai K.P., Coles M.E. Davis R.M., and Muegge E.L., 1991. "CT-Scan-Monitored Electrical- Resistivity Measurements Show Problems achieving Homogeneous Saturation", SPE Formation Evaluation, (June), 134–140.

[9] Gray., Trewin B., Pallat N. and Mitchell P., 1992. "Comparison of Saturation Exponent Data by the Porous Plate and by the Continuous Injection Techniques with In-Situ Saturation Monitoring ", 3rd European Core Analysis Symposium (EUROCAS III), Paris, Sep. 14–16.

[10] Elashahab B.M., Jing X.D. and Archer J.S., 1993. "Experimental Investigation of the Effect of Wettability, Saturation History and Overburden Pressure on Resistivity Index", SPWLA, 15th European Formation Evaluation Symposium, Staranger, May 5–7.

[11] Zeelengerg P.W. and Schipper B.A., 1992. "Developments in I-Sw Measurements", 3rd European Core Analysis Symposium (EUROCAS III), Paris, Sep. 14–16.

[12] Arps, J.J., 1953. "The Effect of Temperature on the Density and Electrical Resistivity of Sodium Chloride Solutions", Trans. AIME, **198**, 327–330.

[13] Stalheim S.O. and Eidesmo T., 1995. "Is the Saturation Exponent n A constant?", SPWLA, 36th Annual Logging Symposium, Paris, June.

[14] Worthington P.F. and Pallatt N., 1990. "Effect of Variable n upon the Evaluation of Hydrocarbon Saturation", SPE 20538, 65th SPE Conf. New Orleans, Sep. 23–26.

[15] Wafta M., 1991. Using Electrical Logs to obtain the Satu-

ration Exponent in the Article Equation, SPE 21415, SPE Middle East Oil Show, Bahrain, Nov. 16–19.

[16] Argud M., Giouse H., Straley C., Tomanic J. and Winkler K., 1989. Salinity and saturation Effects on Shaly Sandstone Conductivity, SPE 19577, 64th Ann. Tech. Conf. and Exh. of SPE, San Antonio, TX, Oct. 8–11.

Petroleum Res.J. Vol. 9 (1997); P. 9–26, 8 FIGS.

Petrography and Palaeoenvironment of the Sidi as Sid Formation in Northwest Libya

M.T. El-Bakai*

بتروغرافية وبيئة ترسيب تكوين سيدي الصيد في شمال غرب ليبيا

محمود الطاهر البكاي

يتألف تكوين سيدي الصيد المتكشف ضمن سلسلة جبل نفوسة من عضوين هما: عين طبي ويفرن. يتكون عضو عين طبي من الدلوميت الذي يتفاوت في حجم حبيباته بين الدقيقة والخشنة. أما عضو يفرن فإنه يتكون من الأحجار الجيرية الطينية والدولوميتية مع تداخلات من حجر الطين والجبس.

تم تمييز خمسة أنواع من الدولوميت ضمن عضو عين طبي وهي:

النوع الأول: بلورات دقيقة شبه منتظمة الأوجه حلت محل حجر جيري يحتوي على القليل من الحفريات ويظهر متجانس اللون تحت المجهر (CL).

النوع الثاني: بلورات دقيقة جدا، غير منتظمة إلى شبه منتظمة الأوجه حلت محل حجر جيري غني بالحفريات وتتميز بلون برتقالي متلألئ وأصفر تحت المجهر (CL).

النوع الثالث: بلورات دقيقة إلى متوسطة الحجم شبه منتظمة الأوجه متجاورة مع المرو ولها لون برتقالي غير نقي تحت المجهر (CL) بمركز البلورة ولون برتقالي متلألئ عند الحواف.

النوع الرابع: بلورات متوسطة إلى كبيرة شبه منتظمة إلى منتظمة الأوجه وتتميز بلونها البرتقالي غير النقي في المركز ولون برتقالي غامق عند الحواف.

النوع الخامس: بلورات الباروك وهي كبيرة إلى كبيرة جداً شبه منتظمة الأوجه لها حواف ملتوية تتميز بلونها البرتقالي عند المركز غني بالخطوط ولون غامق نقي في الحواف.

البيئة التي ترسب فيها تكوين سيدي الصيد هي جزء من منحدر يقع بين سطحين مستويين من الأرض يتراوح بين منحدر محصور وبرك شاطئية إلى منحدر مفتوح أو شبه محصور يتدرج باتجاه الشمال إلى وسط المنحدر أو حوافه. يمثل عضو يفرن بيئة المنحدر المحصور وعضو عين طبي المنحدر الشبه محصور إلى المفتوح. أما الرسوبيات التي تمثل حاجز المنحدر فقد تمت إزالتها نتيجة لعوامل التعرية التي حدثت بعد إنتهاء الحقبة الطباشيرية أما المنحدر الخارجي فيمثله التكوين المكافئ لتكوين سيدي الصيد في العمر وهو ما يطلق عليه بتكوين العلالقة الذي يقع في المنطقة المغمورة من الرف القاري الليبي.

Abstract *The Sidi as Sid Formation (Upper Cretaceous) outcropped in Jabal Nafusah in NW Libya is composed of very fine to very coarse-grained dolomite of the Ain Tobi Dolostone Member and marly limestone, dolomites and calcareous shales interbeds with bedded gypsum of the Yifran Member. Five diagenetic dolomite types are recognized in the Ain Tobi Member. They are Type-1, fine and subhedral replaces mudstone/wackestone facies that show homogeneous luminescence pattern; Type-2, very fine, anhedral to subhedral replaces packstone/grainstone facies and characterized by bright orange and yellow luminescence pattern; Type-3, fine to medium, subhedral associated with quartz and has dirty orange luminescent cores and bright*

*Petroleum Research Center, P.O. Box 6431 Tripoli – Libya

orange rims; Type-4, medium to coarse, euhedral to subhedral crystalline fabric with orange luminescent cloudy cores and dully luminescent clean rims; Type-5 (baroque), coarse to very coarse, subhedral with curved crystal faces and characterized by orange luminescent inclusion-rich cores and dully luminescent inclusion-free rims.

The environment of deposition of the Sidi as Sid Formation is part of inner ramp which ranged from restricted or lagoonal ramp and open to semi-restricted ramp environments which graded northwards to mid- and outer ramp environments. The Yifran Member represents restricted ramp environment and the Ain Tobi Dolostone Member represents open- to semi-restricted ramp environment. The ramp margin had been removed due to post-Cretaceous erosion and the outer ramp environment is represented by the Sidi As Sid Formation's equivalent (Alalgah Formation) in the offshore Basin.

INTRODUCTION

Sidi as Sid Formation (Cenomanian) is outcropped along Jabal Nafusah in northwestern Libya (Fig. 1). Jabal Nafusah Escarpment extends from the coast of the Mediterranean Sea near Al Khums in a broad arc 350 km south and west to the Libyan–Tunisian border where it is 130 km from the coast. Jabal Nafusah continues into Tunisia, turns north, and dies out near Gabes, and it is known in that area as the Jifarah Escarpment.

Christie (1955) described Ain Tobi and Yifran as separate formations, but El Hinnawy and Cheshitev (1975) assigned the term Sidi as Sid Formation which includes two members (Ain Tobi Member below and Yifran Marl Member above). It is difficult to demarcate these two rock units in many places, so that were mapped together by all authors.

Ain Tobi Member is previously described by El Hinnawy and Cheshitev (1975), Megerisi and Mamgain (1980a,b) as it is composed of greyish limestone and dolomitic limestone with marly intercalations in the lower part and well bedded white to light yellow limestone and dolomitic limestone in the upper part.

The lithotypes of the Ain Tobi Member have been evaluated by systematic measurements and description of the units encountered in the NW Libya. A total of twelve sections have been measured along Jabal Nafusah Escarpment. Two hundred ordinary thin section and same number polished thin sections

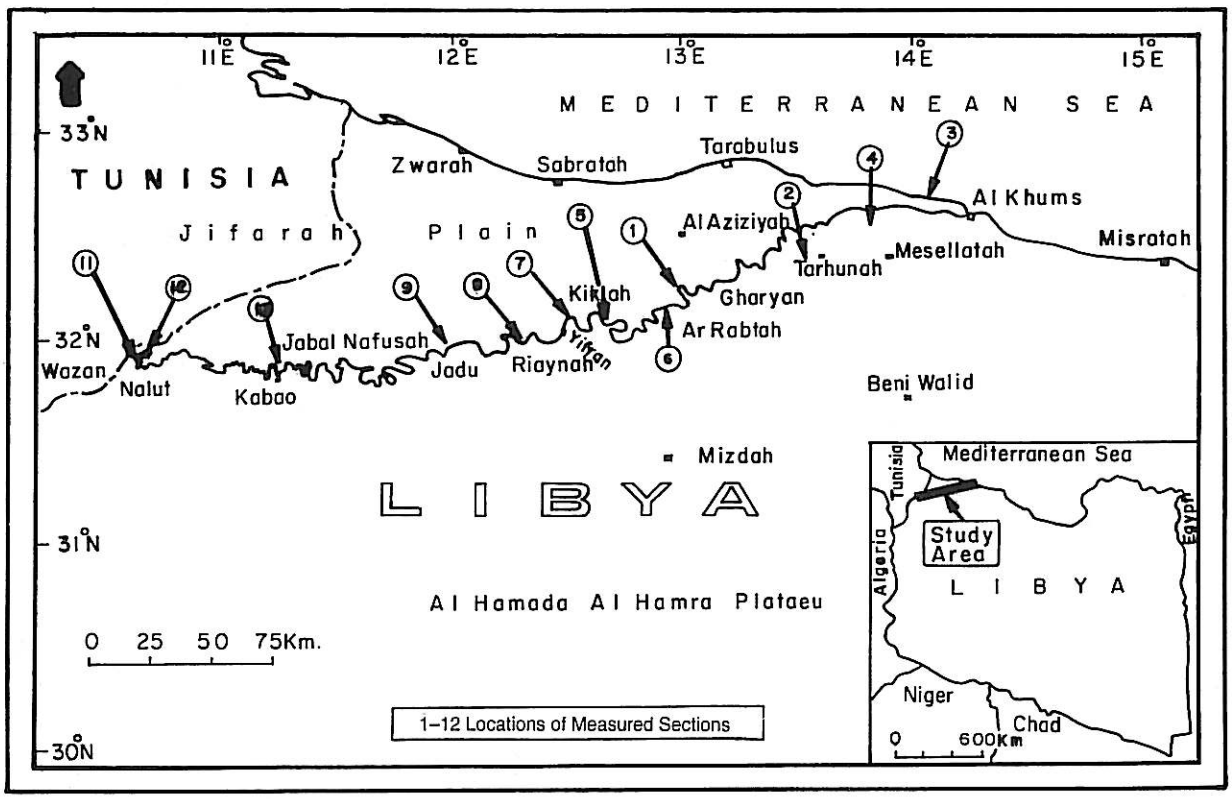


Fig. 1. Location for measured sections: (1) Abu Ghaylan section; (2) Ras Fam Mulghah section; (3) Al Khums (Wadi Ghanimah) section; (4) Wadi Jabbar section; (5) Kiklah section; (6) Ar'Rabtah section; (7) Taghmah section; (8) Riaynah section; (9) Jadu section; (10) Kabao section; (11) Wazan section; (12) Nalut section.

were examined petrographically and by Cathodoluminescence Microscope to determine mineral composition and texture. All ordinary thin sections were stained by alizarin red S and potasium ferricynide according to Dickson (1965). They are all unstained which indicate the completeness of dolomitization and dolomites contain less than 1% FeO (Sperber *et al.*, 1984). 154 sample were analysed by X-ray diffraction and they also show the total replacement by dolomite.

PALAEOGEOGRAPHY AND FIELD OBSERVATIONS

Cenomanian Palaeogeography in Northwestern Libya:

The Ain Tobi sediments were deposited during a major marine transgression which began in northwest Libya at the beginning of the Cenomanian and culminated in the Late Turonian.

The Ain Tobi Dolomite Member is a part of a shelf deposit which covers all or part of Algeria, Tunisia, Libya, Egypt, Niger and Chad (Reyre, 1966). The isopach map (Fig. 2) shows that the region of the present Jabal Nafusah in northwest Libya is a part of a wedge of Cenomanian strata which thicken to the south toward the axis of the Ghadamis Basin. The Jabal Nafusah area was adjacent to a topographically high or non-subsident region to the north.

There is a general decrease in carbonate content from northeast to southwest and increasing in siliciclastics. This reflects generally the gradient between an onshore clastic source and offshore carbonate production.

In the subsurface from northwest Libya into the Sirt Basin there are lithologic and nomenclature changes in the Cenomanian section. The Bahi and Lidam Formations (subsurface) are equivalent to the Sidi as Sid and Nalut Formations (outcrop). The Bahi Formation is a siliciclastic composed of interbedded sandstone, siltstone, conglomerate and shale with common glauconite pellets in the uppermost part. The lower part is thought to be non-

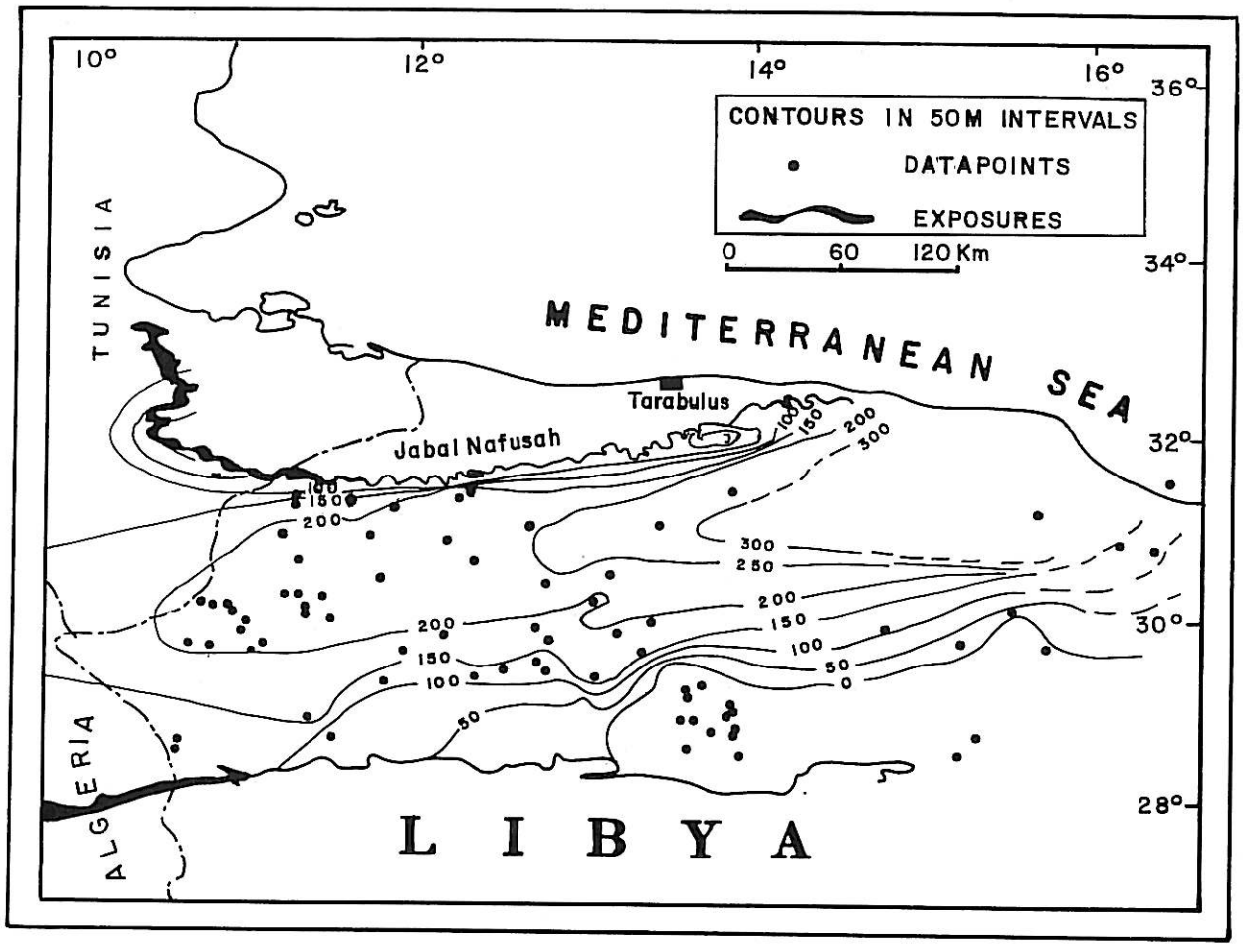


Fig. 2. Cenomanian isopach map in northwestern Libya (Tunisia after Busson, 1970).

marine, but the glauconitic upper part is apparently marine (Sghair, 1993), and is believed to be diachronous unit, ranging in age from Cenomanian to Maastrichtian. The Bahi Formation is conformably overlain by the marine Lidam Formation or other younger Upper Cretaceous strata.

The Lidam Formation is dated as Cenomanian in age (Barr and Weegar, 1972). It is composed mainly of argillaceous dolomite with common glauconite pellets and quartz grains in the lower portion, oolitic packstone and grainstone in the middle part, and fine to medium dolomite associated with anhydrite at the upper part (El-Bakai, 1989; 1991). It was deposited in a shallowing upward ramp in the northwestern part of the Sirt Basin (El-Bakai, 1989; 1992).

The Ain Tobi Dolostone Member is a part of a transgression sequence that can be found throughout most of North Africa. As in the case of Ain Tobi Dolostone Member, most of the transgressive units were deposited on a carbonate platform, possibly a carbonate ramp. The dominance of carbonates and presence of evaporites reflect a warm possibly dry Cretaceous climate. The Sidi as Sid (Ain Tobi and Yifran Members) transgressive sequence is part of a major worldwide Mid-Cretaceous rise in sea-level.

Main Lithologic Units of the Ain Tobi Member:

The Ain Tobi Dolostone Member is widely distributed rock unit, along Jabal Nafusah Escarpment and it forms the topmost of this escarpment. Generally, the thickness of the Ain Tobi sediments increases from southwest to the northeast direction. The thickness ranges from 5 m in Wazan area to more than 110 m in the area between Mesellatah and Qasr Khiar. The maximum thickness of Ain Tobi was observed in Jadu section in the western part of the escarpment, and this is due to the percentage of coarse clastics which was the highest in the area. Ain Tobi Dolostone Member is unconformably underlain by Kiklah Formation (Fig. 3a) and overlain by Yifran Marl Member.

Ichthyosarcolites Band:

The *Ichthyosarcolites* Band is a marker bed across the whole Jabal Nafusah. It is consistently present at each locality at the lower and/or middle of the Ain Tobi Dolostone Member. The band was recognized and described by Christie (1955) in eastern Jabal Nafusah because of leached moulds of the rudist *Ichthyosarcolites* sp. commonly found at its top. Rudists have been destroyed probably by silicification at the western Jabal Nafusah, but the band can still be recognized due to its prominent position, thickness and relatively resistance to weathering comparing with the other beds (Fig. 3b).

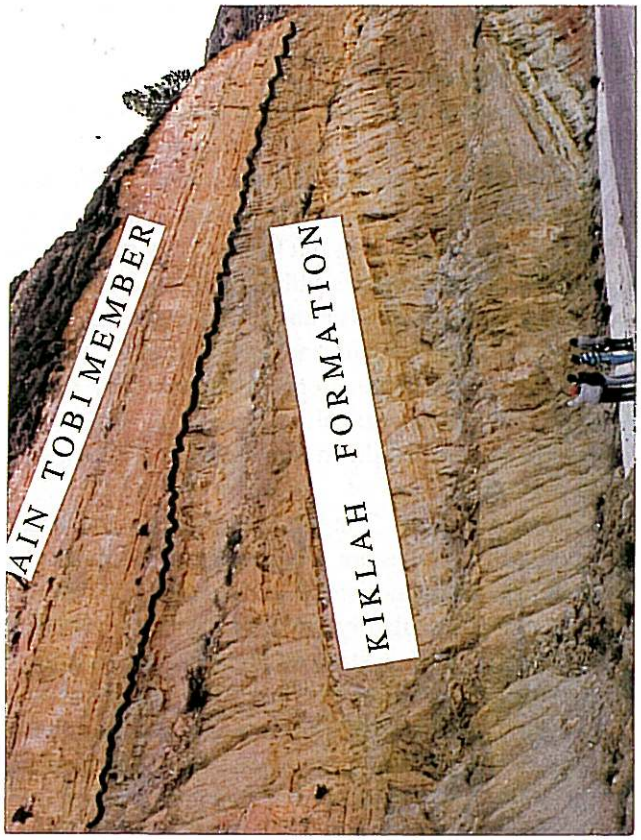
The *Ichthyosarcolites* Band is an unusually thick unit compared to other bedded intervals in the Ain Tobi. It ranges from 3 to 18 m in thickness although it is sometimes difficult to locate the base (specially at the western Jabal Nafusah) due to the diagenetic alteration. The band is composed of dolomite, chert and some quartz sand. Generally, the band is cross-bedded in the central and eastern Jabal Nafusah areas and appears to be uniformly bioturbated in the western area of Jabal Nafusah. In addition to rudists (Fig. 3c), which gives the band its name, other bivalves, gastropods, echinoids, bryozoans and foraminifera occur mainly as moulds. Ooids are also present.

The *Ichthyosarcolites* Band makes a gross change from the dominance of thicker bioturbated beds below to thinner beds above. The overlying beds contain sedimentary structures which indicate deposition in shallower water and some show signs of current activity (e.g. cross-bedding and microbial). Beds below the band are more resistant to weathering than those above. The upper beds are often soft and powdery while the underlying beds tend to be crystalline. This is due to differences in depositional lithology across the band. Sediments above the band contain more argillaceous material and gypsum than those below it, thus this part of the Ain Tobi Member has the steepest weathering profiles found in the section. The *Ichthyosarcolites* Band may be the result of a facies change in response to a change in sea level. The change in bedding thickness, dominated types of sedimentary structures, and lithology are probably due to a shift from deposition in tens of meter to less than that. The coincidence of the band and sea level fluctuation is only suggested here because the microfuna does not provide the necessary biostratigraphic detail.

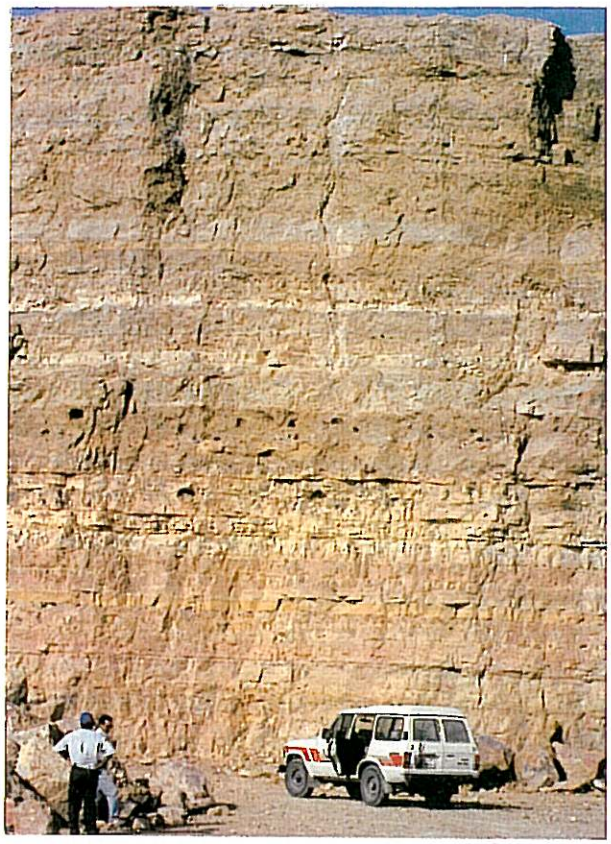
In summary, the *Ichthyosarcolites* Band of the Ain Tobi Dolostone Member is a distinctive marker bed throughout Jabal Nafusah. In the eastern part of the escarpment it is characterized by a distinc-

Fig. 3. Field photographs showing: (a) The angular unconformity between the Kiklah Formation below and the Ain Tobi Member above at Abu Ghaylan area: (b) Tabular bedding which is the dominant sedimentary structure within the Ain Tobi Dolostone Member; (c) General view of the *Ichthyosarcolites* Band at Tarhunah area; (d) The extensive bioturbation at Wadi Jabbar section. →

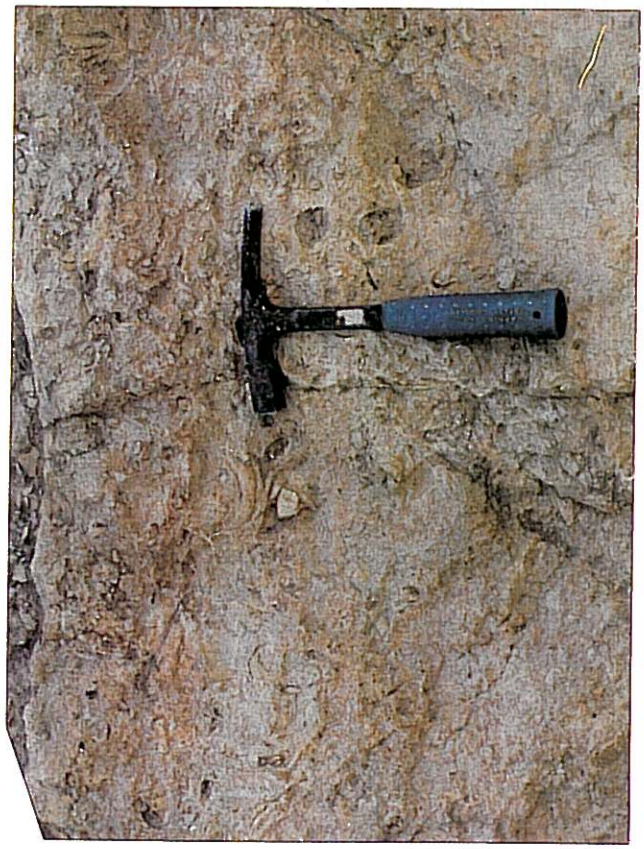
a



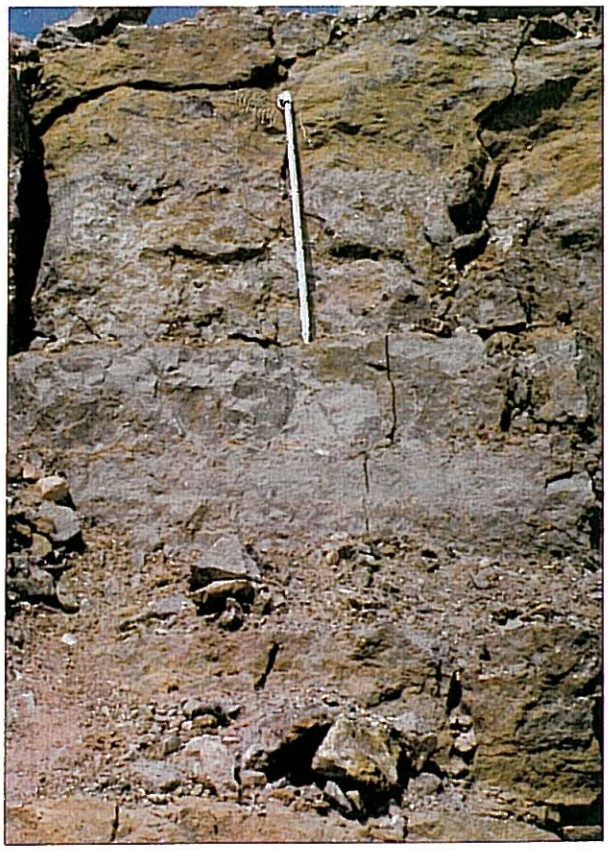
b



c



d



tive fauna including rudist bivalves. In the west it is represented by dolomite. The band represents the culmination of a basin filling sequence which may mark a drop and subsequent rise in sea level. Because water depths were different before and during deposition of the band versus after the band it makes at least a facies change if not a minor disconformity due to change in sea level.

Bioturbation Unit:

Bioturbation structures are the most common form of structures found in units of the Ain Tobi of Jabal Nafusah (Fig. 3d). They are the most continuous in the escarpment, commonly extending for 5 km. The *Ichthyosarcolites* Band is bioturbated throughout Jabal Nafusah in NW Libya where diagenesis has had a less obscuring effect on primary fabric. Bioturbated units can be found above and below any of the other sedimentary units.

Generally, dolomitization has obscured most of the primary deposition textures of the bioturbated beds. Most of the grains have either been leached and left as mouldic porosity or they have been replaced. The precursor matrix material was probably limestone because of the random orientation of dolomite crystal axes and the uniform crystal size (Evamy, 1967). Intercrystalline and leached mouldic porosity averages between 10–20% (estimates from thin sections). If each of the leached mouldic pores is assumed to be precursor grain, bioturbated units were wackestones, packstones and possibly grainstones. The original bioturbated sediments of the Ain Tobi Member were probably bioturbated by the combined activity of worms, enhinoderms and molluscs.

Interpretation: Deposition of Ain Tobi sediments probably has occurred on an open marine platform with alternating periods of storm reworking and bioturbation. Storm generated currents and bioturbation rather than tidal currents are thought to be principally responsible for disturbing sediments over the Ain Tobi platform. Bioturbation is indicated by lack of internal layering. Storm activity is indicated by cross-bedded carbonate sand units up to 4 m thick in and above the *Ichthyosarcolites* Band. Tidal currents are thought to play a minor roll in the Ain Tobi deposition particularly in the oolitic intervals because of the absence of extensive channel development, absence of levees and limited development of distinctly intertidal or supratidal environments.

Laminated Unit:

Laminated units are found principally in the dolomudstone units (Fig. 4a), but may be present in dolowackestones and dolopackstones. The laminated units are generally less than 1 m thick, but may range up to 2 m in thickness. They may extend laterally for kilometres although units are difficult to trace because of differences in weathering. These lamination are smooth and flat to slightly undulatory. Individual laminations extend laterally from 1 to 30 m. Narrow vertical burrows (Fig. 4b) may be present and extend down for 5 to 6 cm. The burrows do not branch.

Interpretation: The flat to undulatory laminated units with fenestra are most easily recognizable as cryptalgal stromatolites. The fenestrs, fine laminations, flat to undulatory surfaces are the criteria used to identify them as stromatolites. Most of fenestral and non fenestral units are flat, therefore could have been originated in several environments. Laminated units of the Ain Tobi are attributed to the trapping and binding of algae. The inferred location of microbial development is in some type of lagoonal setting in the intertidal zone.

The thickness of the flatness laminae, the lack of fenestra and probably the aridity of the climate of the Ain Tobi sedimentary environment (judging from Cretaceous palaeotemperature curves of Savin, 1977 and the presence of gypsum in Yifran Marl Member of Jabal Nafusah and Ghadamis Basin) indicate that Ain Tobi laminated units probably deposited in intertidal environment.

Cross-bedding Unit:

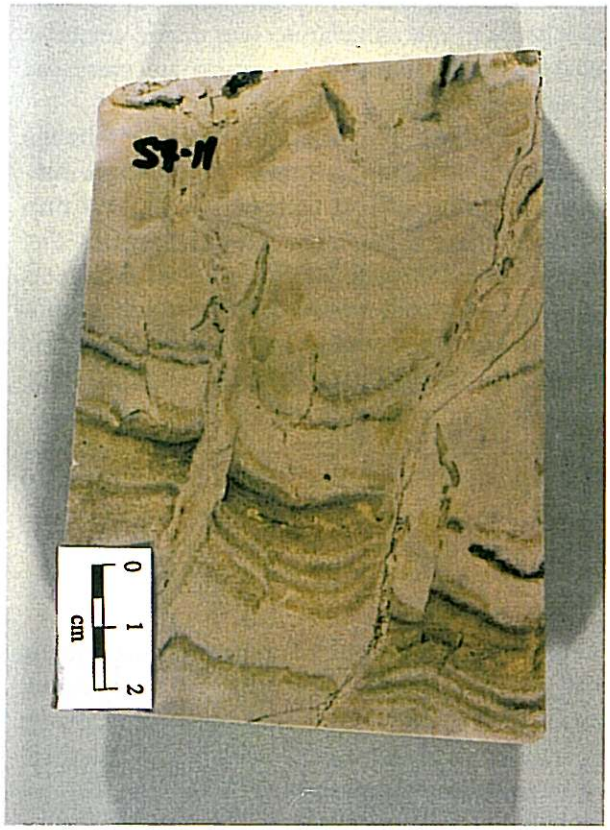
The cross-bedding units of the Ain Tobi Member increase in thickness towards the northeast. The dominant types of cross-bedded units are dune or tabular which mainly occurred in the Ras Fam Mulghah (Section #2) and Taghmah (Section #7). Trough cross-bedding occurs at the Abu Ghaylan (Section #1, Fig. 4c). The thick cross-bedded unit in the Ras Fam Mulghah is composed of dolograinstones. The grains which form these carbonate sands include ooids, peloids, foraminifera, quartz grains and fragments of gastropods, bivalves and echinoids.

Fig. 4. (a) Field photographs showing laminated dolomudstone unit at Wadi Jabbar section; (b) Polished slab photograph of sample taken from Taghmah section. Note well preserved lamination in a completely dolomitized mudstone. Some laminae are disturbed by burrows; (c) Outcrop photograph at Abu Ghaylan section showing small-scale cross-bedded oolitic doloplackstone/dolograinstone; (d) Field view showing mudcracks structure at Abu Ghaylan section. →

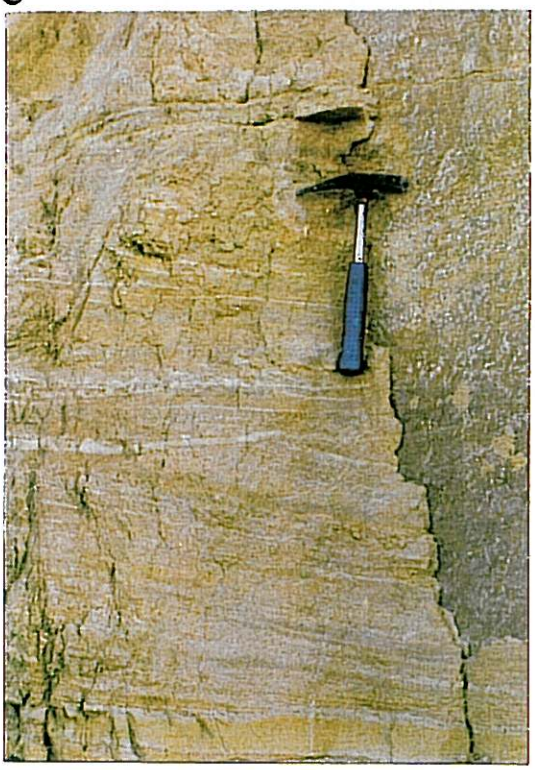
a



b



c



d



Cross-bedded carbonate sands are the only units that commonly contained recognizable ooids. These units are the only ones in which grains can be identified because dolomitization, was fabric retentive and the exterior forms of the grains are preserved (non-mimetic replacement).

Interpretation: The generation of ooid grains and grainstone sand bodies in Recent carbonate environments occurs in shallow agitated waters, less than 2 m (Milliman, 1974). Hine (1977) suggests that ooids generated through interaction of tidal currents and storm generated waves. Tidal currents are primarily responsible for ooid generation while storm currents distributed them. Because ooids make up a significant proportion of the grains in these units, some tidal activity is indicated. These cross-bedded units represent the highest energy environment of the Ain Tobi Member and probably are shoal deposits.

Collapse Breccia:

Units interpreted as solution breccias occurred in small intervals in most of the measured sections. Solutions breccia has implied dissolution of evaporite minerals and the subsequent collapse of interbedded or overlying material. In the Ain Tobi Member true solution breccias are rare. This type of feature occurs commonly on sabkhas (Wilson, 1975). In this case precipitation and dissolution of the gypsum may have occurred during a brief period of exposure, despite the fact that there is little real evidence of subaerial exposure in the Ain Tobi. Distinct mudcracks are found only in the Tarhunah area (Ras Fam Mulghah section), the Wadi Jabbar section and Abu Ghaylan section (Fig. 4d). The lack of horizontal surface may have hindered the recognition of mud cracks and makes positive identification of vertical cross sections through possible mud cracks difficult. The mud cracks generally are uncommon, and suggests that subaerial exposure was rare during the deposition of the Ain Tobi Member.

LITHOTYPES OF AIN TOBI MEMBER

The Ain Tobi Member is an arenaceous to argillaceous dolostones. The dolomitized limestone or dolostone contains a varying proportion of poorly sorted, subangular to subrounded quartz sand. According to the field observations and petrographic studies of samples from twelve measured sections, Ain Tobi Member can be divided into five lithotypes:

Lithotype 1. Cross-bedded dolograinstones and dolopackstones. The scale of cross-bedded locally decreases upward and may show erosional relief at the basal surfaces. Channel geometry is suggested in some areas by the lateral changes into marls.

Lithotype 2. Bioturbated dolowackestones and dolopackstones. These contain subhorizontal fractures and burrows belonging to trace fossils.

Lithotype 3. Bedded dolomudstones and dolopackstones with rare wavy laminations and bioturbation. This facies is generally interbedded with bioturbated dolowackestones and dolopackstones.

Lithotype 4. Laminated dolomudstones and dolowackestones with microbial, birds-eye structure and gypsum.

Lithotype 5. Solution breccias consisting of angular clasts, commonly silicified in a dolomitized matrix.

These lithotypes of the Ain Tobi Dolostone Member are interpreted as a shallow-shelf or ramp carbonate deposit (discussed below). These represent a shoaling-upward cycles deposited during regressive phases.

Ain Tobi Dolostone Member is overlain by Yifran Marl (upper member of the Sidi as Sid Formation). It consists of yellow soft marls, marly limestone and dolomites and calcareous shales with uncommon interbeds of bedded gypsum, gypsiferous shales and oolitic limestone. Marls with bedded gypsum predominate west of Yifran whereas to the east the thickness decreases and dolomitic limestone predominate. Recrystallization makes identification of textures difficult, mudstones, wackestones, and wackestones/packstones occurred with occasional oolitic grainstone. Parallel lamination is the most common sedimentary structure and sparse fauna generally consists of molluscs. Bioturbation is commonly occurred throughout the member. The lithology of Yifran Marl Member is interpreted as a restricted ramp (inner-ramp) in the western and south of Jabal Nafusah, and as an open to semi-restricted ramp in the eastern Jabal.

PETROGRAPHY

In this study Ain Tobi Member is assigned as "Ain Tobi Dolostone Member" because the petrographic details and XRD analysis of samples taken from 12 measured sections scattered throughout the study area (Fig. 1) show that all Ain Tobi sediments have been completely dolomitized (more than 95% dolomite) and only traces of calcite occurred in

the form of calcitization or dedolomitization. Yifran Marl Member will not be treated petrogaphically in this study.

According to the crystal shape and size distribution, five different types of dolomite recognized in the studied sections. These differences may reflect the variation of origin, mechanisms, chemistry and may be the timing of dolomitization. Detailed geochemistry and origin of these types of dolomite is a separate study now in progress. Some individual samples of these sections composed of more than one type of dolomite. The dolomite types are classified according to Friedman (1965) and Sibley and Gregg (1987). All types of dolomite are calcian, nonferroan and have more than 52% $CaCO_3$, except Type-1 which is stoichiometric (49–50% $CaCO_3$). All types are moderately to well ordered as determined by XRD.

Hand Specimen Petrography

Type-1 dolomite is yellowish-grey, porous and laminated mainly replaced wackestone/packstone. The laminae usually pinkish in colour. This type of dolomite is associated with birds-eye structure, ripples and microbial with gypsum nodules or collapse breccia and quartz grains in the western part of the study area. Type-2 dolomite is very fine, whitish-grey, cross-bedded, slightly porous and calcareous crystalline replaced mainly packstone and grainstone facies. Type-3 is also laminated, tan to grey, calcareous and interbedded with quartz sandstone. Type-4 dolomite is light-grey to yellowish, slightly porous and calcareous being replaced the highly fossiliferous sediments and occurred mainly at all positions of almost all measured sections. Type-5 dolomite is grey, coarse to very coarse, porous crystalline with pearly lustre appearance (Fig. 5a) replaced calcerenitic packstone lithofacies. This type is restricted to the eastern part of the study area and rarely occurred at western part of the study area.

Transmitted Light and Cathodoluminescent Microscopy:

Type 1 dolomite:

It is an early and pervasively non-ferroan dolomite, generally consists of unimodal or very fine to fine (10–100 μm, average 70 μm), closely packed nonplanar-*a* or xenotopic (anhedral) dolomite crystalline (Fig. 5b). These dolomite cystals have totally replaced the precursor sediments which probably were lime mudstones and wackestones and its crystals have inclusions. The cores of some crystals are selectively dissolved out leaving intracrystalline pores. The texture is mainly xenomorphic. The commonly observed cathodoluminescence pattern in Type-1 dolomite is homogeneous orange luminescence at zones succeded dissolved cores and very thin bright yellow luminescent outer rims (Fig. 5c). Type-1 dolomite is the most common type in the Ain Tobi Dolostone Member and occurred at all locations.

Type 2 dolomite:

The crystals of this type of dolomite are made up of unimodal or very fine mainly less than 10 μm, closely packed nonplanar-*a* or xenotopic dolomite crystalline (Fig. 7a). The crystals are usually dirty or cloudy and mainly nonmimetically replaced skeletal and non-skeletal allochems. Crystals of Type-2 dolomite exhibit bright yellow orange luminescent pattern whereas late crystals occurred as a cement around pores show red to dark brown luminescent appearance (Fig. 7b). In fabric-destructive or non-mimetic replacement, original fabrics are commonly outlined by abundant inclusions. Mouldic, interparticle and vuggy porosities are commonly occurred within this xenomorphic mosaic dolomite and has been found in the lower and middle intervals of most measured sections.

Type 3 dolomite:

Type-3 dolomite is unimodal (average 100 μm), nonplanar- *a* and planar-*s* replacive crystalline. This type is mainly associated with quartz grains (Fig. 5d) and may be occured post-compaction. It is mainly found at bottom of all measured sections. Quartz grains associated with this type are subrounded medium to coarse and unicrystalline, cemented by quartz overgrowth. They are usually coarser than dolomite crystals and sometimes fractured probably due to compaction. Type-3 dolomite is characterized by dully luminescent cores and orange luminescent rims (Fig. 6a).

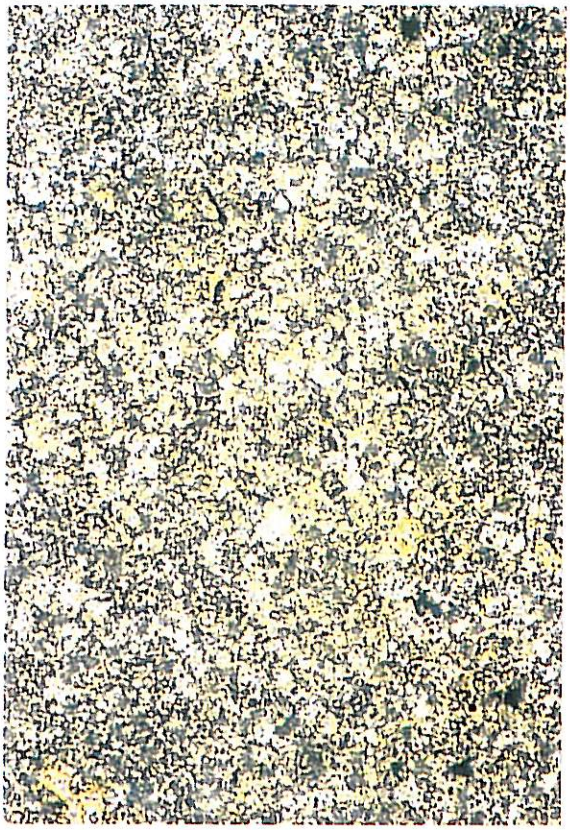
Type 4 dolomite:

It is polymodel or fine to medium (average 200 μm), nonplanar-*s* or hypidiotopic and non-ferroan dolomite crystalline (Fig. 6b). The crystals are cloudy at cores and more cleaner rims, and exhibits undulose extinction. Some times this type occurred as an isolated euhedral rhombs (Fig. 6c). This type believed to be an intermediate to late diagenetic dolomite and has completely replaced the original sediments which probably were bioclastic wackestone/packstone. Some crystals show replacement or recrystallization of precursor fine and nonplanar-*a* (Type-1) dolomite crystals, whereas others have

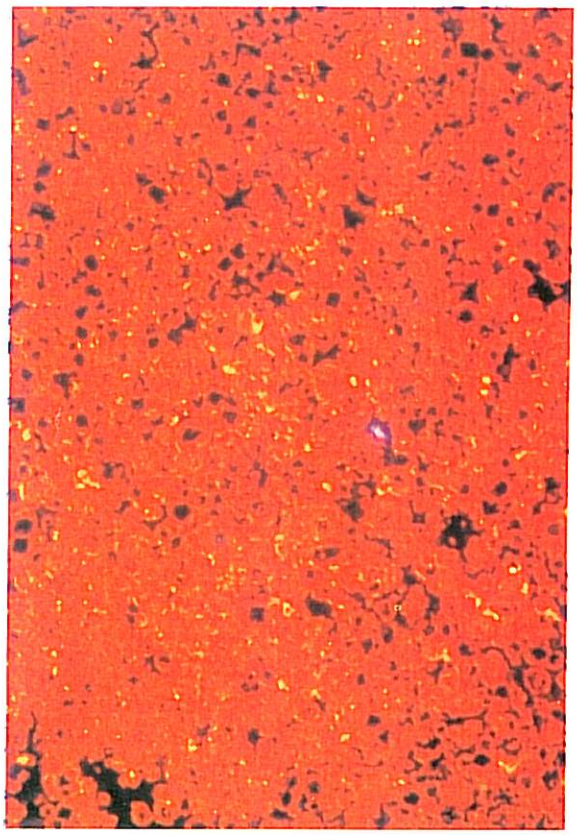
a



b



c



d



their cores partially or completely dissolved out due to continued dissolution, leaving irregular voids indicating dedolomitization. In some instances dissolution has proceeded to the point where almost the whole crystal has been dissolved out leaving a rhombic moulds. The texture of Type-4 dolomite is generally hypidiomorphic. Cathodoluminescence microscopy shows that the cores are mainly dirty orange luminesent due to inclusion-rich, whereas inclusion-free rims exhibit dully orange luminescent (Fig. 6d). These differences reflect that the Fe and Mn values are considerably lower in the inclusion-rich than in the inclusion-free zones (Fairchild, 1980; Coniglio and James, 1988; Amthor and Friedman, 1991; 1992) due to recrystallization (Nielsen *et al.*, 194). Intercrystalline, mouldic and vuggy porosities are associated with this dolomite type which occurs in various stratigraphic intervals.

Type 5 dolomite:

This type of dolomite occurred in the eastern Jabal Nafusah only and has been observed in Al Khums and Wadi Jabar areas. Type-5 dolomite is composed of coarse to very coarse or polymodal (500 μm–2 mm), planar-*s* and zoned baroque or saddle crystalline (Fig. 7c). These replacive crystals have curved faces or boundaries and cleavage planes. They show extremely undulose extinction. The crystals characterized by euhedral cloudy cores and clean rims, which indicate their replacement to the original micritic sediments. The cloudy cores exhibit orange luminescent and rims show dully luminescent, but the cleavage lines have bright yellow pattern (Fig. 7d).

Dedolomitization:

The term dedolomitization was first proposed by Von Morlot (1848) to describe a possible mechanism by which the mineral calcite replaces the mineral dolomite. Evidences for dedolomitization have been observed under the microscope and by XRD analysis of whole rock of the Ain Tobi dolomite sediments. Presence of euhedral or idiomorphic dolomite crystals with their cores leached out leaving itracrystalline pores and sometimes the whole rhomb dissolved out leaving euhedral mouldic pores, indicating dedolomitization. The dissolved cores of some crystals are filled or replaced by calcite (Fig. 8a). Some other rhombohedral crystals are replaced by large or blocky non-ferroan, and late calcite crystals. These calcite crystals being as an overgrowth with an optical continuity with dolomite substrates. In some cases the dolomite rhombs are corroded or rounded crystals, whereas elsewhere some dolomite crystals float in a coarser calcite crystals with irregular contacts between them indicating dedolomitization. Under cathodoluminescence microscope the dedolmitizated crystal show complex zonation (Fig. 8b). Dolomite zones show bright yellow luminescent pattern whereas the replacive calcite zone exhibit dully orange luminescent.

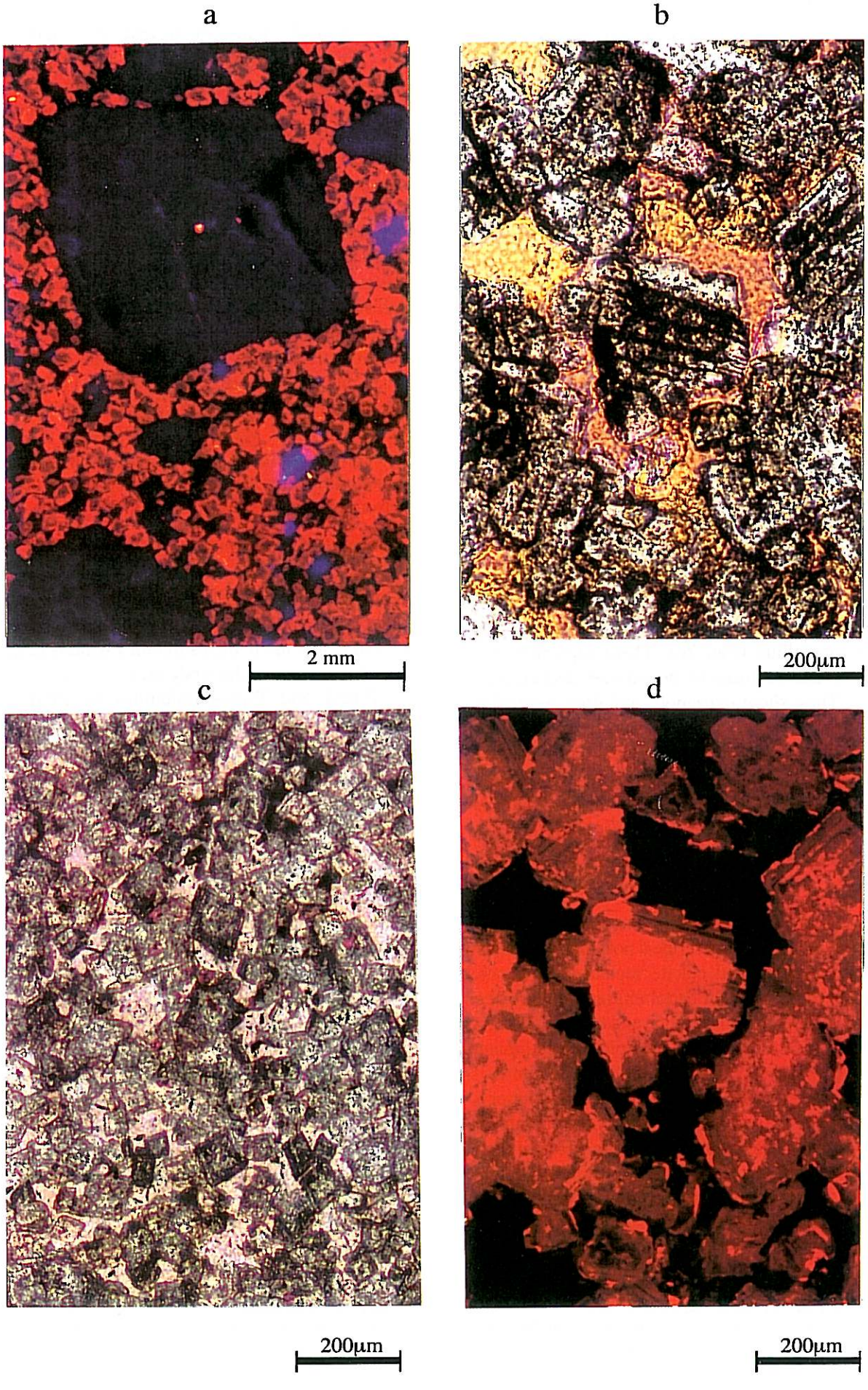
Several authors attributed the phenomenon of dedolomitization to early diagenesis and/or surface chemical weathering (Evamy, 1967; Braun and Friedman, 1970; Magaritz and Kafri 1981) or to oxidation of pyrite (Evamy, 1963), all epigenetic process. Budai *et al.* (1984) pointed out that dedolomitization can occur any where (surface and subsurface) conditions are favourable for it.

Distribution of dolomite

Dolomite has been found to replace all Ain Tobi sediments in all measured sections, only traces of limestone remain. Sandstone occurred in the lower part or below the *Ichthyosarcolites* band occurred in the western part of the study area.

Type-1 and Type-4 dolomites occurred in all sections in different stratigraphic positions. Type-3 dolomite is mainly occurred at bottom of all sections and in higher position in section #9 at Jadu area. Type-2 dolomite has been found mainly at the middle parts of measured sections in the western and central parts of the study area within the *Ichthyosarcolites* band or replacing packstone and grainstone facies. It replaces the oolitic grainstone intervals in the lower and middle parts of the measured sections at the eastern part of Jabal Nafusah (east Wadi Ghan). Finally, Type-5 dolomite restricted to the eastern part of the study area at the top of measured sections in Fam Mulghah, Wadi Jabbar and Al Khums area and rarely at Riaynah and Jadu area. Dedolomitization or the replacement of the dolomite by calcite crystals has been observed at various stratigraphic positions. It has been found at the bottom of section #9 and section #10, close to the unconformity between Kiklah Formation below and Ain Tobi Member above, and occurred also at top of sections #4, #5, $6, #8, and section #9 (Fig. 1).

← Fig. 5. (a) Polished slab photograph showing the very coarse saddle dolomite seen at Al Khums coast; (b) Photomicrograph of Type-1 dolomite (PPL); (c) Luminescence microscopy of the same sample (b) showing the homogeneous orange luminescence pattern; (d) Photomicrograph of Type-3 dolomite associate with quartz grains (PPL).


a
2 mm
b
200μm
c
200μm
d
200μm

ENVIRONMENT OF DEPOSITION

A sedimentary model was proposed for the Sidi as Sid Formation (El Hinnawy and Cheshitev, 1975) in the Jabal Nafusah escarpment and Ghadamis Basin to the south. In this section the term facies is avoided because the depositional environments could be defined on the basis of sedimentary structures and because dolomitization has obliterated most of the criteria used to define microfacies based on textures and grain types.

The Cenomanian depositional environments, found on the Jabal Nafusah escarpment and in the Ghadamis Basin are part of inner ramp sequence according to definition of Ahr (1973); Buxton and Pedley (1989); Elrick and Read (1991); Burchette and Wright (1992) which ranged from open to semi-restricted ramp and a restricted or lagoon ramp. In this study the open to semi-restricted and restricted ramps will be discussed, because they occur in the exposures of the Sidi as Sid Formation and in the subsurface of Ghadamis Basin where well logs are available. In the offshore Gabes–Tarabulus–Misratah Basin most drilled wells did not penetrate deeper than the Maastrichtian and in Tunisia the data are not available. Published data on the Gabes–Tarabulus–Misratah Basin and Tunisia areas and data gathered during this study from outcrop and subsurface Ghadamis Basin will be used in order to propose a model for the Cenomanian in northwestern Libya.

Inner Ramp:

Restricted or lagoon Ramp:

The restricted ramp environment is represented by the Yifran Marl Member of the Sidi as Sid Formation in the subsurface of Ghadamis Basin, southern Nafusah uplift and in Jabal Nafusah. Yifran Member is composed of approximately 70 m of marls, marly limestone, dolomites and calcareous shales interbeds of bedded gypsum in western Jabal Nafusah and dominated by limestone in eastern part of the study area. In the subsurface (Ghadamis Basin) it consists of 150 m of interbedded dolomite, shale and evaporites. In both Jabal Nafusah and the Ghadamis Basin it overlies open to semi-restricted dolostones of the Ain Tobi Member and is overlain by Nalut Formation. Units associated with restricted ramp occurred commonly above the *Ichthyosarcolites* Band close to the contact between Ain Tobi and Yifran Marl.

The rare fauna present in the Yifran Marl suggest deposition in a shallow, marine, neritic environment (Fig. 9) with restricted lagoonal conditions (intertidal and supratidal) with no tidal channels in the western part of the basin (Megerisi and Mamgain, 1980a). A lagoonal palaeoenvironment is suggested because it could impound water whose evaporation would result in evaporite deposition indicated by the solution breccias in the Ain Tobi Dolostone Member (lithotype-5) and in actual evaporite layers in the Yifran Marl Member.

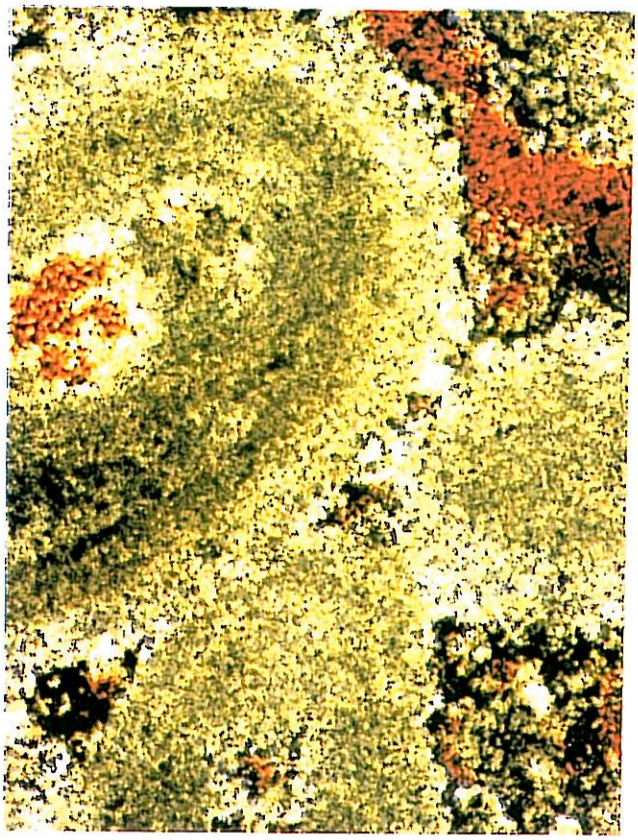
Open to Semi-Restricted Ramp:

The open to semi-restricted ramp environment is represented by the Ain Tobi Dolostone Member of the Sidi as Sid Formation in the Jabal Nafusah escarpment and in the subsurface of Ghadamis Basin where it can be traced on completion logs. In the Ghadamis Basin the open to semi-resricted ramp consists of dolomite which overlies Early Cretaceous siliciclastics of the Kiklah Formation and underlies lagoonal rocks of the Yifran Marl Member. The Ain Tobi Member thins to the south as the Yifran Marl thickness. In the Jabal Nafusah escarpment the open to semi-restricted ramp consists of dolostones, sandy dolomite, chert and quartz sandstone. It is composed mainly of bioturbated bedded carbonate units, with cross-bedded oolitic dolograinstones and laminated dolomudstones. The bioturbated units especially those containing rudists such as the *Ichthyosarcolites* Band and cross-bedded sands are more abundant towards the north of the Nafusah escarpment. The carbonate muds and associated evaporites are more abundant south of the escarpment and at the top of the escarpment (Yifran Marl Member) towards the restricted or lagoon ramp.

The vertical change from dolowackestones/dolopackstones through dolomudstones and dolowackestones to thinly bedded dolomudstones probably represent cycles of shoaling-upward deposited during regressive phases. The lower part of each cycle is composed of interbedded, bioturbated dolowackestones/dolopackstones and bedded dolomudstones (lithotype-2 and 3). The upper part consists of thinly bedded dolomudstones with gypsum nodules, algal

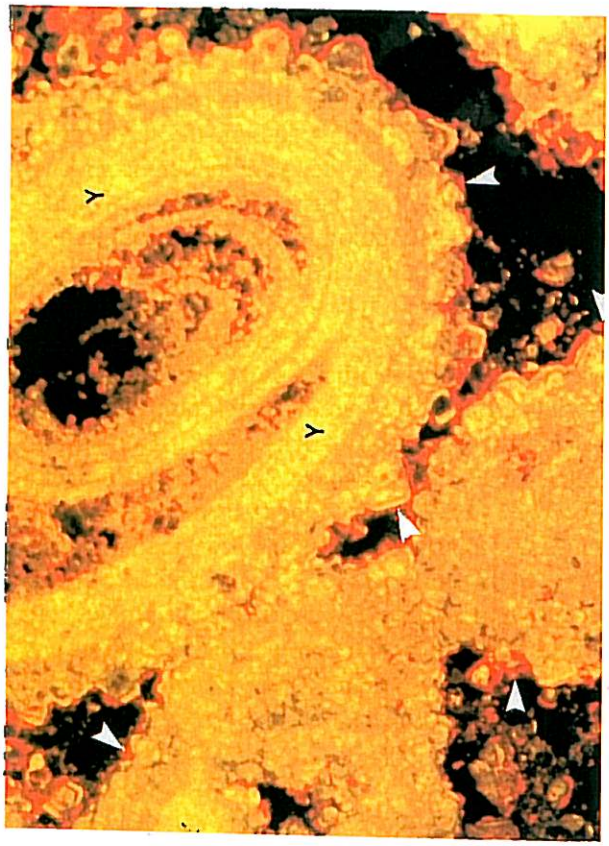
← Fig. 6. (a) Luminescence microscopy of same sample shown in (Fig. 5d). Note that Type-3 dolomite, which is associated with quartz, has a dull luminescent core and bright rims; whereas quartz shows dark blue colour; (b) Photomicrograph of Type-4 dolomite, characterized by cloudy cores and clean rims; (c) Photomicrograph of sample taken from Jadu section showing isolated crystals of Type-4 dolomite. Note the crystal shapes are planar-*e* and are loosed interlocking (PPL).

a



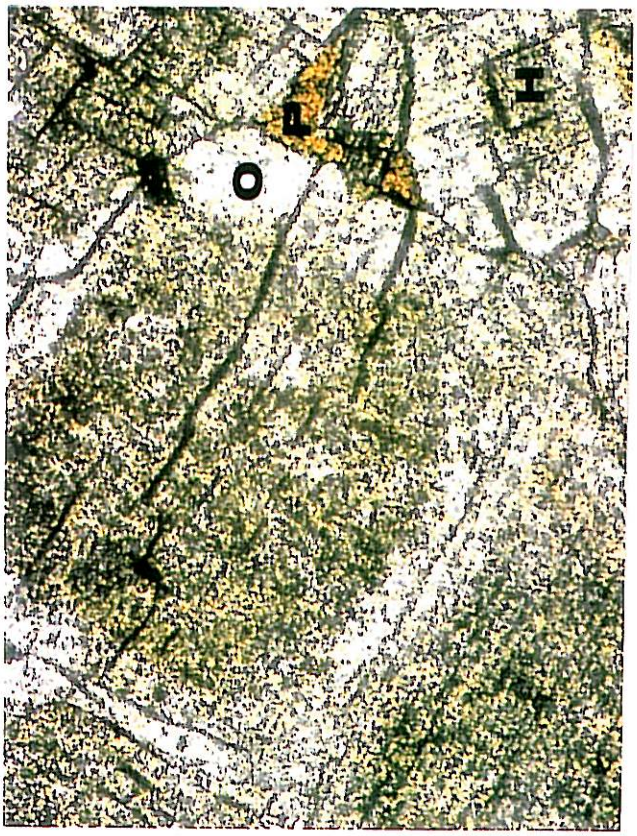
200 µm

b



200 µm

c



400 µm

d



400 µm

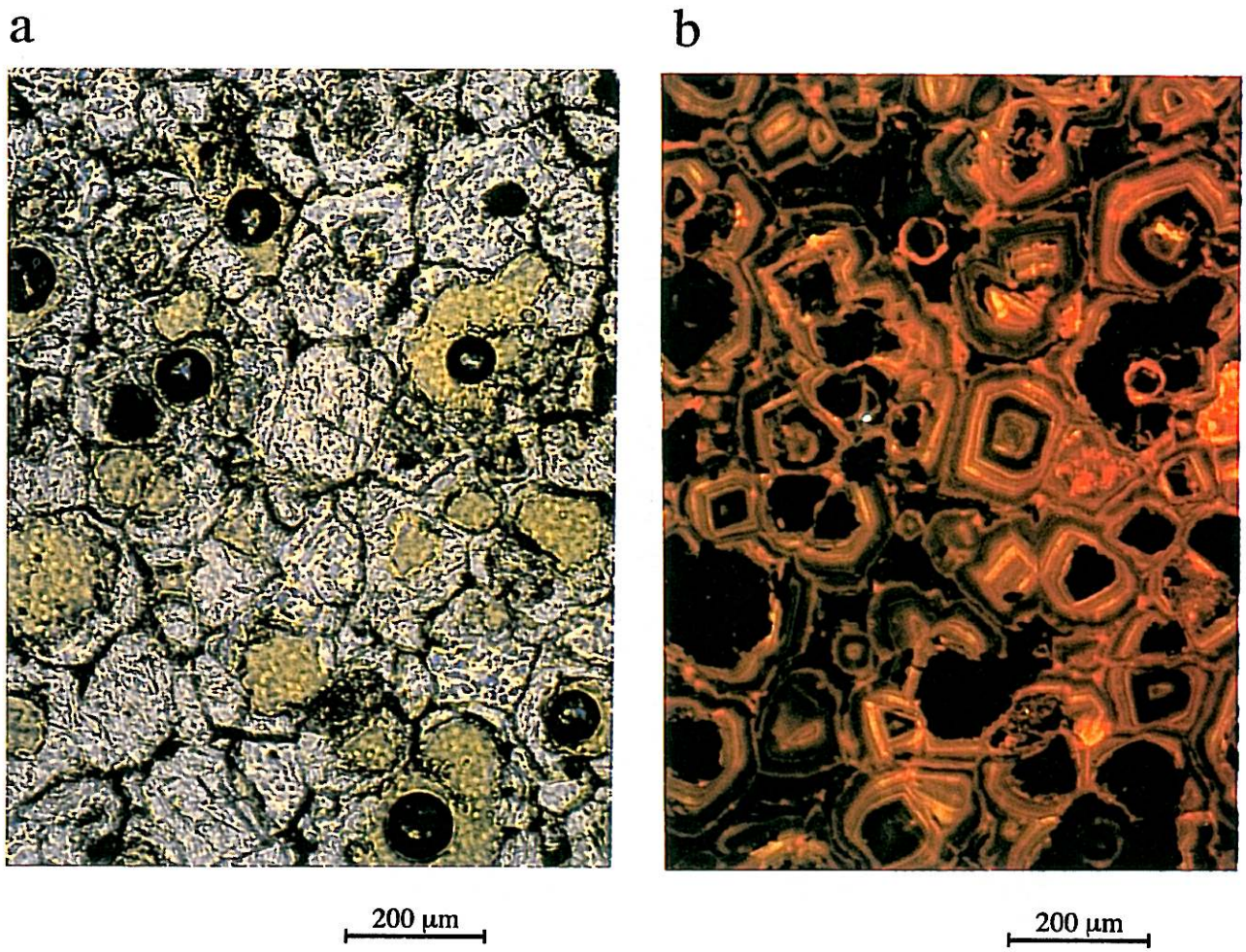


Fig. 8. (a) Thin-section photomicrograph of sample taken from Kabao section showing dedolomitization and dissolution. Note that cores of some crystals are selectively dissolved out leaving intracrystalline pores and some of them are replaced by calcite in later stage (PPL); (b) Luminescence microscopy of sample shown in (a). Note the complex zonation of the dedolomitization where dolomite zones show bright luminescent and calcite zones show dull luminescence and the pores are black.

laminations and solution breccias (lithotype-4 and 5). Each cycle was initiate by a rapid rise in sea level, a conditions suggested by the sharp contact between the intertidal lithotype-4 and the overlying carbonates lithotype-2 at Tarhunah and in the Abu Ghaylan area. Gradual shallowing as a result of sedimentation created extensive tidal flats and evaporitic sabkhas in which lithotype-3 and 4 were deposited. The bedded dolomudstones and dolopackstones of lithotype-3 were deposited in a low intertidal zone, and the algal mats or microbial of lithotype-4 were deposited in a higher intertidal zone.

Evaporites formed at the top of the cycles in sabkha type environment were probably extensive at the time of deposition. However, subsequent leaching, during subaerial exposure, removed many of the evaporite layers, now represented by solution breccias (lithotype-5). These are best developed in the thinner sequences of western outcrops (Wazan and Nalut area), which show rather restricted marine aspect. Cycles involving lithotype-1 (large-scale cross-bedded dolograinstones and dolopackstones) are well developed in sequence northeast at Tarhunah area. This cycle is interpreted as a tidal-channel deposit. Deposition occurred during progradation of broad shoals or lateral migration of tidal channels.

Based on the subsurface data it is thought that the lithotypes of the Sidi as Sid Formation (Ain Tobi

← Fig. 7. (a) Photomicrograph showing Type-2 crystalline dolomite which is very fine nonplanar-*a* being replaced by oolitic grainstone (PPL); (b) Luminescence microscopy of same view (a). The very fine dolomite replacing concentric structure of ooids have bright yellow luminescence (Y), whereas dolomite within intraparticle porosity or lining interparticle pores have red luminescence (arrow); (c) Thin-section photomicrograph of Type-5 saddle dolomite crystalline. It shows cloudy cores and clean rims (PPL); (d) Luminescence microscopy of same view shown in (c). Note that cloudy cores have brighter luminescence than clean rims whereas cleavage lines show bright yellow luminescent pattern (arrow).

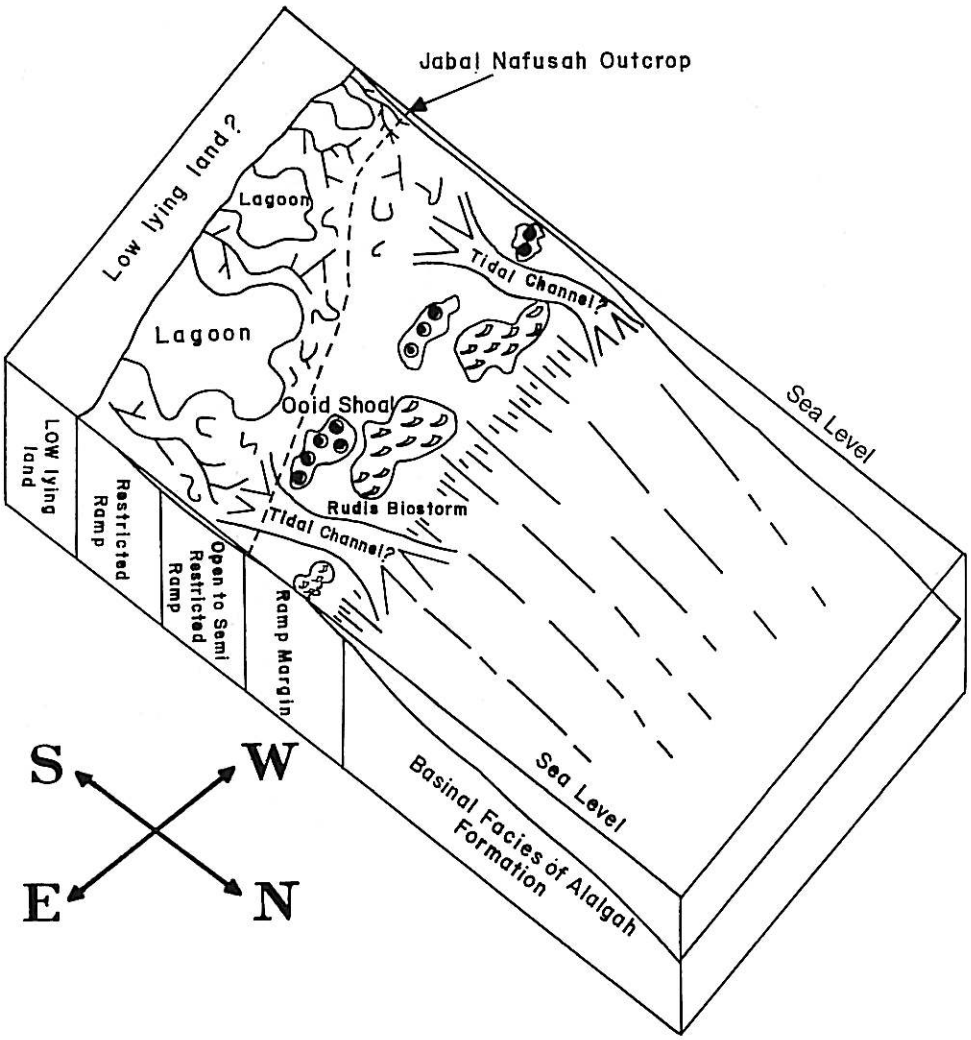


Fig. 9. Schematic block diagram of proposed Cenomanian sedimentary environment in NW Libya.

and Yifran members) regressive megasequence conditions could be more evaporitic south of Jabal Nafusah, with better development of sabkha sequences could be expected.

Mid-Ramp or Ramp Margin:

Stratigraphic sequences in wells drilled on the Jifarah Plain north of Jabal Nafusah indicate that post-Cretaceous erosion has removed the Sidi as Sid and the remainder of the Cenomanian in at least part of that area. The open to semi-restricted ramp environment probably graded northwards into mid-ramp or ramp margin environment. The margin is thought to occupy a narrow band in the subsurface that parallels the present coastline.

The presence of ramp margin is inferred on the basis of Cenomanian rudist debris in the Ain Tobi Member of the Jabal Nafusah, from oyster debris found at a point southeast of Tarabulus in Jabal Nafusah where its orientation changes from north-south to east-west, and from oyster packstones and grainstones of the Sidi as Sid's equivalent (Zebbag Formation) in Tunisia (Pedley *et al.*, 1982). This deposition environment probably also contains cross-bedded carbonate bodies and bioturbated units such as those found in the Ain Tobi Member in the Nafusah Escarpment. The presence of the *Ichthyosarcolites* Band as a series of buildups and the absence of a visible shelf-slope break on seismic lines implies that this is a ramp margin. The extensive post-Cretaceous erosion which removed the Cretaceous deposits along the coast may have resulted in obliteration of any ramp margin that was present.

Outer Ramp:

The Gabes–Tarabulus–Misratah Basin lies to the north of the ramp margin (Fig. 10). The Cenomanian

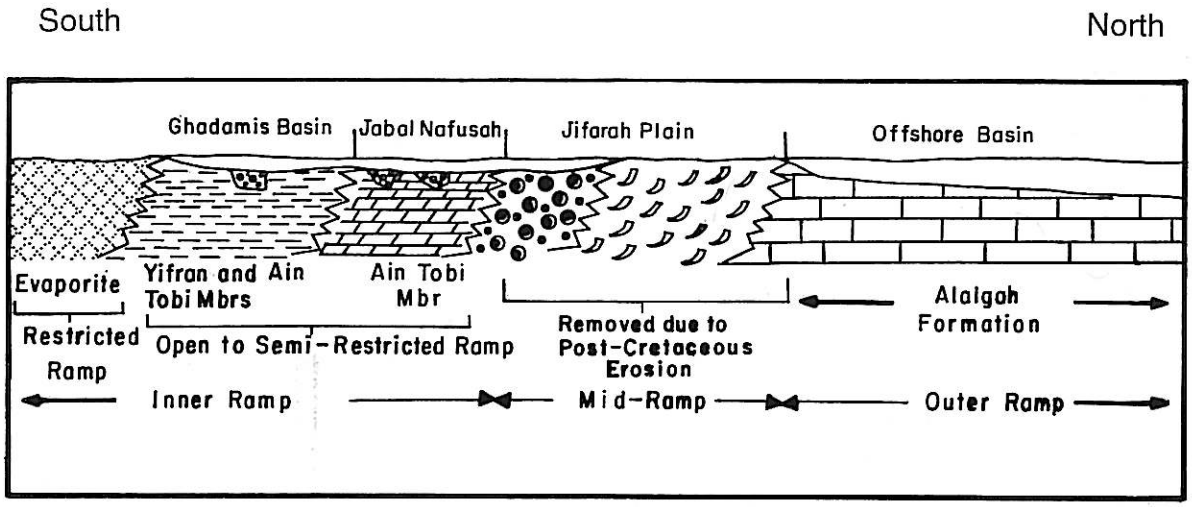


Fig. 10. Postulated changes in Cenomanian lithofacies in onshore and offshore NW Libya.

strata in this basin is represented by the Alalgah Formation (Hammuda *et al.*, 1985). The outer ramp environment is only known from the description of completion logs which reached the Cretaceous in offshore Libya (e.g. K1-137, H1-137, L1-137 and J1-NC35A wells).

Cenomanian sediments of the Alalgah Formation consist of laminated dolomitic marls containing miliolid and pelagic foraminifera and rudist material. The miliolid and rudist are thought to be derived from higher up the slope near the crest of the uplift. The pelagic foraminifera represent normal sediment accumulations for this environment.

Because of the paucity of the Upper Cretateous subsurface data, and absence of surface data in the northwestern Libyan offshore region, elaboration upon the basinal and slope environments is not possible.

Conclusion

1. The Sidi as Sid Formation includes two members. They are the Ain Tobi Dolostone Member which previously describe as dolomitic limestone and the Yifran Marl Member.

2. Bioturbation, lamination and cross-bedding structures are the most common form of structures found in units of the Ain Tobi Member. Units interpreted as solution breccias occurred in small intervals in most of the measured sections.

3. *Ichthyosarcolites* Band of Christie (1955) found in the lower and middle part of the Ain Tobi Member and vary the thickness from 3 to 18 m. The band is a marker bed across the whole Jabal Nafusah. The *Ichthyosarcolites* Band makes a gross change from the dominance of thicker bioturbated beds below to thinner beds above.

4. The Ain Tobi sediments have completely been dolomitized and five diagenetic types are identified. Dolomite Type-1 as early, fine, subhedral and nonferroan. Cores of crystals of this dolomite type are selectively dissolved leaving intrapores. Crystals of dolomite Type-1 have homogeneous luminescence pattern. Dolomite Type-2 is early, very fine, and anhedral to subhedral replacing packstone/grainstone facies, Crystals of dolomite Type-2 have bright orange-yellow luminescent pattern. Dolomite Type-3 occurs in the lower part of the Ain Tobi sequence in all measured sections and interbedded with quartz sandstone. Its crystals are fine to medium, subhedral probably formed post-compaction. Type-3 dolomite is characterized by dirty orange luminescent cores and very thin bright luninescent rims. Type-4 dolomite is medium to coarse, euhedral to subhedral and characterized by cloudy cores and clean rims. Crystals of this type have orange luminescent cores and dull rims. Dolomite Type-5 (baroque dolomite) found only in the eastern part of the study area. Crystals of this type are coarse to very coarse with cloudy cores and clean rims and characterized by curved faces. Dolomite Type-5 has orange luminescent cores, dull rims and bright cleavage lines. Early calcitization or replacement of dolomite by early calcite occurs close to the unconformity surface and show complex zonation. However, replacement of dolomite by late calcite occurs in the top of the sequence and show dull to no luminescence.

5. The Sidì as Sid Formation represents part of inner ramp sequence, which ranged from open to semi-restricted ramp and restricted or lagoon ramp. The restricted ramp environment is represented by the Yifran Marl Member, the open to semi-restricted ramp environment is represented by the Ain Tobi Member in Jabal Nafusah areas and in the subsurface Ghadamis Basin. The open to semi-restricted ramp probably graded northwards into mid-ramp or ramp margin environment which are removed by post-Cretaceous erosion from the Jifarah Plain. The outer ramp environment is represened by the Alalgah Formation in the offshore Gabes–Tarabulus–Misratah Basin. It consists of laminated dolomitic marls containing miliolid and pelagic forminifera.

REFERENCES

Ahr, W.M., 1973. The Carbonate Ramp – an alternative to the Shelf Model. *Trans., Gulf Coast Ass. Geol Soc.*, **23**: 221–225.

Amthor, J.E. and Friedman, G.M., 1991. Dolomite-rock textures and secondary porosity development in Ellenberger Group Carbonates (Lower Ordovician), West Texas and southeastern New Mexico. *Sedimentology*, **38**: 343–362.

Amthor, J.E. and Friedman, G.M., 1992. Early-to late- diagentic dolomitization of platform carbonates: Lower Ordovician Ellenburger Group, Permian Basin, West Texas. *J Sed. Petr.*, **62(1)**: 131–144.

Barr, F.T. and Weegar, A.A., 1972. Stratigraphic Nomenclature of the Sirte Basin, Libya. *Publ. of the Petr. Expl. Soc. of Libya*: 179 p.

Braun, M. and Friedman, G.M., 1970. Dedolomization fabric in peels: A possible clue to unconformity surfaces. *J. Sed. Petr.*, **40**: 417–419.

Budai, J.M., Lohmann, K.C. and Owen, R.M., 1984. Burial dedolmitization in the Mississippian Madison Limestone, Wyoming and Utah Thrust Belt. *J. Sed. Petr.*, **54**: 276–288.

Burchette, T.P. and Wright, V.P., 1992. Carbonate ramp depositional systems. *Sed. Geol.*, **79**: 3–57.

Busson, G., 1970. Le Mesozoique Saharian Essai de Syntheses des Donnes des Sondages Algero-Tunisiens. *Centre de Recherches sur les Zones Arides, Serie: Geologie*, **11**, *Editions du Centre National de la Recherche Scientifique, Paris*: 811 p.

Buxton, M.W.N. and Pedley, H.M., 1989. A standardized model for tethyan carbonate ramps. *J. Geol. Soc. London*, **146**: 746–748.

Christie, A.M., 1955 reprinted, 1966. Geology of the Garian Area, Tripolitania, Libya. *Geol. Section, Bull.*, **5**, *Kingdon of Libya, Ministry of Industry: Willimer Bros. Ltd. Birkenhead, UK*: 64 p.

Conoglio, M. and James, N.B., 1988. Dolomitization of deep-water sediments, Cow Head Group (Cambro–Ordovician), western Newfoundland. *J. Sed. Petr.*, **58(6)**: 1032–1045.

Dickson, J.A.D., 1965. A modified staining technique for carbonate in thin section. *Nature*, **205**: p. 587.

El-Bakai, M.T., 1989. The Sedimentology of the Lidam Formation in northwest Sirte Basin, Libya. *Unpubl. M. Sc. Thesis, Geology Department, Hull University, England:* 172 p.

El-Bakai, M.T., 1991. Petrography and diagenesis of the Lidam Formation (carbonate units): from selected wells in Sirt Basin, Libya. *Petroleum Res. J., Petroleum Research Center, Tarabulus, Libya*, **3**: 35–43.

El-Bakai, M.T., 1992. Environment of deposition of the Lidam Formation in NW Sirte Basin, Libya. In: A. Sadek (ed.) Geology of the Arab World *Proc. of the 1st. Inter. Conf. on Geol. of the Arab World, Cairo University* **1**: 343–352.

El Hinnawy, M. and Cheshitev, G., 1975. Geological map of Libya, 1:2500,000, Sheet: Tarabulus, NI 33-31, Explanatory Booklet. *Industrial Research Centre, Tripoli, Libya:* 75 p.

Elrick, M. and Read, J.F., 1991. Cyclic ramp-to-basin carbonate deposits, Lower Mississipian, Wyoming and Montana: A combined field and computer modeling study. *J. Sed. Petrol.* **61(7)**: 1194–1224.

Evamy, B.D., 1963. The application of a chemical technique to a study of dedolomitization. *Sedimentology*, **2**: 164–170.

Evamy, B.D., 1976. Dedolomitization and the development of rhombohedral pores in limestones. *J. Sed. Petr.*, **37**: 1204–1215.

Fairchild, I.J., 1980. Stages in a Precambrian dolomitization, Scotland: cementing versus replacement textures. *Sedimentology*, **27**: 631–650.

Friedman, G.M., 1965. Terminology of crysallization textures and fabrics in sedimentary rocks. *J. Sed. Petr.*, **35(3)**: 643–655.

Hammuda, O.S., Sbeta, A.M., Mouzughi, A.J. and Eliagoubi, B.A., 1985. Stratigraphic Nomenclature of the Northwestern Offshore of Libya. *The Earth Sciences Soc. Libya, Tarabulus, Libya*: 166 p.

Hine, A.C., 1977. Lily Bank Bahamas: History of an active oolite sand shoal. *J. Sed. Petr.*, **47**: 1554–1583.

Magaritz, M. and Kafri, U., 1981. Stable isotope and Sr^{2+}/Ca^{2+} evidence of diagenetic dedolomitization in a schizohaline environment: Cenomanian of northern Israel. *Sed. Geol.* **28**: 29–41.

Megerisi, M.F. and Mamgain, V.D., 1980a. The Upper Cretaceous-Tertiary formations of northern Libya: A synthesis. *Industrial Research Centre, Tripoli, Libya, Bull.* **12**: 85 p.

Megersi, M.F. and Mamgain, V.D., 1980b. The Upper Cretaceous-Tertiary formations of northern Libya. In.: M.J., Salem and M.T. Busrewil (eds.), *The Geology of Libya, Academic Press*, **1**: 67–72.

Milliman, J.D., 1974. *Marine carbonates*. Springer-Verlag, New York, 375 p.

Nielsen, P., Swenen, R. and Keppens, E., 1994. Multiple-step recrystallization within massive ancient dolomite units: An example from the Dinantian of Belgium. *Sedimentology*, **41**: 567–584.

Pedley, H.M., Bell, B.S., Thunell, R. and Arthur, M.A., 1982. The Zebbag Formation in central Tunisia, *Earth Science and Resources Institute, University of South Carolina, Unpub. Report*: 53 p.

Radke, B.H. and Hathis, R.L., 1980. On the formation and occurrence of saddle dolomite. *J. Sed. Petr.*, **50**: 1149–1168.

Reyre, D., 1966. Particularites geologiques des bassins cotiers de l'ouest African. In: bassins sedimentaires du littoral African, symposium, 1st. re partie, littoral Atlantique, *Union Int. Sci. Geol. Assoc. Serv. Geol African*: 253–301.

Savin, S.M., 1977. The history of the earth's surface temperature during the past 100 millian years. *Ann. Rev. Earth and Planetary Sci.*, **5**: 319–356.

Petroleum Res.J. Vol. 9 (1997); P. 27–44, 3 FIGS.

Planktonic Foraminiferal Zonation of the Oligocene–Miocene Succession of Well H1-NC41, NW Offshore, Libya

I.I.M. Kassab*, A.K. Abusrewil*, and F.E. Abuhmida*

المنخربات الهوائم، الطباقية الحياتية للتتابع الطبقي لعصريْ الأوليجوسين والمايوسين للبئر H1-NC41، شمال غرب الرف القاري، ليبيا

إسماعيل إبراهيم محمد قصاب، أحمد خليفة أبو سريويل، وفيصل الهادي أبو حميدة

من خلال المحتوى الأحاتي للمنخربات الهوائم لعدد 183 عينة فتاتية ولبية من التتابع الطبقي لعصري الأوليجوسين والمايوسين في المقطع تحت السطح للبئر H1-NC41 في شمال غربي الرف القاري لليبيا أمكن تقسيم التتابع إلى أحد عشر نطاقاً حياتياً للمنخربات الهوائم والمرتبة تصاعدياً كما يلي:

1 – النطاق The *Globigerina ampliapertura* Zone

2 – النطاق The *Globorotalia opima opima* Zone

3 – النطاق The *Globorotalia kugleri* Zone

4 – النطاق The *Globoquadrina dehiscens* Zone

5 – النطاق The *Globigerinoides altiapertura* Zone

6 – النطاق The *Globigerinoides bisphericus* Zone

7 – النطاق The *Praeorbulina glomerosa glomerosa* Zone

8 – النطاق The *Orbulina suturalis* Zone

9 – النطاق The *Orbulina universa* Zone

10 – النطاق The *Globorotalia acostaensis* Zone

11 – النطاق The *Globigerinoides extremus* Zone

تمت مقارنة التتابع الطبقي الحياتي لعصري الأوليجوسين والمايوسين للبئر H1-NC41 مع الأنطقة الحياتية P-N، وكذلك مع الظواهر الطبقية الحياتية للأعمار مقدرة بملايين السنين، ومع الحدود الطبقية الأوروبية.

إن عدم وجود الأنطقة الحياتية P19, P18, P17 وكذلك احتمالية عدم وجود الجزء الأسفل من النطاق الحياتي P20 قد يدل على فترة تعرية وعدم ترسيب أثناء الحد الفاصل بين عصري الأيوسين والأوليجوسين. إن عدم وجود النطاق الحياتي P22 واحتمالية عدم وجود الجزء الأسفل من النطاق الحياتي N4a يدل على وجود فترة زمنية مفقودة خلال عصر هذيْن النطاقيْن، وكذلك فان عدم وجود الأنطقة الحياتية N10 (جزء)، N14, N13, N12, N11 (جزء) قد يعزي إلى وجود فترة عدم ترسيب، أو تغيير في البيئة الترسيبية أو كليهما. كما أن عدم وجود أعلى النطاق N17 يدل على وجود فترة عدم توافق في نهاية عصر المايوسين.

Abstract *Analysis of the planktonic foraminiferal contents of 183 cutting and sidewall core samples from the Oligocene–Miocene sequence of well H1-NC41, NW offshore, Libya enabled to subdivide the sequence into eleven planktonic foraminiferal zones, they are in ascending order:*

(1) *The Globigerina ampliapertura Zone.*
(2) *The Globorotalia opima opima Zone.*

*Petroleum Research Centre, P.O. Box 6431, Tripoli, Libya, G.S.P.L.A.J.

(3) *The Globorotalia kugleri Zone.*
(4) *The Globoquadrina dehiscens Zone.*
(5) *The Globigerinoides altiapertura Zone.*
(6) *The Globigerinoides bisphericus Zone.*
(7) *The Praeorbulina glomerosa glomerosa Zone.*
(8) *The Orbulina suturalis Zone.*
(9) *The Orbulina universa Zone.*
(10) *The Globorotalia acostaensis Zone.*
(11) *The Globigerinoides extremus Zone.*

The Oligocene–Miocene planktonic foraminiferal biosequence of well H1-NC41 has been correlated with P-N Zones, the biostratigraphic events age estimates in million years, and the European stage boundaries.

The absence of Zones P17, P18, P19, and possibly the lower part of the Zone P20 may indicate a period of erosion and non deposition at the Eocene/Oligocene boundary. In the Late Oligocene, Zone P22 and possibly the lowermost Zone N4a are missing indicating a hiatus at this interval. The missing of Zones N10 (part), N11, N12, N13, N14 (part) may due to nondeposition (hiatus), change in depositional environment or both.

The top of Zone N17 is also missing indicating unconformity at the end of the Miocene.

INTRODUCTION

The biozonation of the Oligocene–Miocene sediments of well H1-NC41 is part of the biostratigraphic study of the Oligocene–Pleistocene of the Tarabulus Basin, Pelagin Platfrom, NW offshore, Libya.

A large number of foraminiferal specimens were picked in order to precisely determine the character of the biozones, their age, boundaries, and to correlate them with the P–N Zones and the European stage boundaries. Utilizing the vertical extension of the planktonic foraminferal index species, several time gaps are postulated during the deposition of the Oligocene–Miocene sequence.

Well H1-NC41 is one among more than 60 exploratory wells drilled in the offshore area (Fig. 1), it is situated in the middle of the Tarabulus Basin (long. 12° 43′ 07″, lat. 33° 26′ 05″), and was drilled by NOC-Agip Name in 1979. It penetrated 12532 ft. (3820.7 m) sedimentary sequence ranging in age from the Palaeocene-to the Pleistocene.

The sea bed was encountered at 769 ft. (234.4 m), water depth at 662 ft. (201.8 m), and first recovery at D.D. around 1055 ft. (321.6 m) from the lower Pleistocene (*Hyalinea balthica* Zone) portion of the

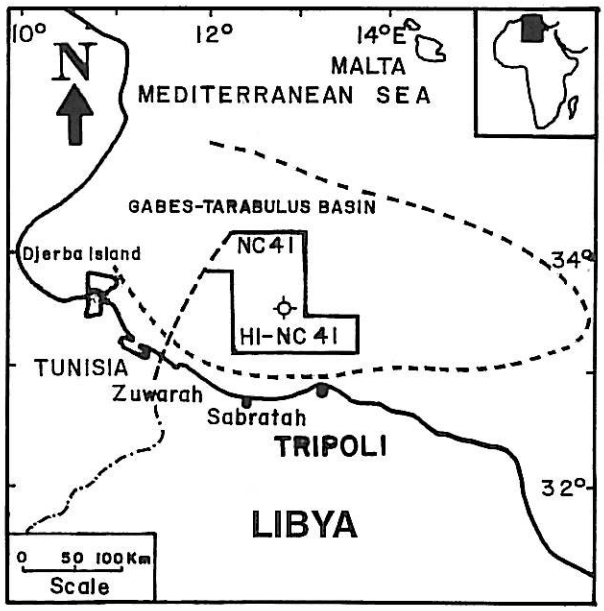


Fig. 1. Location Map

Sbabil Formation. The Oligocene–Miocene sedimentary sequence in this well is 7224 ft. (2202.4 m) thick (including 44 ft. belonging to the larger foram *Nummulites vascus* Zone).

The planktonic foraminiferal biostratigraphy of the Oligocene–Miocene of the subsurface, NW offshore, Libya have been investigated previously by Van Hinte *et al.* (1980, well B1-NC35A, Messinian–Tabianian), Cococcetta (1982, well H1-NC41, Palaeocene–Pleistocene, unpublished NOC-Agip Name report), Hammuda *et al.*, (1985, 16 wells, 32 rock units ranging in age from Triassic–Pleistocene), Duronio (1985, Bouri Field, 7 wells, 10 rock units and groups ranging in age from Palaeocene to Pleistocene), and Hammuda *et al.*, (1991, 11 wells, 15 rock units involving two rock groups, ranging in age from Santonian to Pleistocene). Salem and Spreng (1980) and Sherif (1991) dealt in detail with onshore (NW Libya) Al Khums Formation (Miocene).

One hundred and sixty one cutting and 23 sidewall core samples were supplied by NOC-Agip Name, Tripoli, Libya, they were processed using standard micropalaeontological techniques, the fossils contents of all size fractions were picked (in proportional quantity) and identified.

STRATIGRAPHY

The Oligocene–Miocene succession in well H1-NC41 is 7224 ft. (2202.4 m) thick sequence of distinct stratigraphic units unconformably overlying the Upper Eocene Samdun Formation of Tellil

Group and unconformably underlying the Pliocene–Pleistocene Sbabil Formation. The rock units are in ascending order.

1. Ras Abd Jalil Formation

The Ras Abd Jalil Formation is underlain by the open marine shallow water *Nummulites vascus* marker bed which is 44 ft. (13.41 m) (D.D. 9028 ft.–8984 ft.) nummulitic limestone of late Early Oligocene (late Rupelian) age. Ras Abd Jalil Formation is 2198 ft. (670 m) (D.D. 8984 ft.–6786 ft.) sandy shales, marl, and marly limestone sequence of deep water origin characterized by rich planktonic foraminiferal contents (ranging in apparent percentage from 56% to 99%) indicating 15.6 Ma time duration of deposition from the bottom of the *Globigerina ampliapertura* Zone (Late Oligocene) at 33.2 Ma to the top of the *Globigerinoids altiapertura* Zone at 17.6 Ma (Early Miocene, early Burdigalian).

The lower contact of Ras Abd Jalil Formation in well H1-NC41 is quite sharp corresponding to the change in fauna and lithology from dark grey shale above to whitish nummulitic limestone below, the contact is considered (at present) conformable with the *Nummulites vascus* marker bed. The upper contact with Al Mayah Formation is taken (at present) at D.D. 6786 ft. (below sample 6790) (in accordance with NOC-Agip Name, 1979) corresponding to the *Globigerinoids altiapertura/Globigerinoids bisphericus* zonal boundary, although no major change in lithology was observed as the boundary falls within a silty shale sequence.

2. Al Mayah Formation

Al Mayah Formation is 3806 ft. (1160 m) sequence of grey green silty shale, shale, sandstone, mudstone (H12), shale and sandstone of open shallow platform to middle neritic environment (30–100 m) indicated by a marked decrease in the planktonic Foraminifera up the section (the apparent planktonic foraminiferal percentage ranges from 4.66% to 84.86%). The planktonic Foraminifera indicate Upper Burdigalian (late Early Miocene, the *Globigerinoids bishpericus* Zone) to Early Tortonian (the *Globorotalia acostaensis* Zone, lower part) of slightly more than 7.4 Ma time duration.

The lower boundary of Al Mayah Formation at well H1-NC41 is taken (at present) at the Lower/Middle Burdigalian boundary. There is no clear lithological change at this level as the silty shale of Ras Abd Jalil Formation continues upward, however, the present boundary is following the well log. The upper boundary is taken at the change from silty marl and marl to fossiliferous limestone at D.D. 2980 ft. corresponding to the FA of *Borelis melo* within the Early Tortonian. NOC-Agip Name (1979) followed by Cococcetta (1982) put the boundary 262 ft. below the present boundary at the change from quartzose sand to silty marl, locally grading to shale, with thin levels of limestone corresponding to their *Borelis melo* Zone lower boundary.

3. Tubtah Formation

The Tubtah Formation is 908 ft. (276.8 m) (from D.D 2980 ft.–2072 ft.) thick oolitic, fossiliferous limestone with marly horizons of inner shallow platform (15–25 m water depth) indicated by the dominance of benthonic Foraminifera characterized by *Borelis* spp., *Elphidium* spp., miliolids, and rotaliids.

The planktonic Foraminifera are scarce found only in the marl iterbeds, however, they are characterized by species referable to this upper part of the *Globorotalia acostaensis* Zone and the lower part of the *Globigerinoids extremus* Zone indicating Tortonian age.

The rich and diverse benthonic foraminiferal fauna enabled the subdivision of the Tubtah Formation into two benthonic foraminiferal zones, a lower *Borelis melo* Zone, and an upper *Ammonia–Elphidium* Zone (the later zone continues into the overlying Marsa Zouaghah Formation).

The first introduction of gypsum within the limestone indicates the start of the Marsa Zouaghah Formation overlying the Tubtah Formation at D.D. 7072 ft.

4. Marsa Zouaghah Formation

Marsa Zouaghah Formation is 268 ft. (81.7 m) (D.D. 2072 ft.–1804 ft.) thick gypsum and limestone (fossiliferous, oolitic, miliolids) sequence characterized by poor planktonic and benthonic foraminiferal assemblages indicative of shallow water (± 9.14 m–15.24 m) of deposition of the tidal flat complex. The presence of scarce but variable planktonic species enabled to refer this depth interval to the upper part of the *Globigerinoids extremus* Zone (Messinian),

the benthonic Zone *Ammonia–Elphidium* is also extended to the Marsa Zouaghah Formation.

The Marsa Zouaghah Formation is unconformably overlain by the Sbabil Formation (Lower Pliocene–Pleistocene), the boundary is taken at D.D. 1804 ft. at the change from gypsum and limestone of the Marsa Zouaghah Formation below to the clay, sandy clay and marl of the Sbabil Formation above. The unconformity is indicated by change in lithology and fauna representing the transition from the Miocene to the Pliocene. The *Ammonia–Elphidium*–miliolids–Ostracoda faunal association indicative of shallow restricted marine environment of the Messinian (Late Miocene) Marsa Zouaghah Formation is overlain by the transgressive clays rich in planktonic Foraminifera (*Sphaeroidinellopsis, Globigerinoides, Globigerina, Globorotalia*) of Early Pliocene age.

BIOSTRATIGRAPHY

Based on rich and diverse planktonic Foraminifera of the Oligocene–Miocene characterizing the sedimentary succession of well H1-NC41 NW offshore, Libya, the sequence has been subdivided into eleven planktonic foraminiferal zones. This biosequence is proposed for well H1-NC41 by integrating the vertical planktonic foraminiferal characteristics of this section with equivalent sections in the Mediterranean and other parts of the world, the deviation from other zonal schemes is controlled by the local characteristics of the planktonic Foraminifera at this particular area of the Mediterranean as a result of climatic differentiations and sea level changes. This has resulted in scarcity of some diagnotic species (*Globorotalia peripheroacuta, Globorotalia conomiozea, Globigerinoids diminutus, Globigerinoids ruber, Globigerina nepenthes, 3 occurrence, Globigerinita insueta*, most of the Middle and Upper Miocene keeled *Globorotalias*), diachronous character species (*Catapsydrax dissimilis*,? *Globigerinoids obliquus*,? *Globigerinoids ruber*, *Praeorbulina transitoria*), and absence of other species (*Globorotalia fohsi fohsi, Globorotalia fohsi lobata, Globorotalia fohsi robusta*, and many other keeled *Globorotalia, Pulleniatina* ssp., *Catapsydrax stainforthi*, single occurrence).

The Oligocene–Miocene planktonic foraminiferal biosequence in well H1-NC41 in ascending order is

1. The *Globigerina ampliapertura* Zone

The *G. ampliapertura* Zone is defined by the interval range of the named zonal taxon from its FA immediately above the *Nummulites vascus* marker bed to its last occurrence. It is of Lower Oligocene age of 2.0 Ma time duration.

The zone covers a depth of 64 ft. (19.5 m) from D.D 8984 ft. to D.D 8920 ft. of the lower part of Ras Abd Jalil Formation. Lithologically this interval is dark grey shale grading to sandy marl.

Most characteristic planktonic foraminiferal species of this zone are: *Catapsydrax dissimilis, Globigerina ampliapertura, Globigerina ciperoensis* subspecies, *Globigerina goratanii, Globigerina ochitaensis* subspecies, *Globigerina praebulloides* subspecies, *Globigerina sellii, Globigerina tripartita, Globigerina venezuelana*, and many others including contaminated species occurring in the cutting samples (see Fig. 2).

Based on the analysis of the vertical distribution of *Globigerina ampliapertura, Globigerina ciperoensis angulisuturalis*, and *Globorotalia opima opima* (Blow, 1969, 1979; Berggren, 1969b, 1971: Stainforth *et al.*, 1975; Bolli and Saunders, 1985; Miller and Katz, 1987) the *Globigerina ampliapertura* Zone of well H1-NC41 is correlated with Zone P20 of Blow (1969), and the upper part of Zone P19/20 of Blow (1979) and equivalent P-Zones and biozones (see Fig. 3).

The time duration of the *Globigerina ampliapertura* Zone (=P20) is 2.0 Ma-2.5 Ma (Blow, 1969, 1979; Berggren, 1969b, 1971; Vail and Mitchum, 1979; Lidz, 1984, Bolli and Saunders, 1985; Haq *et al.*, 1987), accordingly a time duration of 2.0 Ma is assumed for the *Globigerina ampliapertura* Zone in well H1-NC41 (considering 0.5 Ma for the *N. vascus* Zone at the lower part of Zone P20). Based on this age estimation 0.97 cm/1000 years rate of sedimentation is calculated for the 64 ft. interval of the *Globigerina ampliapertura* Zone assuming constant rate of subsidence.

2. The *Globorotalia opima opima* Zone

The *Globorotalia opima opima* Zone is a partial range zone of 3.0 Ma time duration in the Oligocene defined by the range of the zonal marker from the LO of *Globigerina ampliapertura* to the LO of the zonal marker.

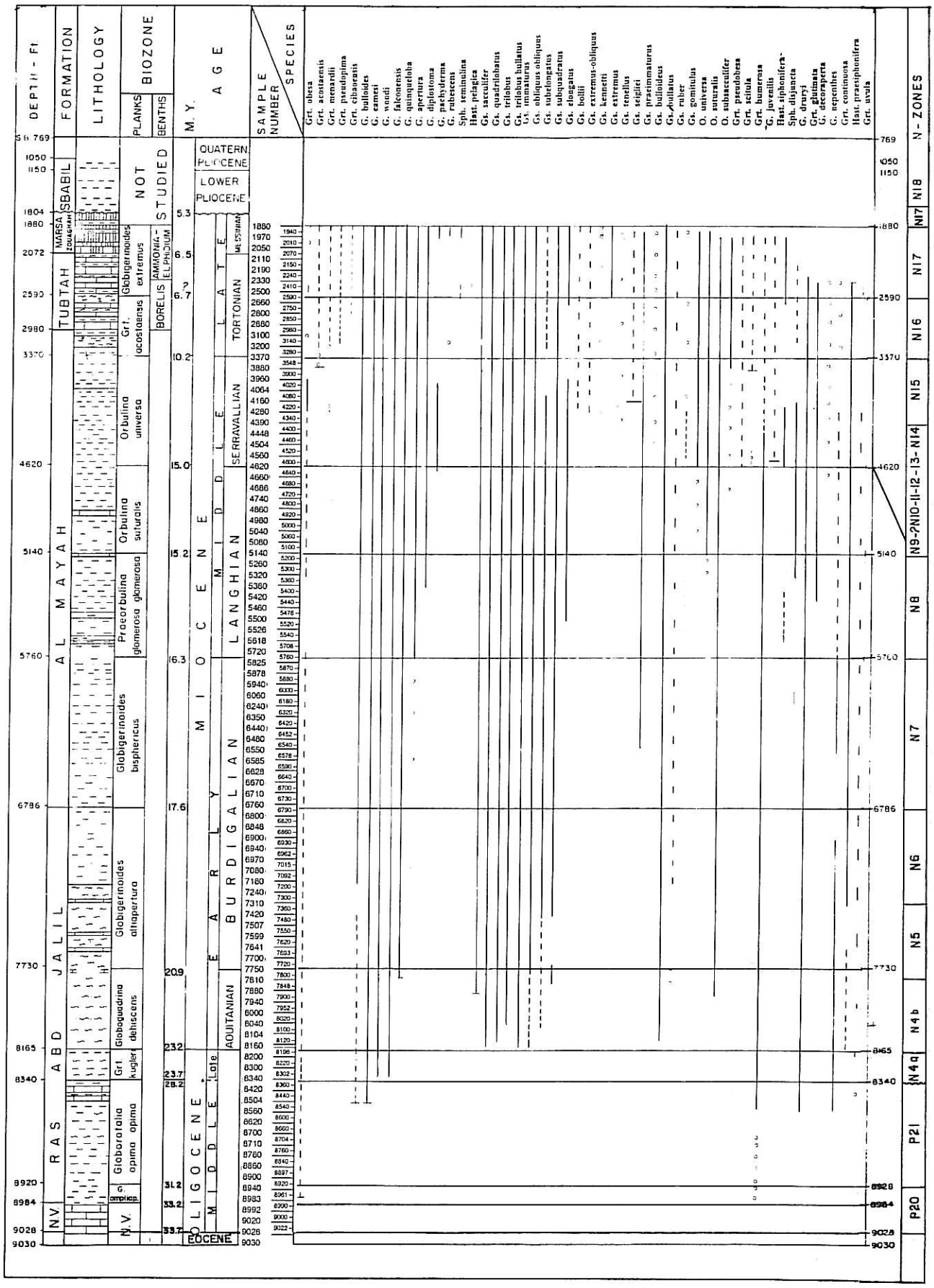


Fig. 2. Ranges of planktonic foraminifera (top occurrence) Oligocene – Miocene, well H1-NC41, NW offshore, Libya.



Fig. 2. (Cont. 1).

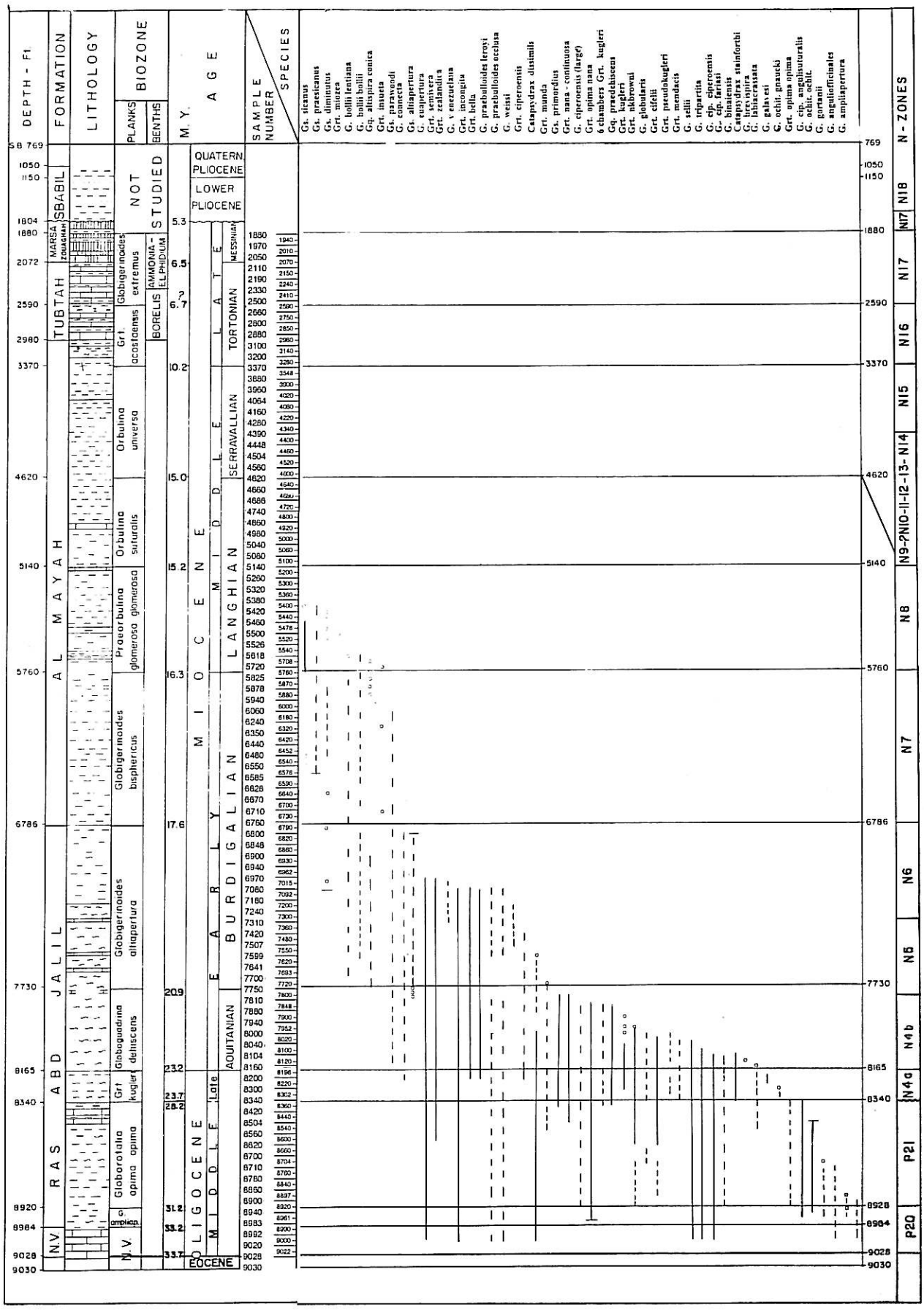

DEPTH - Ft
FORMATION
LITHOLOGY
BIOZONE
PLANKS
BENTHS
M.Y.
AGE
SAMPLE NUMBER
SPECIES
N - ZONES
RAS ABD
JALIL
TUBTAH
SBABIL
NOT STUDIED
QUATERN.
PLIOCENE
LOWER PLIOCENE
MESSINIAN
TORTONIAN
SERRAVALLIAN
LANGHIAN
BURDIGALIAN
AQUITANIAN
EOCENE
Globigerinoides extremus
Grt. acostaensis
Orbulina universa
Orbulina suturalis
Praeorbulina glomerosa glomerosa
Globigerinoides bisphericus
Globigerinoides altiaperturus
Globoquadrina dehiscens
Grt kugleri
Globorotalia opima opima
Gs. siganus
Gs. praesicanus
Gs. diminutus
Grt. miozea
G. bollii lentiana
G. bollii bollii
Gq. altispira conica
Grt. insueta
Gs. parawondi
G. connecta
Gs. altiapertura
G. euapertura
Grt. semivera
Grt. zealandica
G. venezuelana
Grt. incongita
Grt. bella
G. praebulloides leroyi
G. praebulloides occlusa
G. weissi
Grt. cipercensis
Catapydrax dissimilis
Grt. munda
Gs. primordius
Grt. nana - continuosa
G. ciperoensis (large)
Grt. opima nana
6 chambers Grt. kugleri
Gq. praedehiscens
Grt. kugleri
Grt. nkhrowai
G. globularis
Grt. cifelli
Grt. pseudokugleri
Grt. mendacis
G. sellii
G. tripartita
G. cip. ciperoensis
G. cip. farisei
G. binaiensis
Catapydrax stainforthi
G. birnageae
G. galavisi
G. ochit. gnauckl
Grt. opima opima
G. cip. angulisuturalis
G. ochit. ochit.
G. gortanii
G. angulofficinales
G. ampliapertura
P20
P21
N4a
N4b
N5
N6
N7
N8
N9-PN10-11-12-13-N14
N15
N16
N17
N18

Fig. 2. (Cont. 2).

The *Globorotalia opima opima* Zone of well H1-NC41 covers a depth of 580 ft. (176.8 m) from D.D. 8920 ft. to D.D. 8340 ft. within Ras Abd Jalil Formation. Lithologically this depth interval is grey sandy shale, sandy marl, and thin marly limestone.

Most characteristic planktonic foraminiferal species of this zone are: *Globorotalia opima opima, Globorotalia opima nana, Globorotalia mayeri, Globorotalia siakensis, Globorotalia acrostoma, Globorotalia nkbrowni, Globorotalia cifelii, Globorotalia munda, Globigerina praebulloides* subsp., *Globigerina euapertura, Globigerina sellii, Globigerina triapartita, Globigerina ciperoensis ciperoensis, Globigerina ciperoensis angulisuturalis, Globigerina cip. fariasi, Catapsydrax dissimilis, Globorotaloides suteri* and *Cassigerinella chipolensis.*

Based on the vertical distribution of the planktonic foraminiferal species characterizing the boundaries of the *Globorotalia opima opima* Zone (i.e. *Globorotalia opim opima, Globigerina ampliapertura, Globigerina ciperoensis angulisuturalis*) it is correlated with Zone P21 of Blow (1969, 1979) and equivalent P-Zones and biozones (Fig. 3).

The time duration of the *Globorotalia opima opima* Zone is 3.0 Ma (Berggren and Miller, 1988), accordingly the 580 ft. thick *Globorotalia opima opima* Zone sediments have 5.89 cm/1000 years calculated rate of sedimentation assuming constant rate of subsidence.

3. *The Globorotalia kugleri* Zone

The *Globorotalia kugleri* Zone is a partial range zone of 0.5 Ma time duration in the Late Oligocene defined by the range of the zonal marker from the LO of *Globorotalia opima opima* (coincident with the FA of the *Globorotalia kugleri* group and *Globigerinoids primordius*) to the FA *Globoquadrina dehiscens* (coincident with the FA of the genus *Globigerinoides* excluding *Globigerinoids primordius*).

The *Globorotalia kugleri* Zone is 175 ft. (53.35 m) thick dark grey shale and marl (D.D. 8340 ft.–8165 ft.) within Ras Abd Jalil Formation.

The *Globorotalia kugleri* Zone is characterized by many distinctive planktonic species, most characteristic are: *Globigerinoides primordius, Globorotalia opima opima, Globorotalia kugleri*: group, *Globoquadrina praedehiscens, Catapsydrax dissimilis, Globigerina euapertura, Globigerina sellii, Globigereina venezuelana, Globigerina tripartita, and Globigerina binaiensis.*

Based on the analysis of the vertical distribution of *Globorotalia kugleri, Globorotalia mendacis, Globorotalia pseudokugleri, Globigerinoides bullatus, Globigerinoids primordius, Globigerinoids quadrilobatus, Globorotalia opima opima, Globigerina ciperoensis* subsp. and *Globoquadrina dehiscens* (Fig. 2), the *Globorotalia kugleri* Zone of well H1-NC41 is considered equivalent to the lower part of Zone N4 of Blow (1969, 1979) and Bolli and Saunders (1985), Zone N4a of Kennett and Srinivasan (1983), Miller and Katz (1987), Berggren and Miller (1988, 1989) and equivalent N-Zones and biozones (see Fig. 3).

The time duration of the *Globorotalia kugleri* Zone as defined in this study is 0.5 Ma (FA of *Globorotalia kugleri* at 23.7 Ma to FA of *Globoquadrina dehiscens* at 23.2 Ma), the lower boundary is in accordance with Bolli and Saunders (1985), Miller and Katz (1987), and Berggren and Miller (1988), the upper boundary is in accordance with Iaccarino and Salvatorini (1982), Kennett and Srinivasan (1983), and Iaccarino (1985). The definition of Miller and Katz (1987), Berggren and Miller (1988, 1989) (FA of *Globorotalia kugleri* at 23.7 Ma to the LA of *Globorotalia kugleri* at 21.8 Ma =1.9 Ma time duration), and the definition of Bolli and Saunders (1985) (FA of *Globorotalia kugleri* =25.5 Ma to the FA of the *Globigerinoides primordius* =24.6 Ma =0.9 Ma time duration) are not coinciding with the present work definition. Thus in assuming continous sedimentation and a constant rate of subsidence through the *Globorotalia kugleri* Zone of well H1-NC41 time, the 175 ft. (=53.35 m) sediments may had been deposited at 10.67 cm/1000 years rate of sedimentation.

4. The *Globoquadrina dehiscens* Zone

The *Globoquadrina dehiscens* Zone is a partial range zone of 2.3 Ma time duration of Aquitanian age (Early Miocene) define by the range of the zonal marker from its FA (23.2 Ma) (coincident with the FA of *Globigerinoides immarturus* and *Globigerinoides quadrilobatus*) to the FA of *Globigerinoides altiapertura* (20.9 Ma).

The *Globoquadrina dehiscens* Zone is 435 ft. (132.6 m) thick (D.D. 8165 ft.–7730 ft.) dark brown to grey shale and marl within Ras Abd Jalil Formation.

The planktonic Foraminifera are very rich in this zone ranging in apparent percentage from 86.30% to 98.93% dominated by the genus *Globigerinoides*

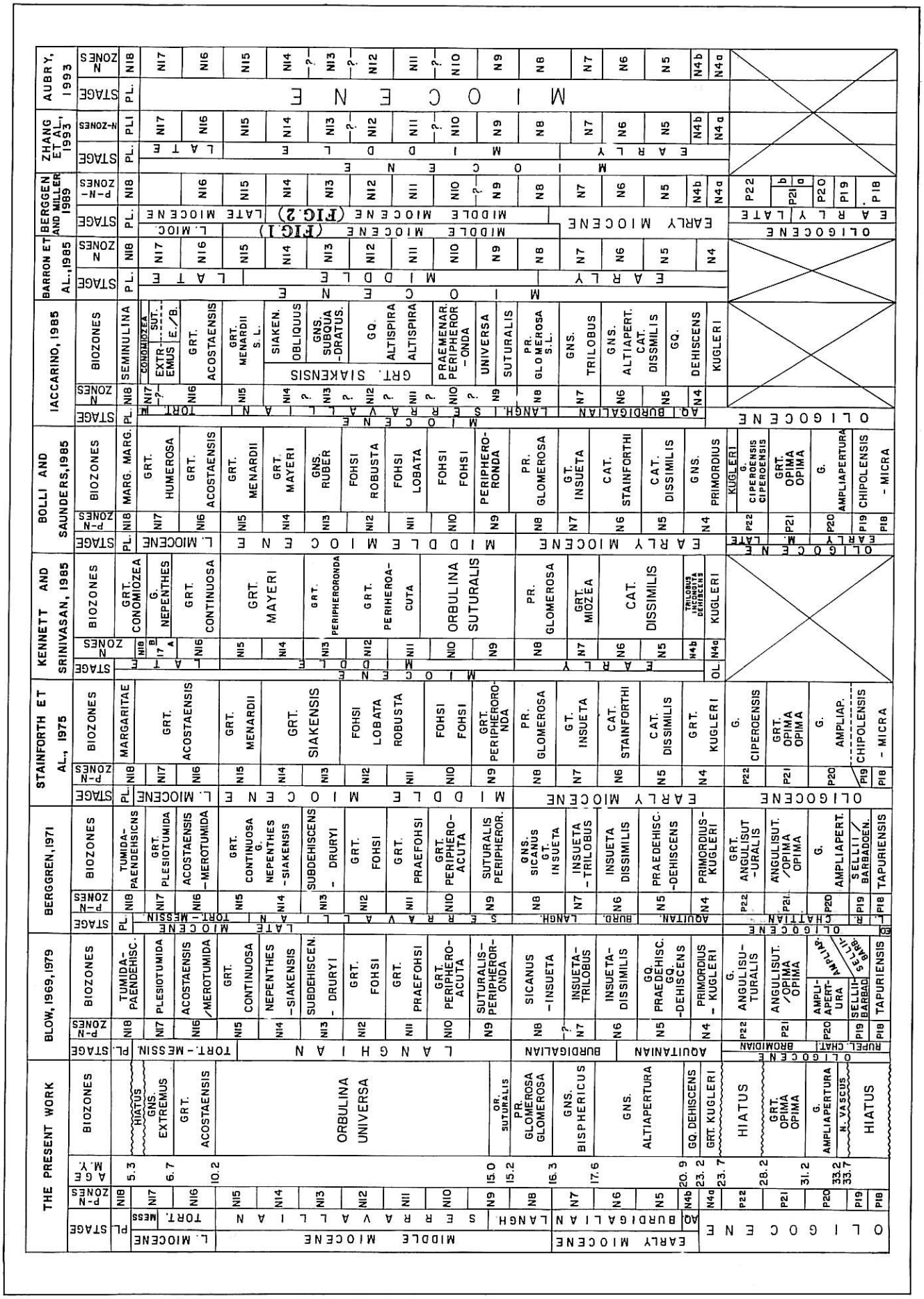


Fig. 3. Correlation of the Oligocene – Miocene zonal schemes of some authors with well H1-NC41 NW offshore, Libya.

(37 species and variants). Most characteristics are the disappearance of *Globigerinoides primordius* and *Globorotalia kugleri* at the top of the zone, the disappearance of *Globorotalia nkbrowni, Globorotalia cifellii, Globorotalia mendacis*, and *Globorotalia pseudokugleri, Globigerina sellii, and Globigerina tripartita* within this zone, and the FA of *Globoquadrina dehiscens* at the lower boundary of the zone.

Based on on the vertical distribution of *Globoquadrina dehiscens* and *Globigerinoides altiapertura*, the *Globoquadrina dehiscens* Zone as defined here can be correlated with the upper part of Zone N4 and the lowermost Zone N5 of Blow (1969, 1979), Berggren (1969b, 1971);? the upper of Zone N4 of Stainforth *et al.*, (1975),? Bolli and Saunders (1985), Zone N4 and lowermost Zone N5 of Iaccarino (1985); Zone N4b and lowermost Zone N5 of Zhang *et al.* (1993); Zone N4b of Kennett and Srinivasan (1983), Miller and Katz (1987), and Berggren and Miller (1988, 1989) and equivalent biozones.

The time span for the *Globoquadrina dehiscens* Zone as defined here from the FA of *Globoquadrina dehiscens* (23.2 Ma) to the LA of *Globorotalia kugleri* coincident with the FA of *Globigerinoides altiapertura* (20.9 Ma) is 2.3 Ma (Berggren and Miller, 1989; Zhang *et al.*, 1993) accordingly, the calculated rate of sedimentation is 9.47 cm/1000years assuming constant rate of subsidence.

5. The *Globigerinoides altiapertura* Zone

The *Globigerinoides altiapertura* Zone is a range zone of 3.3 Ma of early Burdigalian (M. Miocene) age defined by the first evolutionary appearance of *Globigerinoides altiapertura* at 20.9 Ma to its last occurrence at 17.6 Ma coincident with the first evolutionary appearance of *Globigerinoides bisphericus* (not *Globigerinoides sicanus*).

The thickness of the *Globigerinoides altiapertura* Zone is 944 ft. (287.8 m) from D.D. 7730 ft. to D.D. 6786 ft., lithologicaly this depth interval is brown shale and marl representing the upper part of Ras Abd Jalil Formation.

The planktonic Foraminifera are very rich ranging in apparent percentage from 76.67% to 97.32% dominated by the genus *Globigerinoides* (64 species and variants) characterized by the FA of *Globigerinoides altiapertura, Globigerinoides amplus, Globigerinoides subquadratus*, and *Globigerinoides murataii* at or near the lower boundary, the disappearance of *Globigerinoides altiapertura* at the upper boundary, and the disappearance of *Catapsydrax dissimils* within its lower part.

Based on the zonal criteria of the *Globigerinoides altiapertura* Zone(total range of the zonal marker) coincident with the first evolutionary occurrence of *Globigerinoides bisphericus* (not *Globigerinoides sicanus*) at its upper boundary and assuming synchronous first and last occurrence of *Globigerinoides altiapertura*, the *Globigerinoides altiapertura* Zone is considered equivalent to Zone N5 and N6 (or most of it) of Blow (1969, 1979, excluding lowermost Zone N5), Bolli and Saunders (1985, excluding the uppermost Zone N6), Zhang *et al.* (1993, excluding the lowermost part of Zone N5) and equivalent biozones (see Fig. 3).

The N5/N6 zonal boundary is generally based on the FA of *Globigerinita insueta* (18.1 Ma, Barron *et al.*, 1985) (see Blow, 1969, Berggren, 1971; Stainforth *et al.*, 1975; Kennett and Srinivasan, 1985; Barron *et al.*, 1985; Bolli and Saunders, 1985), however, Iaccarino (1985), and Zhang *et al.* (1993) found that the FA of *Globigerinita insueta* is diachronous, it is also scarce in the Mediterranean area, which seems true for well H1-NC41 (Kassab *et al.*, 1995–1996) and the Sirt Basin (Berggren, 1969a), accordingly Zhang *et al.*, (1993) preferred the FA of *Globorotalia praescitula* (19.0 Ma) distinct between the N5/N6 Zones, however, the last and first appearance of *Globorotalia praescitula* seems diachronous as well (Blow, 1969, 1971; Stainforth *et al.*, 1975; Kennett and Srinivasan, 1983; Barron *et al.*, 1985; Bolli and Saunders, 1985; Iaccarino, 1985; Zhang *et al.*, 1993).

The time of deposition of the *Globigerinoides altiapertura* Zone is 3.3 Ma, thus the rate of sedimentation during the deposition of the *Globigerinoides altiapertura* Zone (total thickness 287.8 m would be 8.7 cm/1000 years.

6. The *Globigerinoides bisphericus* Zone

The *Globigerinoides bisphericus* Zone is a Lower Miocene (Upper Burdigalian) partial range zone of 1.3 Ma time duration defined by the range of *Globigerinoides bisphericus* (not *Globigerinoides sicanus*) from its first evolutionary appearance coincidint with the LO of *Globigerinoides altiapertura* (17.6 Ma by correlation with N6/N7 zonal boundary) to the FA of *Praeorbulina glomerosa glomerosa* (16.3 Ma, Iaccarino, 1985, by correlation with Cowie and Basset, 1989; Miller and Katz, 1987; Zhang *et al.*, 1993; Aubry, 1993) and the first

evolutionary appearance of *Globigerinoides sicanus* (16.6 Ma; 16.3 Ma).

The *Globigerinoides bisphericus* Zone covers a thickness of 1026 ft. (312.8 m) from D.D. 6786 ft. to D.D. 5760 ft. in the lower part of Al Mayah Formation. This depth interval is made of quartzose sand, shale, silty and glauconitic horizons.

The Planktonic Foraminifera show a marked decrease in number of individuals relative to the underlying zone, the apparent percentage of the planktonic Foraminifera ranges from 22.4% to 84.86% dominated by the genus *Globigerinoides* (63 species and variants). Most characteristics are the FA of *Globigerinoides bisphericus* (not *Globigerinoides sicanus*) at the lower boundary and the disappearance of *Globigerinoides altiapertura* close to the lower boundary, also characteristics is the abundance of *Globigerinoides immaturus, Globigerinoides obliquus, Globigerinoides quadrilobatus, Globigerinoides sacculifer*, and *Praeorbulina transitoria.*

Assuming synchronous LA of *Globigerinoides altiapertura* and synchronous FA of *Pr. glomerosa glomerosa*, therefore, and in accordance with the zonal definition of the *Globigerinoides bisphericus* Zone (first evolutionary appearance of *Globigerinoides bisphericus*, coincident with the LA of *Globigerinoides altiapertura* to the FA of *Pr. glomerosa glomerosa* coincident with the FA of *Globigerinoides sicanus*) the *Globigerinoides bisphericus* Zone of well H1-NC41 can be correlated with Zone N7 (and may be the lower part of Zone N8) of Bolw (1969, 1979), Zone N7 of Stainforth *et al.* (1975), Iaccarino (1985), Bolli and Saunders (1985, excluding the lowermost part), the upper part of Zone N7 and the lowermost part of Zone N8 of Kennet and Srinivasan (1983), Zone N8 of Barron *et al.* (1985), Miller and Katz (1987), and Zone N7 and the lowermost Zone N8 of Zhang *et al.* (1993).

The lower limit of Zone N7 is widely taken corresponding to the LO of *Catapsydrax dissimilis* (Blow, 1969, 1979; Stainforth *et al.*, 1975; Keller, 1981; Kennett and Srinivasan, 1983; Lidz, 1984; Barron *et al.*, 1985; Bolli and Saunders, 1985; Iaccarino, 1985; Miller and Katz, 1987; Berggren and Miller, 1989, Zhang *et al.*, 1993).

The last occurrence of *Catapsydrax dissimilis* in well H1-NC41 is within the upper part of Zone N5 (similar observation was noted by Zhang *et al.*, 1993, p.302 for diachronous LO of *Catapsydrax dissimilis* in borehole Eureka 68–136, upper De Soto Canyon, NE Gulf of Mexico), thus it is not in the reach of limiting Zone N7 in well H1-NC41, therefore, the taxa *Globigerinoides bisphericus* (not *Globigerinoides sicanus*), and *Globigerinoides altiapertura* are used to limit the lower boundary of the N7 Zone. The N6/N7 boundary is at 17.6 Ma (LA of *Cat. dissimilis* at 17.6 Ma, Barron *et al.*, 1985; Zhang *et al.*, 1993; Aubry, 1993). Accordingly the *Globigerinoides altiapertura/Globigerinoides bisphericus* zonal boundary is considered at 17.6 Ma by correlation with the N6/N7 zonal boundary. Assuming constant rate of subsidence, the rate of sedimentation during the time of deposition (1.3 Ma) of the *Globigerinoides bisphericus* Zone (thickness 312.8 m) is 4.06 cm/1000 years.

7. The *Praeorbulina glomerosa glomerosa* Zone

The early Langhian (Middle Miocene) *Praeorbulina glomerosa glomerosa* Zone is a partial range zone of 1.1 Ma time duration defined by the range of *Pr. glomerosa glomerosa* from its FA (16.3 Ma, Iaccarino, 1985 by correlation with Cowie and Basset, 1989; Miller and Katz, 1987; Zhang *et al.*, 1993; Aubry, 1993) coincident with the FA of *Globigerinoides sicanus* to the FA of *Orbulina suturalis* (15.2 Ma, Iaccarino, 1985 by correlation with Cowie and Basset, 1989).

The zone covers 620 ft. (189.0 m) from D.D. 5760 ft.–to D.D. 5140 ft. thickness of grey green shale; sandy, pyritic glauconitic, and fossiliferous limestone thin levels of the lower part of Al Mayah Formation.

The Planktonic Foraminifera show a noticeable decrease in number of individuals in this zone, their apparent percentage ranges from 9.66% to 60.29%.

The genus *Globigerinoides* is consistent in its dominance of the planktonic Foraminifera (51 species and variants). Most characteristics are the FA of *Pr. glomerosa glomerosa, P. glomerosa curva, Globigerinoides. sicanus, Globigerinoides elongatus, Orbulina bilobata, Globorotaloides variabilis, Grtd. hexagona, Sphaeroidinellopsis* spp., and *Sphaeroidinella* spp.

Based on the zonal definition (range of *Pr. glomerosa glomerosa* from its FA coincident with the FA of *Gns. sicanus*, to the FA of *Orbulina suturalis*), the *Pr. glomerosa glomerosa* Zone is correlated with most of Zone N8 of Blow (1969, 1979), and Berggren (1969b, 1971), Zone N8 of Stainforth *et al.* (1975), most of Zone N8 of Kennett and Srinivasan (1983), Barron *et al.*, (1985), Zone N8 of Bolli and Saunders (1985, part), Iaccarino (1985), Miller and

Katz (1987), Berggren and Miller (1989), and most of Zone N8 of Zhang *et al.* (1993) and equivalent biozones (see Fig. 3).

Assuming constant rate of subsidence, the rate of sedimentation during the time of deposition (1.1 Ma) of the *Pr. glomerosa glomerosa* Zone (189 m) at well H1-NC41 is 17.27 cm/1000 years.

8. The *Orbulina suturalis* Zone

The Upper Langhian (Middle Miocene, 0.2 Ma time duration) *Orbulina suturalis* Zone is a partial range zone of 520 ft. (158.5 m) thickness from D.D. 5140 ft. to D.D. 4620 ft., it is defined by the range of *Orbulina suturalis* from its FA (15.2 Ma, Barron *et al.*, 1985; Zhang *et al.*, 1993; Aubry, 1993) to the FA of *Orbulina universa* (15.0 Ma, Iaccarino, 1985 by correlation with Cowie and Basset, 1989). Lithologically it is grey green shale with levels of limestone, silstone and marl falls within the upper part of Al Mayah Formation.

The planktonic Foraminifera range in apparent percentage from 7.07% to 68.87%. The genus *Globigerinoides* still the dominant planktonic genus (44 species and variants). Most characteristics of the zone is the FA of *Orbulina suturalis* and the disappearance of the *Praeorbulina glomerosa* group in this zone.

The zonal criteria of the *Orbulina suturalis* Zone as defined by the FA of *Orbulina suturalis* to the FA *Orbulina universa* correlates it with the lower part of Zone N9 and equivalent N-Zones (Blow, 1969, 1979; Berggren, 1969b, 1971; Stainforth *et al.*, 1975; Kennett and Srinivasan, 1983; Bolli and Saunders, 1985; Iaccarino, 1985; Miller and Katz, 1987) and possibly the lower part of Zone N9 of Barron *et al.* (1985), Berggren and Miller (1989), and Zhang *et al.* (1993) and equivalent biozones (see Fig. 3).

The 158.5 m thick *Orbulina suturalis* Zone of 0.2 Ma time duration is thought to have been deposited at a rate 79.25 cm/1000 years in case of constant rate of subsidence.

9. The *Orbulina universa* Zone

The *Orbulina universa* Zone is a partial range zone of Middle Miocene age (Serravallian) of 4.8 Ma time duration (in well H1-NC41). It is defined by the range of the zonal marker from its FA (15.0 Ma, Iaccarino, 1985 by correlation with Cowie and Basset, 1989) to the FA of *Globorotalia acostaensis* (10.2 Ma, Miller and Katz, 1987; Berggren and Miller, 1989; Zhang *et al.*, 1993). It is made of 1250 ft. (381 m) (D.D. 4620 ft. to D.D. 3370 ft.) of thin grey marly limestone, grey marl, grey green shale, and quartzose sandstone of the upper part of Al Mayah Formation.

The planktonic Foraminifera range in the apparent percentage from 4.66% to 61.22%. The genus *Globigerinoides* is represented by 49 species and variants (most of them are rare to very rare), most characteristics are the FA throughout this zone of *Globigerinoides seigliei, Globigerinoides Kennetti, Globigerinoides tenellus*,? *Globigerinoides conglobatus* and transitionals, *Globorotalia scitula, Globorotalia humerosa, Globorotalia menardii, Globorotalia pseudobesa, Globigerina regina, Globigerina praenepenthes, Globigerina umblicata, Globigerina multiloba, Globigerina pachyderma, Globigerina nepenthes, Sph. hancocki, Grtd. falconarae*, and *Orbulina universa*.

Based on the present definition of the *Orbulina universa* Zone (FA of *Orbulina universa* to the FA of *Globorotalia acostaensis*), the lower boundary of the zone may fall within the middle of Zone N9 or the lower third of it (Blow, 1969, 1979; Stainforth *et al.*, 1975; Kennett and Srinivasan, 1983; Bolli and Saunders, 1985; Iaccarino, 1985). The upper boundary of the *Orbulina universa* Zone has been drawn differently. Iaccarino (1985) put the upper boundary corresponding to the FA of *Globorotalia praemenardii* at the base of Zone N-10 in the Lower Serravallian, Hammuda *et al.* (1991) put it at the FA of *Globorotalia fohsi lobata-robusta* or the FA of *Borelis melo* at a similar stratigraphic position to Iaccarino (1985), while Cita and Premoli Silva (1971–1973 in 1976), Borsetti *et al.* (1979), Agip Minerraria (1980), and Duronio (1985) extended the upper boundary of the *Orbulina universa* Zone almost to the end of the Serravallian (and by correlation within Zone N15 or the base of N16, fide Kassab *et al.*, 1995–1996). Similarly in well H1-NC41, the *Orbulina universa* Zone upper boundary coinciding with the FA of *Globorotalia acostaensis* at the base of Zone 16.

The planktonic Foraminifera indicative of Zones N10–N15 are either very scarce (*Globorotalia mayeri, Globorotalia praemenardii, Globorotalia peripheroacuta, Globorotalia siakensis, Globigerina nepenthes*), or absent (*Globorotalia fohi fohsi, Globorotalia fohsi lobata, Globorotalia fohsi robusta*).

A possible hiatus within the *Orbulina universa* Zone may be questionably concluded due to the

ill representation (or absence) of the planktonic Foraminifera indicative of N-Zones (10, 11, 12, 13,? 14). However, in case of continuous deposition the *Orbulina universa* Zone of well H1-NC41 is correlated with the upper part of Zone N9-N15 of Blow (1969, 1979) and equivalent N-Zones and biozones (Blow, 1969, 1979; Berggren, 1969b, 1971; Stainforth *et al.*, 1975; Thunell, 1979; Kennett and Srinivasan, 1983, Bolli and Saunders, 1985; Iaccarino, 1985) (see Fig. 3).

Assuming constant rate of subsidence during the time of deposition of the *Orbulina universa* Zone (4.8 Ma) in the area of well H1-NC41, the 381.09 m would have been deposited at rate of 7.93 cm/1000 years.

10. The *Globorotalia acostaensis* Zone

The *Globorotalia acostaensis* Zone is a partial range zone of Lower Tortonian (low Upper Miocene) age. It is defined by the range of *Globorotalia acostaensis* from its FA (10.2 Ma Zhang *et al.*, 1993; 11.3 Ma, Bolli and Saunders, 1985; 10.0 Ma, Kennett and Srinivasan, 1983) to the first evolutionary occurrence of *Globigerinoides extremus* (6.7 Ma, Zhang *et al.*, 1993; 8.2 Ma, Bolli and Saunders, 1985; 7.7 Kennett and Srinivasan, 1983).

The *Globorotalia acostaensis* Zone is 690 ft. (210.3 m) thick (from D.D. 3280 ft. to D.D. 2590 ft.) sandstone, shale, silty clay, fossiliferous limestone, bryozoan limestone, marly limestone, and *Borelis* limestone representing the uppermost part of Al Mayah Formation and the lower part of the Tubtah Formation.

The planktonic foraminiferal assemblage of this zone is rather poor, its apparent percentage ranges from 0.76% to 35.34%. The genus *Globigerinoides* shows noticeable decrease in number of individuals and to a less extent in the number of species (44 species and variants, 34 of them are rare to very rare). Other Planktonic genera are also poorly represented. *Globorotalia acostaensis, Globorotalia cibaoensis, Globigerinoides? conglobatus, Globigerinoides elongatus*, and *Globigerinoides seigliei* made their FA in this zone. *Globigerinoides extremus* limits its upper boundary.

Based on its definition (the range of *Globorotalia acostaensis* from its FA to the FA of *Globigerinoides extremus*), the lower boundary of the *Globorotalia acostaensis* Zone is correlated with the lower limit of Zone N16 (Blow, 1969, 1979; Strainforth *et al.*, 1975; Kennett and Srinivasan, 1983; Bolli and Saunders, 1985; Iaccarino, 1985; Miller and Katz, 1987; Berggren and Miller, 1989; McLaughlin, 1989; Zhang *et al.*, 1993)

The FA of *Globigerinoides extremus* is within Zone N16 (Blow, 1969, 1979 lower part, Iaccarino, 1985, middle part), within lower part of Zone N17 (Zhang *et al.*, 1993), and at the base of Zone N17 corresponding to the FA of *Globorotalia humerosa* and *Globorotalia plesiotumida* (Kennett and Srinivasan, 1983; Barron *et al.*, 1985; Bolli and Saunders, 1985; McLaughlin, 1989). The restriction the FA of *Globigerinoides extremus* to the base of Zone N17 is in accordance with the last four authors.

Accordingly, the *Globorotalia acostaensis* Zone is correlated with Zone N16 of Blow (1969, 1979) and equivalent N-Zone and biozones (ignoring the FA of *Globigerinoides extremus* at the lowest part of Zone N16 of Blow, 1969, 1979).

The *Globorotalia acostaensis* Zone is of 3.5 Ma, 3.1 Ma, 2.3 Ma time duration (Zhang *et al.*, 1993; Bolli and Saunders, 1985, Kennett and Srinivasan, 1983) and in assuming a continuous deposition in the area of H1-NC41, the 210.3 m of sediments could have been accumulated at a rate of 6.0 cm/1000 years, 6.7 cm/1000 years, or 9.1 cm/1000 years.

11. The *Globigerinoides extremus* Zone

The Upper Miocene (Upper Tortonian-Lower Messinian) *Globigerinoides extremus* Zone is a partial range zone defined by the range of the zonal marker from its first evolutionary appearance (6.7 Ma, Zhang *et al.*, 1993; 7.7 Ma, Kennett and Srinivasan, 1983; 8.2 Bolli and Saunders, 1985) to the top of the studied section just below the unconformity separating the Miocene/Pliocene boundary.

The 710 ft. (216.46 m) thick interval depth from D.D. 2590 ft. to D.D. 1880 ft. covered by *Globigerinoides extremus* Zone is lithologically made of (in ascending order *Borelis* limestone, oolitic limestone, marly limestone, anhydrite, marl, gypsum, fossiliferous oolitic limestone, and gypsum belong to the upper part of the Tubtah Formation and most of the Marsa Zoughah Formation.

The planktonic Foraminifera are extremely rare (with exception of 2 samples which gave a good yield from the fine size fraction), the planktonic foraminiferal percentage ranges from 1.82% to 50.0%. The genus *Globigerinoides* is represented by 29 species and variants most of them are rare to

very rare. Other planktonic genera are also poorly represented.

The base of the *Globigerinoides extremus* Zone as defined here (the first evolutionary appearance of *Globigerinoides extremus*) marks the base of Zone N17 (Kennett and Srinivasan, 1983; Barron *et al.*, 1985; Bolli and Saunders, 1985; McLaughlin, 1989).

The top of the zone in well H1-NC41 is marked by unconformity at the Messinian (Upper Miocene)/Lower Pliocene boundary, therefore, the *Globigerinoides extremus* Zone of the present work is considered equivalent to most part of Zone N17 of Blow (1969, 1979) and equivalent N-Zones and biozones.

The top of this zone is not determined due to missing samples, however, the top of the Marsa Zouaghah Formation may represent the top of this zone and in any case an unconformity is indicated at the top of the Marsa Zouaghah Formation (NOC-Agip Name, 1979; Cococcetta, 1982, well H1-NC41 report), indicating missing time at the end of the Miocene, therefore an age older than 5.3 Ma is supposed for the top of the *Globigerinoides extremus* Zone in well H1-NC41, in this case the calculated time duration of the *Globigerinoides extremus* Zone in well H1-NC41 would be < 1.4 Ma, < 2.4 Ma, and < 2.9 Ma (see definition), accordingly the calculated rate of sedimentation would be: $>$ 15.46 cm/1000 years, $>$ 9.0 cm/1000 years, or $>$ 7.46 cm/1000 years.

HIATUSES

1. Eocene/Oligocene

Previous studies of the Eocene–Oligocene sequences in the subsurface NW offshore, Libya, assumed unconformable relations between the Upper Eocene Samdun Formation and the overlying Lower Oligocene *Nummulites vascus* marker bed (Panci *et al.*, 1976, well A1-NC41; NOC-Agip Name, 1979, well H1-NC41, 1981, well P1-NC41; 1982, well N1-NC41; Bristot, 1982, well M1-NC41). Eocene/Oligocene unconformity has also been detected between the Oligocene-Lower Miocene Ras Abd Jalil and Dirbal Formations and the underlying Tellil Group (Samdun Formation) (wells NC41: R1, S1, F1, F2, J1, B1-B8, C1-C8, well D1-NC35A; NOC-Agip Name, 1979, 1980, 1981, 1982, 1984, 1989, 1994, 1995; Drughi, *et al.*, 1978; Bristot and Cassan, 1982; Sirt Oil Co., 1983; Hammuda *et al.*, 1985; Duronio, 1985; Hammuda *et al.*, 1991). Assuming the Eocene–Oligocene boundary (i.e. the Priabonian-Rupelian boundary) is at 36.5 Ma (Berggren and Miller, 1988, 1989; Cowie and Basset, 1989) and consequently considering this boundary coinciding with the P17/P18 Zone (*T. cerroazulensis/Cassigerinella chipolensis* Zone), and as this planktonic foraminiferal boundary is not usually well detected in subsurface NW offshore, Libya due to the non-planktonic dominant foraminiferal fauna of the Upper Eocene–Lower Oligocene in the south central part of the basin, an unconformable relation is expected. Hammuda *et al.* (1991) considering the Lower Oligocene base of 37.0 Ma postulated unconformity ranging in magnitude from 4.5 Ma to 18.5 Ma for 9 wells in the NW offshore, Libya subsurface across the Eocene/Oligocene boundary.

The time span for *Cassigerinella chipolensis-pseudohastigerina micra* Zone may be in the range 2.5 Ma–3.0 Ma (see Bolli and Saunders, 1985; Berggren and Miller, 1988, 1989). In well H1-NC41 the *Globigerina ampliapertura* Zone (Zone P20) is underlain by the *Nummulites vascus* Zone (0.5 Ma by correlation with Ben Ferjani *et al.*, 1990), marks the base of the Oligocene, the time duration of both zones is around 2.5 Ma (*Globigerina ampliapertura* Zone is 2.0 Ma–2.5 Ma according to Blow, 1969, 1979; Berggren, 1969, 1971; Vail and Mitchum, 1979; Lidz, 1984; Bolli and Saunders, 1985; Haq *et al.*, 1987) consequently it is concluded that the hiatus time span at the base of the *Nummulites vascus* Zone (base of Oligocene) in well H1-NC41 may range from 2.5 Ma to 3.0 Ma (uppermost Zone N17, Zone P18, Zone P19,? lowermost Zone P20).

2. Oligocene

Based on the analysis of the vertical distribution (first and last occurrence) of the planktonic foraminiferal species *Globorotalia opima opima* (LA 28.2 Ma, Aubry, 1993), *Globorotalia kugleri*, (FA 23.7 Ma-LA 21.8 Ma, Zhang *et al.*, 1993), *Globigerina ciperoensis* (FA $\pm$35.5 Ma-LA $\pm$2.5 Ma, Bolli and Saunders, 1985), *Globigerinoides primordius* (FA $\pm$26.7 Ma-LA $\pm$23.7 Ma, Berggren and Miller, 1989), and *Globoquadrina dehiscens* (FA 23.2 Ma, Zhang *et al.*, 1993, Aubry 1993), it is possible that Zone P22 of Blow (1969, 1979) (equivalent to the *Globigerina ciperoensis* Zone of Bolli 1957, and *Globigerina angulisuturalis* Zone of Blow, 1969, 1979), and lowermost part of Zone

N4a are not represented in well H1-NC41 as it is explained by the overlap of the vertical ranges of *Globorotalia opima opima*, *Globorotalia kugleri* s.1. and *Globigerinoides primordius* (see Fig. 3). The duration of Zone P22 is 4.5 Ma (Berggren and Miller, 1988, 1989). This interval or at least most part of it (3.0 Ma–4.5 Ma) is not represented because of the overlap of the Zone N4 zonal markers with the P21 Zone (FA event of *Globigerinoides primordius* may start within the upper part of Zone P22, according to Miller and Katz, 1987; Berggren and Miller, 1988, 1989), accordingly this would give 1.0 Ma time of Zone P22 may be questionably represented in well H1-NC41.

3. Oligocene/Miocene

The present planktonic foraminiferal analysis does not reveal missing time at the transition from the Oligocene *Globorotalia kugleri* Zone to the Miocene *Globoquadrina dehiscens* Zone. However, previous studies by Panci *et al.* (1976, well A1-NC41), and Sirt Oil Co. (1983, 1984, 1985, wells NC35A D1, H1, I1) show unconformable relation across the Oligocene/Miocene boundary. Moreover, further studies may include the *Globorotalia kugleri* Zone within the Miocene, thus indicating unconformity at the base of the Miocene.

4. Middle Miocene

In well H1-NC41 the *Orbulina universa* is in normal biosequential relation with the underlying *Orbulina suturalis* Zone within Zone N9. The biozonal sequential relationship with the overlying biozones is not exactly determined due to the scarcity of the well known zonal markers. The planktonic Foraminifera indicative of Zone N10-N15 are either very scarce or absent. A possible hiatus within the *Orbulina universa* Zone may be questionably concluded due to the ill representation (or absence) of the planktonic Foraminifera indicative of N-Zones (10, 11, 12, 13,? 14)

5. Miocene/Pliocene

The uppermost Miocene is not determined due to missing samples, however, NOC-Agip Name (1979 well log) followed by Cococcetta (1982, well H1-NC41 report) indicated missing time at the end of the Miocene involving part of the Messinian, it includes the top of Zone N17 (*Globigerinoides extremus* Zone of the present work), therefore, an age older than 5.3 Ma is supposed for the top of the Miocene in well H1-NC41.

CONCLUSIONS

(1) Based on the vertical distribution of the planktonic Foraminifera, eleven planktonic foraminiferal biozones are recognized and are correlated with P-N Zones, and by their integration enabled to determined possible hiatuses as follows:

(a) The *Globigerina ampliapertura* Zone (2.0 Ma) is underlain by the *N. vascus* marker bed (0.5 Ma) both representing Zone P20 (2.5 Ma) with Zone P18-P19 of the Lower Oligocene missing.

(b) The *Globorotalia opima opima* Zone is correlated with Zone P21 (3.0 Ma).

(c) The *Globorotalia kugleri* Zone (0.5 Ma marking the top of the Oligocene is correlated with the Zone N4a (lower part of Zone N4) with Zone P22 (3.0 Ma-4.5 Ma) missing.

(d) The *Globoquadrina dehiscens* Zone (2.3 Ma) marking the Lower Miocene (Aquitanian) is correlated with the upper part of Zone N4 and the lowermost part of Zone N5.

(e) The *Globigerinoides altiapertura* Zone (3.3 Ma) (Lower Burdigalian) is correlated with Zone N5 (excluding its lowermost part) and Zone N6. Its lower boundary marks the Aquitanian/Burdigalian boundary.

(f) The *Globigerinoides bisphericus* Zone (1.3 Ma) (Upper Burdigalian) is correlated with Zone N7. Its upper boundary marks the Burdigalian/Langhian boundary.

(g) The *Praeorbulina glomerosa glomerosa* Zone (1.1 Ma) (Lower Langhian) is correlated with Zone N8. Its lower boundary marks the Burdigalian/Langhian boundary.

(h) The *Orbulina suturalis* Zone (0.2 Ma) (Upper Langhian) is correlated with the lower part of Zone N9. Its upper boundary marks the Langhian/Serravallian boundary.

(i) The *Orbulina universa* Zone (4.8 Ma) (Ser-

ravallian) is correlated with the upper part of Zone N9 to N15, however, there is a possibility of missing Zones N10 (part)–N15 (part) due to scarcity or absence of zonal index planktonic Foraminifera, the possibility of a hiatus in the Serravallian is not excluded. The top of this zone marks the Serravallian/Tortonian boundary.

(j) The *Globorotalia acostaensis* Zone (3.5 Ma, 2.3 Ma, 3.1 Ma) (Lower Tortonian) is correlated with Zone N16.

(k) The *Globigerinoides extremus* Zone (< 1.4 Ma, < 2.4 Ma, < 2.9 Ma) (Upper Tortonian/Lower Messinian) is correlated with Zone N17. The upper part of Zone N17 is considered missing and the top of the *Globigerinoides extremus* Zone unconformably marks the Messinian/Lower Pliocene boundary.

(2) The Eocene/Miocene boundary is taken at 33.7 Ma involving a hiatus older than 2.8 Ma.

(3) The Oligocene/Miocene boundary is taken at 23.2 Ma corresponding to the base of the *Globoquadrina dehiscens* Zone (base of Aquitanian).

(4) The Aquitanian/Burdigalian boundary is taken at (20.9 Ma) corresponding to the *Globoquadrina dehiscens/Globigerinoides altiapertura* Zones boundary.

(5) The Burdigalian/Langhian (Early Miocene/ Middle Miocene boundary) (16.3 Ma) is taken corresponding to the *Globigerinoides bisphericus/Pr. glomerosa glomerosa* Zones boundary.

(6) The Langhian/Serravallian (15.0) boundary is taken corresponding to the *Orbulina suturalis/Orbulina universa* Zones boundary.

(7) The Serravallian/Tortonian (Middle Miocene/ Late Miocene boundary) (10.2 Ma) is taken corresponding to the *Orbulina universa/ Globorotalia acostaensis* Zones boundary.

(8) Due to the scarcity of planktonic Foraminifera in the Late Miocene of well H1-NC41, the Tortonian/Messinian boundary is taken within the *Globigerinoides extremus* Zone following the NOC-Agip Name (1979, well log).

(9) The Miocene/Pliocene boundary is at the top of Marsa Zouaghah Formation possibly at the top of the *Globigerinoides extremus* Zone (+5.3 Ma).

(10) Based on the planktonic foraminiferal contents of the studied rock units, they are considered of Oligocene–Miocene age as follows:

(a) Ras Abd Jalil Formation (Lower Oligocene–Lower Miocene, lower Burdigalian).

(b) Al Mayah Formation [late Lower Miocene (upper Burdigalian) – early Upper Miocene (lower Tortonian)].

(c) Tubtah Formation (lower upper Miocene, Tortonian).

(d) Marsa Zouaghah Formation (upper Miocene, Messinian). The uppermost Miocene is not represented and the Lower Pliocene Sbabil Formation is unconformably overlying the Marsa Zouaghah Formation.

ACKNOWLEDGEMENTS

The authors wish to sincerely thank the management of the Petroleum Research Centre headed by Mr. M. Idris for supporting this research, the scientific committee at P.R.C. for follow up and encouragement, Agip–Name, Tripoli for supplying the samples and our colleagues in the Geology Department, Exploration Office, P.R.C. for their various help. Mr. Sefau Tshakrin and Miss Layla Hafidh are greatly acknowledged for their taking part in the preliminary stage of this research, Mr. M. Gumati and Miss Mufida El-Mesallati are also acknowledged for drafting the text-Figures.

The senior author would like to thank Mr. Abdel Majid Musrati and all other personnel and management of P.R.C. for various help to carry out this research.

REFERENCES

Agip Mineraria, 1980. Foraminifera Padani (Terziario e Quaternario), Altante I congrafico e distribuzione stratigrafica. *Agip Mineraria*, Milano, 68 pls., 2nd Edition.

Aubry, M.P., 1993. Neogene allostratigraphy and depositional history of De soto canyon area, northern Gulf of Mexico. *Micropaleontogy*, vol. **39**, no. **4**, pp. 327–366, 19 text-figs., 3pls., 5 tables.

Barron, J.A., Keller, G. & Dunn, D.A. 1985., A multiple microfossils biochronology for the Miocene. *Mem. Geol. Soc. Amer.*, **163**, 21–36., 6 text-figs., 4 tables.

Ben Ferjani, A.; Burollet, P.F.; and Mejri, F., 1990. *Petroleum Geology of Tunisia.* Enterprise Tunisienne d'Activites Petrolieres, Tunisia, 194 P., 68 text-figs., 23 photos.

Berggren, W.A., 1969a. Biostratigraphy and Planktonic Foraminifera Zonation of the Tertiary system of the Sirt Basin of Libya, North Africa. *Proceeding of the first Interna-*

tional Conference on Planktonic Microfossils, v. (**1**). Geneva (1967), P. Brronnimann and H.H. Renz (Eds.) Leiden, E.J. Brill. vol. **1**, pp. 104–120, 4 text-figs.

Berggren, W.A. 1969b. Rate of evolution in some Cenozoic planktonic Foraminifera, Micropal., vol. **15**, no. **3**, pp. 351–366, 8 tables, 13 figs.

Berggren, W.A. 1971. Tertiary boundaries and correlations. In: *The Micropaleontology of Oceans*, Proceed. Symp. Cambridge (1967) Micropal. of Marine Bottom Sed. B.M. Funnell and W.R. Riedel (Eds). Cambridge Univ. Press (1971) pp. 693–809, 52 tables.

Berggren, W.A., and Miller, K.G., 1988. Paleogene tropical planktonic foraminiferal biostratigraphy and magnetobiochronology. *Micropaleontology*, vol. **34**, no. **4**, pp. 362–380, 13 text-figs., 1 tab.

Berggren, W.A., and Miller, K.G., 1989. Cenozoic bathyal and abyssal calcareous benthonic foraminiferal zonation. *Micropaleontology*, vol. **35**, no. **4**, pp. 308–320, 2 text-figs.

Blow, W.H., 1969. Late Middle Eocene to Recent planktonic foraminiferal biostratigraphy. In: P. Bronnimann and H.H. Renz (Eds.), *Proceed. Ist. Conf. Plankt. Microfoss.*, Leiden: E.J. Brill, **I**, 199–422, 54 pls., 43 figs.

Blow, W.A., 1979. *The Cainozoic Globogerinida.* Leiden: E.J. Brill, 3 vols., 1413 p., 264 pls., 65 figs.

Bolli, H.M., 1957. Planktonic Foraminifera from the Oligocene–Miocene Cipero and Lengua Formations of Trinidad, B.W.I.U.S. *Natl. Mus., Bull.* **215**: 97–123.

Bolli, H.M., and Saunders, J.B., 1985. Oligocene to Holocene low latitude planktonic Foraminifera In: H.M. Bolli, J.B. Saunders and K. Perch–Nielsen (Eds.) and K.E. Fancett (Assist.), *Plankton Stratigraphy, Planktonic Foraminifera, Calcareous Nannofossils and Calpionellids.* Cambridge, Earth Sc. Ser., Cambridge Univ. Press, Cambridge, U.K., **I**, 155–262, 46 figs.

Borsetti, A.M., Cati, F., Colalongo, M.L. and Sartoni, S. 1979. Biostratigraphy and absolute age of the Italian Neogene. *Ann. Geol. Hellen., 7th Internat. Congr. Medit. Neogene, Athens*, pp. 183–97.

Bristot, B., 1982. Final well log M1-NC41, NOC-Agip Name, Explorat. Div., Subs., Tripoli, Libya.

Bristot, B., and Cassan, B.DE, 1982. Final well log R1-NC41. NOC-Agip Name, Explorat. Div. Subs., Tripoli, Libya.

Cita, M.B. and Premoli Silva, I., 1971–1973 In: Cita, M.B., 1976. Planktonic Foraminiferal biostratigraphy of the Mediterranean Neogene. *Progress in Micropaleontology.* pp. 47–68, Special Publication Micropaleontology Press, The American Museum of Natural History, New York. (Fide Iaccarino, 1985).

Cococcetta, V. 1982. *Stratigraphy & Paleoecology report* of well H1-NC41. Agip Name, Libyan Branch, Explorat. Div. Tripoli, Libya, 24 pp., 1 table, 1 text-fig.

Costa, V., Fandi, A., Drughi, M., 1977. Final well log B2-NC41. NOC-Agip Name, Explorat. Div. Subs., Tripoli, Libya.

Costa, V., Fandi, A., Drughi, M., and Sbeda, H., 1977. Final well log B1-NC41 (copy). NOC-Agip Name, 1977. Tripoli, Libya.

Cowie, J.W., and Basset, M.G., 1989. Global stratigraphic chart with geochronometric and magnetostratigraphic calibration. Bureau of International Comission on Stratigraphy (ICS: IUGS), Episodes, vol. **12**, no. **2**.

Drughi, M., and Costa, V., 1978. Well log F1-NC41. NOC-Agip Name, 1978. Libyan Branch, Tripoli, Libya.

Duronio p., 1985, Stratigraphy of the Bouri Field, In: Bristot, B. and Duronio, P. 1985. Bouri Oil Field Handbook for wellsite geologists. NOC-Agip Name, Tripoli, Libya.

Hammuda, O.S., Sbeta, A.M., Mouzughi, A.J. and Eliagoubi, B.A., 1985 *Stratigraphic Nomenclature of the Northwestern offshore of Libya.* Earth Sc. Soc. Libya, Tarabulus, Libya, 166 pp.

Hammuda, O.S., Van Hinte, J.E. and Nederbracht, S., 1991. Geohistory analysis mapping in central and southern Tarabulus Basin, northwestern offshore of Libya, In: M.J. Salem, O.S. Hammuda and B.A. Eliagoubi (Eds.). *The Geology of Libya.* Amsterdam, Elsevier IV, pp. 1657–1680, 13 figs.

Haq, B.U. Hardenbol, J. and Vail, P.R., 1987. Chronology of fluctuating sea levels since the Triassic. *Science*, 235: 1156–1167.

Iaccarino, S., 1985. Mediterranean Miocene and Pliocene Planktonic Foraminifera. In: H.M. Bolli, J.B. Saunders, and K. Perch–Nielsen (Eds.) and K.E. Fancett (Assist.) *Plankton Stratigraphy, Planktonic Foraminifera, Calcareous Nannofossils and Calpionellids.* Cambridge Earth Sc. Ser. Cambr. Univ. Press, Cambridge, **I**, 283–314, 6 figs.

Iaccarino, S. & Salvatorini, G. 1982. A Framework of planktonic foraminiferal biostratigraphy of the Early Miocene to Late Pliocene Mediterranean area. *Paleontol. Stratigr.* vol. **2.**, 115–25 (fide Iaccarino, 1985).

Kassab, I.I.M., Abusrewil, A.K. and Abuhamida, F.E., 1995–1996. Biostratigraphy of the Oligocene–Miocene of subsurface offshore, northwestern Libya typified by well H1-NC41. *Unpubl. Rep. Pet. Res. Cent.* (N.O.C.), Tripoli, Libya.

Keller, G., 1981. Origin and evolution of the genus *Globigerinoides* in the Early Miocene. *Micropal.* vol. **27**, no. **3**, pp. 293–304, 4 pls., 2 text-figs.

Kennett, J.P. and Srinivasan, M.S., 1983. Neogene planktonic Foraminifera, a phylogenetic *atlas. Hutchinson Ross publishing*, 1983, 265 pp., 61 pls., 26 text-figures, 1 table.,

Lidz, B.H., 1984. Oldest (Early Tertiary) subsurface carbonate rocks of St. Croix, USVI, revealed in a turbidite-mudball. *Journal of Foraminiferal Research*, v. **14**, no. **3**, p. 213–227, 4pls, 6 text figs.

McLaughlin, P.P., Jr. 1989. Neogene planktonic foraminiferal biostratigraphy of the southwestern Dominican Republic. *Journal of Foraminiferal Research*, vol. **19**, no. **4**, pp. 394–310, pl. 1–3, 6 figures, 3 tables.

Mercati, Carlin, S. and Drughi, M. 1979. Composite well log: G1-NC41. N.O.C.-Agip Name, Tripoli, Libya, Encl. No.1.

Miller, K.G., and Katz, M.E. 1987. Oligocene to Miocene benthonic foraminiferal and abyssal circulation change in the north Atlantic. *Micropaleontology*, **33**, no. **2**, 1987, pp. 97–149, 24 text-figures, pls 1–13.

NOC-Agip Name, 1979. Final well log H1-NC41, NOC-Agip Name, Explorat. Div. Subs., Tripoli, Libya.

NOC–Agip Name, 1979. Final well log J1-NC41, IBID.

NOC–Agip Name, 1980. Final well log C2-NC41, F1, IBID.

NOC–Agip Name, 1981. Final well log P1-NC41, B3, IBID.

NOC–Agip Name, 1982. Final well log NC41: B4, F2, N1, L1, IBID.

NOC–Agip Name, 1989. Final well log NC41: S1, B4-09, B1-10, B4-11, B8, IBID.

NOC–Agip Name, 1994. Final well log NC41: C3, C4, C5, C6, C7, IBID.

NOC–Agip Name, 1995. Final well log C8-NC41 IBID.

Panci, G., Costa, V., Drughi, M. and Fandi, A., 1976, N.O.C composite well log: A1-NC41. N.O.C.–Agip Name, Tripoli, Libya, Encl. No.2.

Panci, G., Costa, V. and Sbeda, H., 1977. NOC–Agip Name composite well log: B1-NC41 (copy).

Stainforth, R.M., Lamb, J.L., Luterbacher, H., Beard, J.H. and Jeffords, R.M., 1975. Cenozoic planktonic foraminiferal zonation and characteristics of index forams. *Univ. Kansas Paleont. Contribution*, Article **62**, Lawrence, Kansas, pp. 1–425, fig. 1–213, tables 1–9.

Salem, M.J. and Spreng, A.C. 1980. Middle Miocene stratigraphy, Al Khums, northwestern Libya- In: M.J. Salem and M.T. Busrewil (Eds.) *The Geology of Libya*, London, Academic Press, **I**, 97–116, 20 figs.

Sherif, K.H.A.T. 1991. Biostratigraphy in Al Khums area, northwestern Libya. In: M.J. Salem, O.S. Hammuda, and B.A. Eliagoubi (Eds.), *The Geology of Libya*, Elsevier, **IV**. 1421–1456, pls. 1–7, 23 figs.

Sirt Oil Company, 1983. Final well log D1-NC35A, Sirt Oil Co., Libya.

Sirt Oil Company, 1984. Final well log H1-NC35A, Sirt Oil Co., Libya.

Sirt Oil Company, 1985. Final well log D1-NC35A, Sirt Oil Co., Libya.

Thunell R.C., 1979. Mediterranean Neogene planktonic foraminiferal biostratigraphy: Quantitative result from DSDP **125**, **132** and **172**. *Micropaleontology*, vol. **25**, no. **4**, pp. 412–437, pls. 1–6.

Vail, P.R. and Mitchum, Jr., 1979. Global cycles of relative changes of sea level from seismic stratigraphy. In: Geological and Geophysical investigations of continental margins. AAPG Memoir, **29**, Tusla, Oklahoma, USA. 1979, J.S. Watkins, L. Montadert, and P.W. Dikerson (Eds.). pp. 469–472, 3 figs.

Van Hinte, J.E. Colin, J.P. and Lehman, R., 1980. Micropaleontologic record of the Messinian Event at Esso Libya Inc. well B1-NC35A on the Pelagian Platform In: M.J. Salem and M.T. Busrewil (Eds.), *The Geology of Libya*, London, Academic Press, **I**. 205–243, Pls 1–13, 8 figs.

Zhang, J., Miller, K.G. and Berggren, W.A., 1993. Neogene planktonic foraminiferal biostratigraphy of the northeastern gulf of Mexico. *Micropaleontology*, vol. **39**, no. **4**, pp. 299–326, plates 1–3, text-figures 1–14, tables 1–5.

Petroleum Res.J. Vol. 9 (1997); P. 45–50, 4 FIGS.

Petrography of the Triassic Phosphorites in Gharyan Area, NW Libya

Salem Lagha

بتروغرافية صخور الفوسفورايت التابعة للحين الترياسي بمنطقة غريان – شمال غرب ليبيا

سالم علي لآغا

أوضحت هذه الدراسة البتروغرافية أن رسوبيات فوسفات منطقة غريان بشمال غرب الجماهيرية تتواجد في الجزء السفلي من تكوين أبوشيبة الذي يرجع عمره إلى الدور الترياسي حيث وجد أنها عبارة عن مجموعة من مكونات فوسفاتية من الكريّات وبقايا عظام الأسماك والبيفتات والأنتركلاست والكبروليت وأخرى غير فوسفاتية تتمثل في خليط من حبيبات كلسية ومن المرو والفلدسبار وتوضح الدراسة البتروغرافية أن رسوبيات الفوسفات كانت قد تكونت أولاً كفوسفات طيني ثم أعيد ترسيبها كفوسفات غني بالرمل.

Abstract *The studied Triassic phosphorites are located in Gharyan area, north-western Libya. The phosphorites form the lower part of Abu Shaybah Formation, and are composed of phosphate elements, such as pellets, micronodules, intraclasts, coprolites and bone fragments plus a mixture of carbonate and quartz grains. Petrographic study of the Gharyan Triassic phosphorites shows that they were formed by deposition as phosphate mud, followed by reworking and redeposition as phosphate sands.*

INTRODUCTION

Ayler (1967) compiled the previous work on the phosphate occurrences in a bulletin for the Ministry of Industry in which he concluded that if commercial phosphate deposits exist in Libya, they would not be easily found. In 1973, the Industrial Research Centre (I.R.C.) carried out (through Polservice) a systematic exploration programme covering four areas in NW Libya. The study included sedimentary rocks of Late Cretaceous to Miocene age, but only a few phosphatized pelecypod shells were noticed. After a quick visit to NW Libya, through the Bureau de Recherches Geologiques et Minieres (B.R.G.M.), Slansky (1974) thought that there were some chances of discovering new phosphate deposits in Gharyan area. In the course of mapping (Tarabulus Sheet at a scale of 1:250 000) El Hinnawy and Cheshitiv (1975) reported the presence of phosphate bands at the top of Al Aziziyah Formation in Gharyan dome and Al Khurmat al Hamra dome. This study presents both petrography and field observations, as very little is as yet known.

GEOLOGICAL SETTING

In the study area the Mesozoic sedimentary sequence shows considerable variation in lithology and thickness, which reflects the shifting of sedimentary environments both laterally and vertically. The Early Triassic rocks are poorly exposed and indicate a continental environment with the development of red micaceous sandstone and siltstone facies. The Middle Triassic sequence shows a mixture of carbonate and terrigenous lithology formed

in an alternating near-shore marine to continental environment. The Late Triassic sediments were deposited in a continental environment that gradually shifted to a shallow water marine environment. (El Hinnawy and Cheshitev, 1975; Fatmi *et al.*, 1978). There are a few prominent domes in the study area which brought the Triassic formations to the surface. These formations are commonly cut by faults (Fig. 1).

Kurrush Formation

Kurrush Formation consists locally of red to brown, fine-grained, micaceous, and glauconitic sandstone. It is poorly exposed and only the upper 23.5 m are exposed (Fig. 2). The contact between Kurrush Formation and the overlying Al Aziziyah Formation is transitional. The upper unit of Kurrush Formation consists of sandy limestone The environment of deposition of this formation was sublittoral and the changes in lithology were related to the fluctuations in sea level (Desio, *et al.*, 1960; 1963; Burrollet, 1963; El Hinnawy and Cheshitev, 1975).

Al Aziziyah Formation

Al Aziziyah Formation consists lithologically of well-bedded limestone characterised by its dark grey colour. The limestone is partly siliceous and partly dolomitic with common clay and chert beds. The thickness of Al Aziziyah Formation in the study area is about 120 m (Fig. 2). Its depositional environment is relatively quiet, water inner shelf environment as indicated by its fossil assemblage (Christie, 1955; El Hinnawy and Cheshitev, 1975).

Abu Shaybah Formation

The Abu Shaybah Formation consists locally of a thin unit of a phosphatic breccia with angular to subrounded grains in the base and cross bedded sandstone in the upper part. The latter is white, red and yellow in colour alternating with green and red bands of clay. The thickness of the formation in the study area is 105 m (Fig. 2). The depositional environment of Abu Shaybah Formation is mainly continental with shallow water, marine to lagoonal

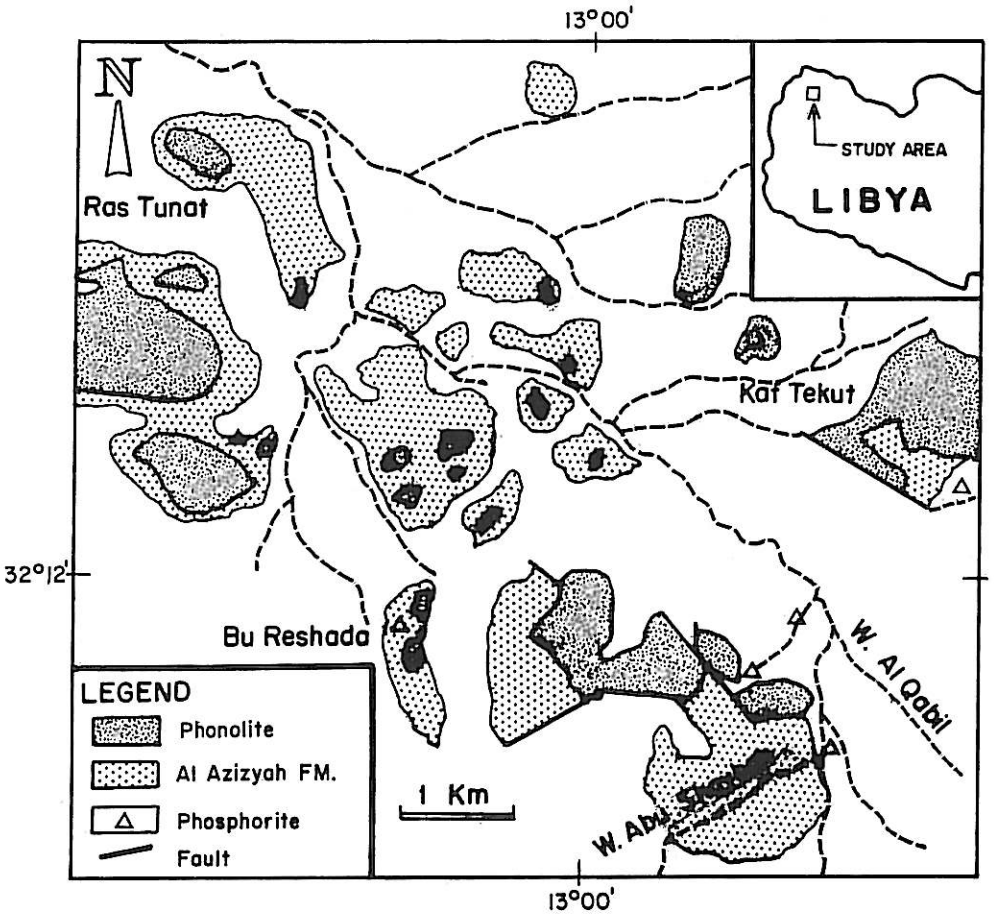


Fig. 1. Geologic map showing location of the Gharyan phosphorite.

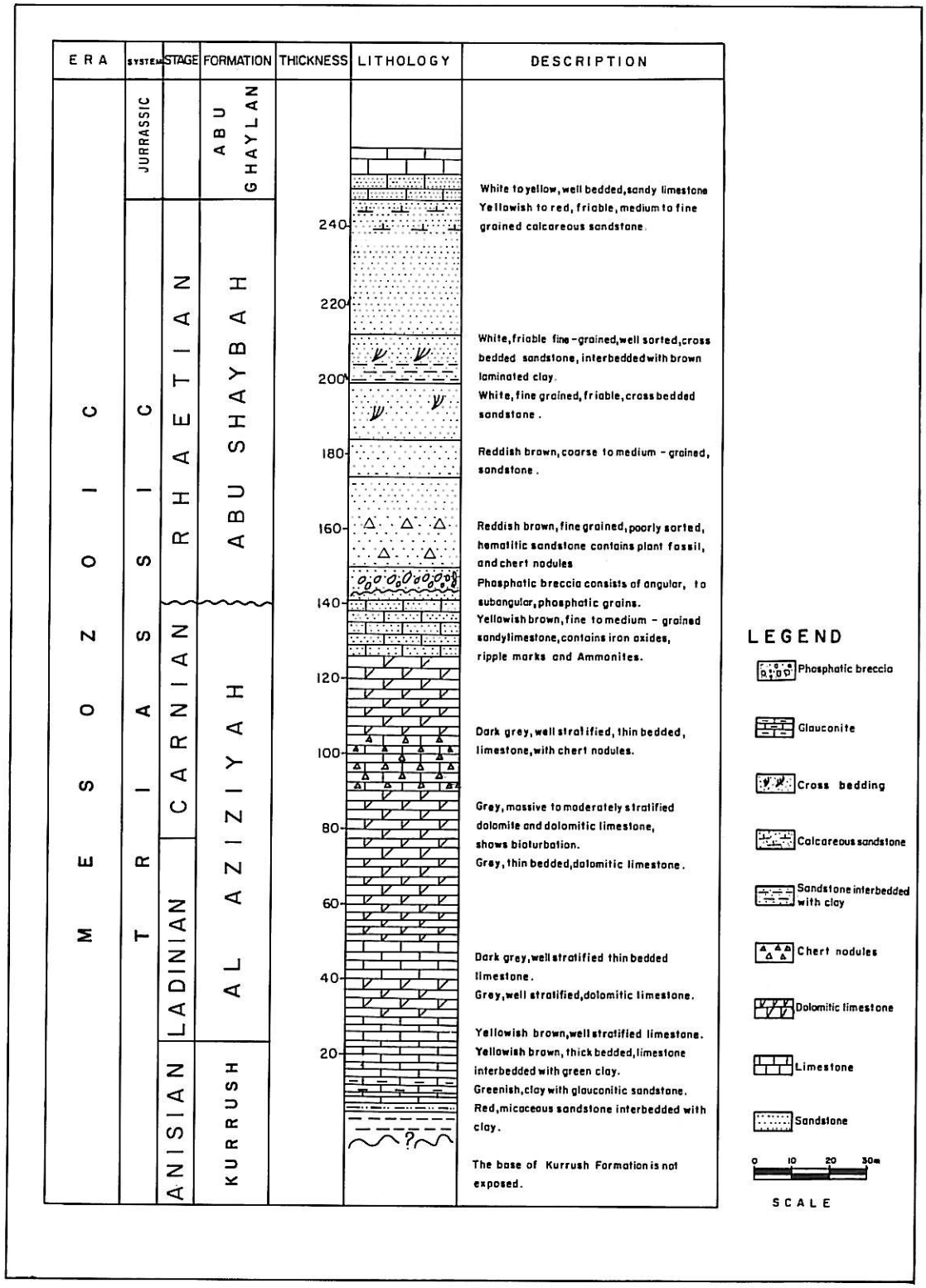


Fig. 2. Stratigraphic section of the Triassic formations in Gharyan area.

and coastal lake facies, particularly in the upper part (Desio, *et al.*, 1960, 1963; El Hinnawy and Cheshitev, 1975; Fatmi *et al.*, 1978).

THE PHOSPHORITES

During their systematic mapping of Tarabulus Sheet, El Hinnawy and Cheshitev (1975) reported

the presence of phosphate bands and described them as the upper part of the marine limestone of Al Aziziyah Formation. The present study suggests that the phosphorite sediments, which overlie the surface unconformity of the upper part of Al Aziziyah Formation, belong to the lower member of Abu Shaybah Formation.

The phosphorite bands show a variation in thickness ranging from 3.9 m at Wadi al Qabil (Fig. 3a) to less than 0.5 m at Kaf Tekut. In Bu Reshada and Ras Tunat areas the phosphorite bands are 0.5 m thick.

PETROGRAPHY

Megascopically the phosphorites are coarse-grained, light brown to light grey in colour with a micro-conglomeratic texture. They include phosphatized pelecypods, gastropods, fish teeth, and bone fragments (Fig. 3b). Most of the phosphorites under consideration show good compaction and poor to moderate sorting. Using Slansky's classification (Slansky, 1986), the Gharyan Triassic phosphorites are mainly phospharenite and phospharudite with some quartz- phospharenite. In thin sections under the microscope phosphatic and non-phosphatic elements and cement can be distinguished.

A-Phosphatic Elements

Pellets

The Gharyan phosphorites show pellets that range from 10% to 15% of the phosphorites in Wadi al Qabil. The grain size ranges from 0.5 to 1.2 mm. The pellets are mostly broken but complete units are sometimes seen (Fig. 4d). Except for very few fine quartz grains no nuclei were noticed in most of the

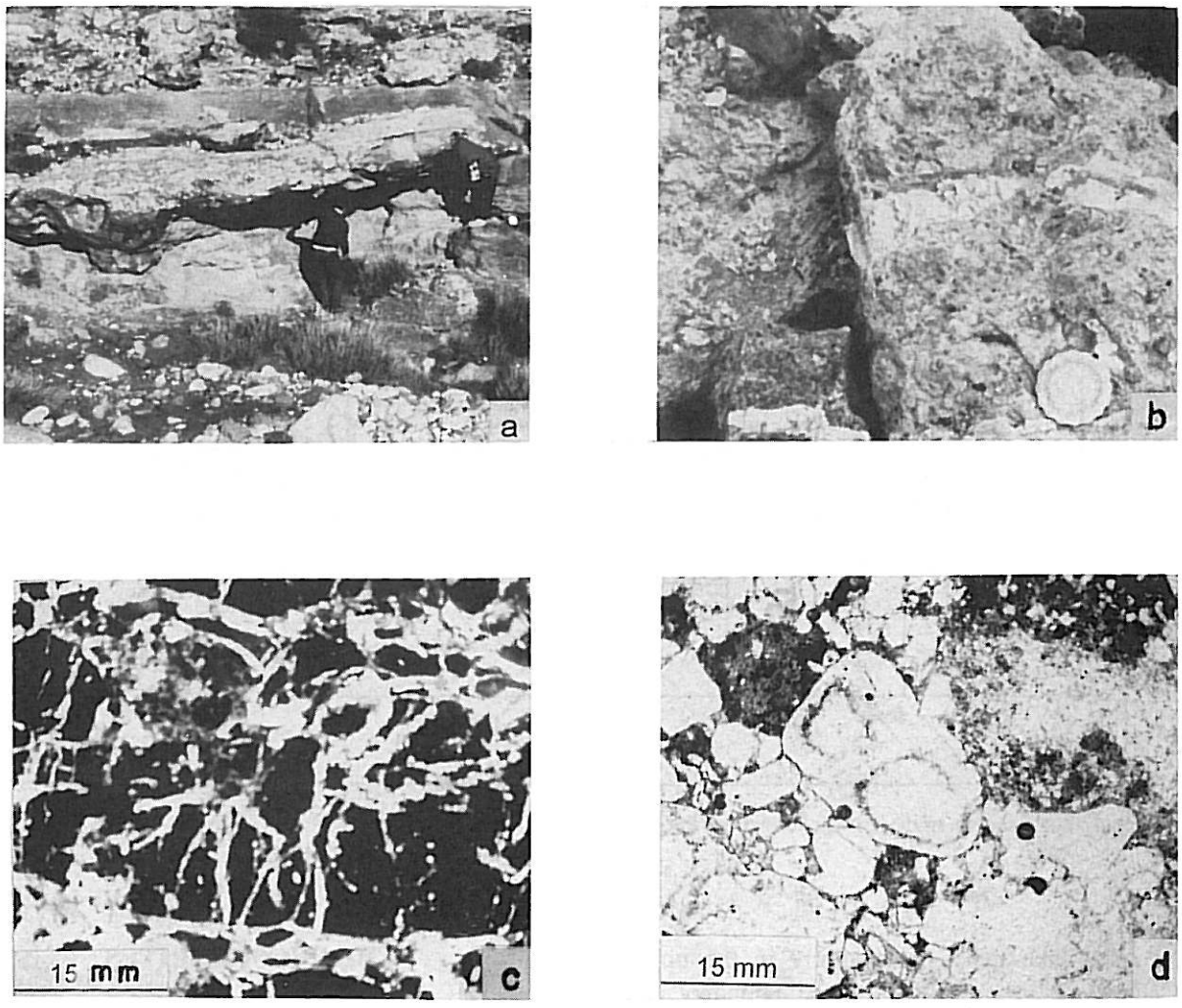


Fig. 3. Phosphorite outcrop in Wadi al Qabil; (b) Bone fragment for aryan phosphorites; (c) Broken pellet filled with microsparite; (d) Microfacies of Gharyan phosphorite pellet showing some organic matter.

examined pellets.

The broken pellets are filled with microsparite (Fig. 3c). Some of the pellets contain organic matter (Fig. 3d). Some others show calcification in the boundaries and less calcification inside. This may be due to chemical substitution.

Micronodules

The micronodules range from 10% to 15% of the studied phosphorites of Gharyan area. The grain size of the micronodules of all the phosphorites ranges from 0.6 to 2.0 mm.

They are composed of rounded to subrounded grains. Their boundaries are broken and the fillings are made of fine grains of quartz, micrite, and microsparite.

Intraclasts

The irregular phosphate elements represent about 4% to 15% of the total component. The grain size of the phosphatic interclasts ranges from 0.4 to 1.8 mm. The endogangue and the exogangue in the intraclast are of fine to medium quartz grains with microsparite, and fine bone fragments, showing some organic matter.

Coprolites

The coprolites represent less than 10% of the total components in most of the examined sections from Gharyan area. (Fig. 4a). Their grain size ranges from 0.2 to 0.7 mm.

Bone fragments

The amount of bone fragments in these phosphorites ranges from 4% to 10%. The studied phosphorite specimens were found to contain broken and fractured vertebrate bone fragments. These fragments are elongated, and filled with microsparite.

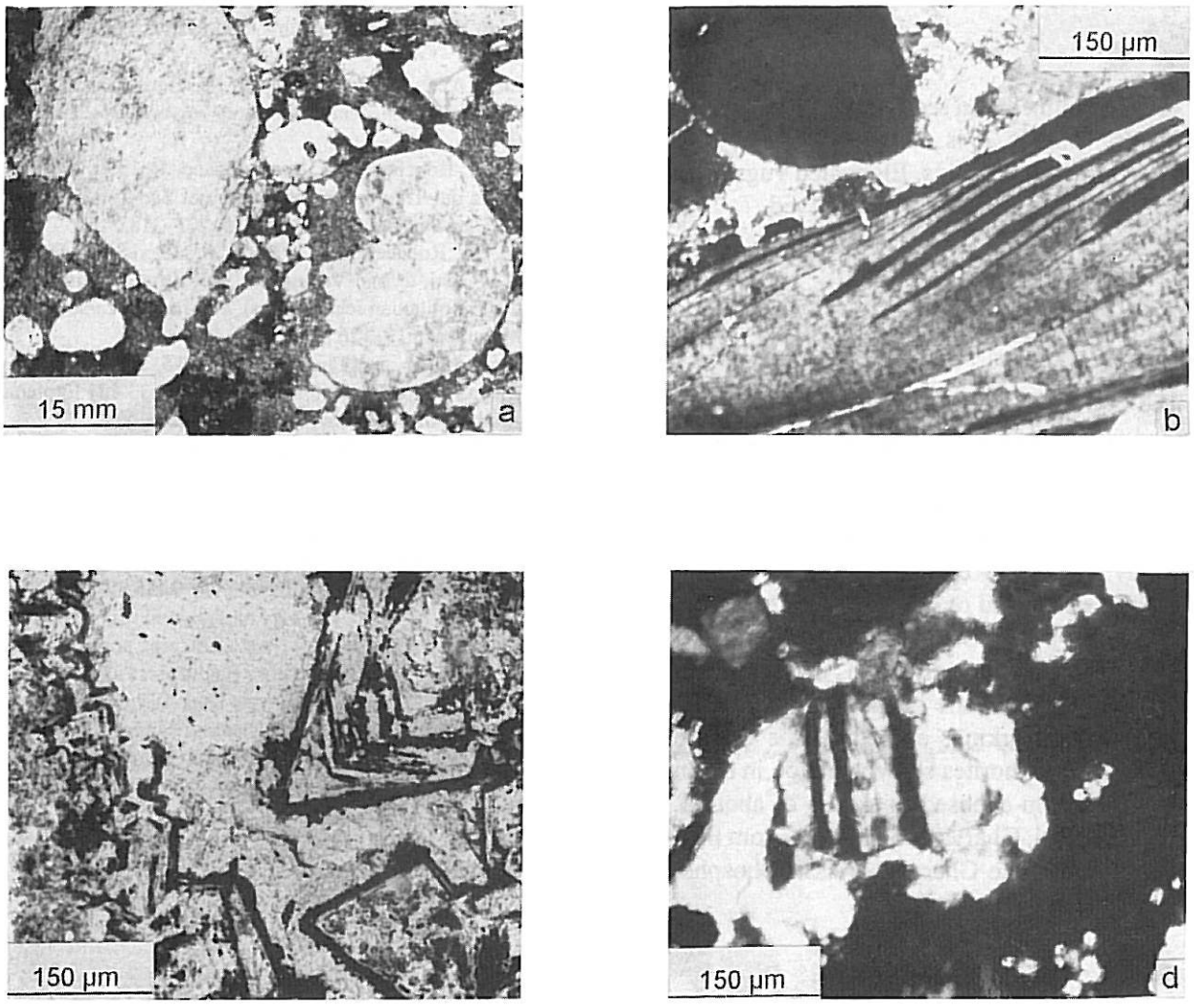


Fig. 4. Microfacies showing (a) coprolite, (b) fish scale, (c) secondary dolomite and (d) plagioclase grain.

The phosphatic sediments are rich in fish teeth and fish scales (Fig. 4b).

B-Other (non-phosphatic) Elements

The main other elements (non-phosphatic) are quartz, feldspar and some carbonate pellets, interclasts, and lithoclasts.

Quartz

Rounded to subrounded, abundant quartz grains represent about 15% of the total volume in the studied phosphorite. The quartz detritus are cemented by calcite and hematite. Some of the detritus are made of secondary dolomite. (Fig. 4c).

Feldspar

The studied phosphorites show grains of plagioclase and microcline. The plagioclase grains occur mostly as exogangue elements and have euhedral form (Fig. 4d). The microcline grains are endogangue in some pellets of the studied phosphorites.

C-Cement

In the examined thin sections cement forms more than 20% volume. It is mainly sparite with some hematite around the grains. Elongated vugs filled by small quartz detritus were also observed.

GENESIS AND CONCLUSION

The studied Triassic phosphorite is coarse-grained, light brown to light-grey in colour with a micro-conglomeratic texture. It includes a phosphatized fauna of pelecypods and gastropods with fish teeth and bone fragments. This phosphorite is generally composed of phosphatized structureless diagenetic grains and ovules with rectangular skeletal grains as intraclasts, together with subangular detrital fine-grained quartz and very fine-grained carbonate cement. Some of the quartz grains show evidence of reworking, especially the exogangue grains. The phosphorites show variation in thickness with a maximum exposed thickness of about 3.9 m in Wadi al Qabil, Gharyan dome area. From this petrographic study, the Gharyan Triassic phosphorites seem to have been formed first by deposition as a phosphate mud and then reworked and redeposited as phosphate sands in a shallow marine environment. The phosphorite particles show deformation as a result of late tectonic movement (faulting and doming) associated with the central Jabal Nafusah uplift. The faults and domes have no relation with the mineralization. The presence of the euhedral feldspar grains is an indication that the phosphorites did not suffer transportation for a long distance. This suggests that the feldspar and phosphorite grains originated from the same area.

REFERENCES

Ayler, M.F., 1967. Phosphate deposits, Tripolitania Libya, Min. Industry *Geol. Sec.*, Tripoli, Bull. **3**, 25 p.

Burollet, P.F., 1960. Lexique Stratigraphique International, N. Afrique, Pt. 4a. Libye Comm. Strat., *Cent. Nat. Rech. Sci.*, 62 p.

Burollet, P.F., 1963. Field trip guide book of the excursion to Jebel Nafusa. 1st. Saharan symp. *Petrol. Explor. Soc.* Libya 19 p.

Christie, A.M., 1955. Geology of the Garian area, Tripolitania, Libya. U.N. Tech *Assistance Program Rept.* TAA/LIB/**2**, 60 p.

Desio, A. Ronchetti, R.C.; and Vigano, P. 1960. Sulla stratigrafia del Trias in Tripolitania e nel Sud-Tunisino. *Milano Riv. Ital. Paleont. Strat.* **66** No. 3, 273–318.

Desio, A., Ronchetti, R.C., Pozzi, R., Clerici, F., Invernizzi, G., Pisoni, C. and Vigano, F. 1963. Stratigraphic studies in the Tripolitanian Jebel (Libya). *Rev. Ital. Paleontol. Stratigr.*, Milan, Mem. **9**, 126 p.

El Hinnawy, M. and Cheshitev, G., 1975. Geological map of Libya, 1:250.000. Sheet Tarabulus (NI 33-13) Explanatory Booklet. *Ind. Res. Cent.*, Tripoli, 65 p.

Fatmi, A.N., 1977. The Upper Triassic (Carnian) ammonite genus *Mojsisovicsites* from Jabal Gharyan (Jaba Nafusa), Libya, *Libyan J. Sci.*, **7A**, 35–48.

Fatmi, A.N. Sbeta, A.M. and Eliagobi, B.A., 1978. Guide to the Mesozoic Stratigraphy of (Jabel Nefusa), Libyan Jamahiriya *Libyan Arab. Dev. Inst.*, Tripoli, No. **7**, 35 p.

Goudarzi, G.H., 1970. Geology and mineral resources of Libya – A reconnaissance. *U.S. Geol. Surv. prof. paper*, **660**, 104 p.

Polservice Company, Consulting Engineers, 1973. Zone Selection Report, Jebel-Jeffara Area. Unpublished Rep., Ind. Res. Cent. Dept. of Geol. Researches and Mining, Tripoli.

Slansky, M., 1974. Some ideas about phosphate research in Libya. In; A proposal for phosphate research in Libya. *Ind. Res. Cent.* Tripoli, 4 p.

Slansky, M., 1986. *Geology of Sedimentary Phosphates*. Oxford Academic Publ. Ltd., London. 211 p.

Petroleum Res.J. Vol. 9 (1997); P. 51–59, 5 FIGS.

Preparation of Activated Carbon from Carbonaceous Industrial Wastes

Latif H. Ali* and Abdurrazzag B. Shebli*

تحضير كربون منشّط من مخلفات صناعية كربونية

لطيف حميد علي وعبد الرزاق بلقاسم الشبلي

تم في هذا البحث تحضير كربون منشّط من مخلفات صناعية يمتلك بعضها قيمة اقتصادية متدنية ويعد البعض الآخر مصدراً ملوثاً للبيئة وتركزت الدراسة حول الآتي:

1 – مخلّفات التقطير الفراغي للنفط فوق 500°م.
2 – أسفلتين مفصول من الترسّبات النفطية لخاميْ السدرة والحمادة.
3 – مخلفات مطاطية من الإطارات المستهلكة لوسائل النقل.
4 – مزيج من الأسفلتين والمطاط المستهلك.

تمت عملية الكربنة بمزج المصدر الكربوني مع عنصر الكبريت بنسبة واحد إلى واحد وزناً وأجريت بمراحل حرارية ثلاث:

– مرحلة أولى عند 250°م وفي ظروف جوية عادية.
– مرحلة ثانية عند 500°م في جو من غاز النيتروجين.
– مرحلة تنشيط حراري أخيرة عند 900°م في جو من غاز النيتروجين.

تم تجميع غاز كبريتيد الهيدروجين (H_2S) الناتج من المراحل الثلاثة في مصائد كيميائية وفي التطبيق الصناعي للطريقة فإن هذا الغاز يحوّل مرة أخرى إلى عنصر الكبريت بطريقة كلاوس المعروفة ويدور الكبريت الناتج إلى مفاعل الكربنة في طريقة صناعية مستمرة.

جرى تقييم فعاليّة أنواع الكربون المنشّط التي تم تحضيرها باستخدام طرق معروفة تضمنت تقييم قابليّة الكربون على امتزاز المواد التالية من محاليلها المائية المخففة:

1 – مادة عضوية (حمض الخليك).
2 – مادة غير عضوية (اليود).
3 – مادة عضوية ملونة كبيرة الوزن الجزيئي (صبغة الميثلين الزرقاء).

وتمت مقارنة النتائج مع فعالية كربون منشط تجاري جيد النوعية في ظروف تجريبية متطابقة.

Abstract *Activated carbon (AC) was obtained by carbonizing the following low value sources and industrial wastes:*

- *500^{+}°C vaccum residue (VR)*
- *Asphaltenes separated from crude oil sludge deposits (SA)*
- *Waste rubber from used tires (WR)*
- *A blend of asphaltenes and waste rubber (AWR)*

A mixture of the carbon source with elemental sulfur in a 1:1 ratio was first carbonized under atmospheric conditions at 250°C followed by a second stage carbonization at 500°C under nitrogen atmosphere in an electrically heated tubular furnace. Carbon was finally thermally activated at 900°C under N_2 gas atmosphere in the same heater.

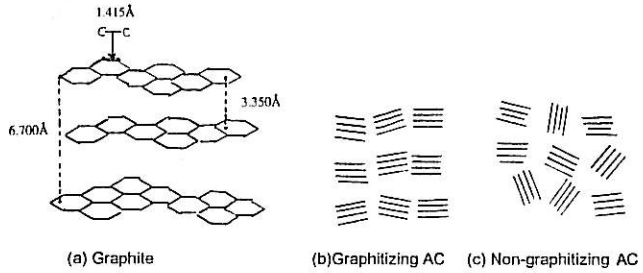
Evaluation of the activity of the prepared carbon types was achieved by measurements on adsorption of acetic acid, iodine, and methylene blue dye from their aqueous solutions.

*Petroleum Research Centre, P.O. Box 6431, Tripoli, Libya.

INTRODUCTION

The importance and world wide recognition of activated carbon as an essential material was through its use in poisonous gas masks during World War 1. Nowadays activated carbon finds an ever expanding uses in the fields of purification of materials, control of environmental pollution and catalysis.

Activated carbon (AC) represents a form of non-crystalline, amorphous material. Its basic unit resembles that of pure crystalline graphite, except that the layers (sheets) of the fused hexagonal carbon rings are not stacked uniformly in a parallel manner on each other:



X-ray examination of graphite (a) and activated carbon shows two types of the latter [1]. One type (b) is a semi-crystalline (graphitized structure), having parallel layers of hexagonal rings but not stacked on each other in a complete uniformity. The other type (c) has no parallel layer connections with a complete randomness in the net formation, thus having pores of vast size and distribution. Thermal activation increases the formation of carbon type (c) resulting in an increased surface area and a diversity of pore formation. The size, shape, and surface area of pores depend on carbonizing and activating temperatures, as well as on the nature of carbonaceous material (CM) [2].

Activated carbon is usually prepared from high carbon content CM such as wood coal, bones, coconut shells, organic waste, petroleum residues, etc. Several methods are available in the literature for the preparation of AC [3, 4, 5, 6, 7].

In this paper, accounts on the preparation, activation and assessment of activated carbon obtained by reacting petroleum carbonaceous materials and waste rubber, with elemental sulfur, will be given.

EXPERIMENTAL

1. Separation of Asphaltenes from Sludge Bitumen (SA)

3g of bituminous material; which was previously extracted from Hamada crude oil sludge with toluene; was mixed with 100 ml of normal heptane (n-C_7) in a 200 ml conical flask. The mixture was shaken 2 h at room temperature, followed by filtration and separation of asphaltenes using a suitable Buchner funnel under water pump suction. Asphaltenes were dried 1 h at 105°C.

The extraction of organics (bituminous like material) from inorganics and water was performed in a modified soxhlet system using toluene as the refluxing solvent which effected the separation of water by azeotropic distillation (see Fig. 1).

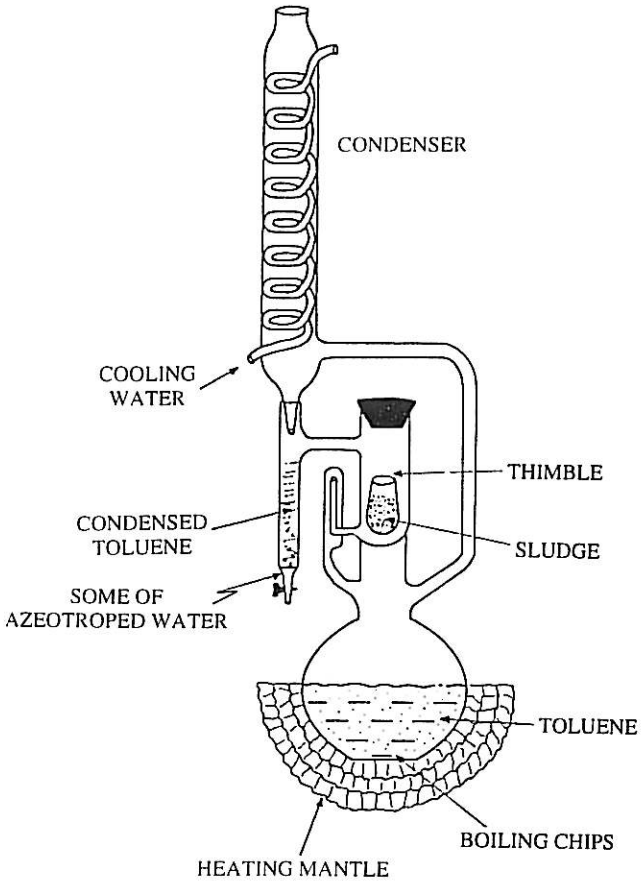


Fig. 1. Real shape of extractor.

2. Preparation of Waste Rubber (WR) as a Feed for Carbonization

Pieces of waste rubber from a used tire were further granulated either by using an electric blender, or by immersing into liquid nitrogen followed by quick hammering in a mortar. WR granules of particle size of 1–3 mm diameter were screened by a suitable sieve.

3. Vacuum Residue (VR), 500^+ °C As a Feed for Carbonization

VR was directly obtained as such from crude oil evaluation laboratory at Petroleum Research Centre.

4. Carbonization and Activation Operations

10 g samples of CM (VR, WR or SA) were mixed with 10 g of elemental sulfur (i.e. 1:1; wt/wt ratio), in a 250 ml round bottom (RB) flask connected to a condenser. The condenser was connected to a cold trap of salt and ice mixture and the latter was connected to solution traps containing 10% aqueous NaOH for the purpose of trapping H_2S gas produced from the carbonization operation (Fig. 2).

The partially carbonized material in the RB flask was crushed and placed in porcelain boats and was further carbonized 1 h at 500°C, under N_2-gas atmosphere in an electrically heated tubular furnace.

Activation was achieved in the same tubular furnace by raising the temperature to 900°C and maintaining a 30 cc/min. flow of N_2-gas for a period of 1 h.

H_2S gas evolved in the second stage carbonization at 500°C and during activation was trapped in 10% aq. NaOH solution in a series of traps connected to the heater (Fig. 3). Final yield of activated carbon is about 60% based on CM.

5. Activated Carbon from a Blend of SA and WR

To 5 g of fully carbonized WR (at 500°C/N_2-atmosphere), 5 g SA was added to form a new carbonization feed AWR. 5 g of elemental sulfur was added to the latter feed and was thoroughly mixed. The mixture was carbonized and activated in exactly the same manner as described in 4 above to yield a new activated carbon denoted AWR-AC.

6. Assessment of Carbon Activity by Acetic Acid Adsorption

To 50 ml samples of 0.1 M acetic acid solution, was added 0.1 and 0.3 g of each activated carbon prepared in the course of this work and to a commercial powdered activated carbon obtained from Merk. The mixture was shaken 30 min., filtered and the first 5 ml discarded. 20 ml of the filtrate was titrated against 0.1 N NaOH using phenolphthalein as indicator. The titration was repeated twice

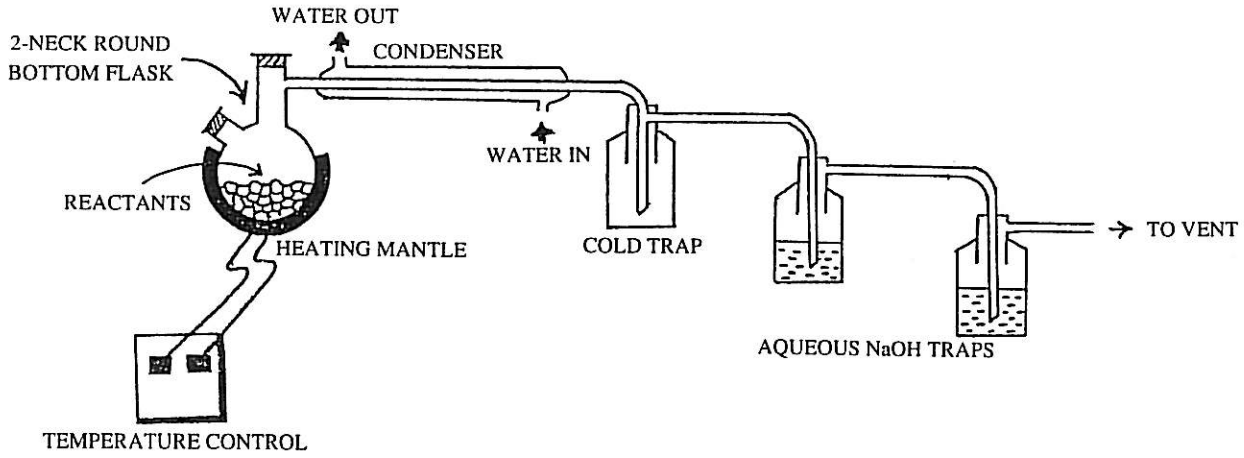


Fig. 2. First stage atmospheric carbonization.

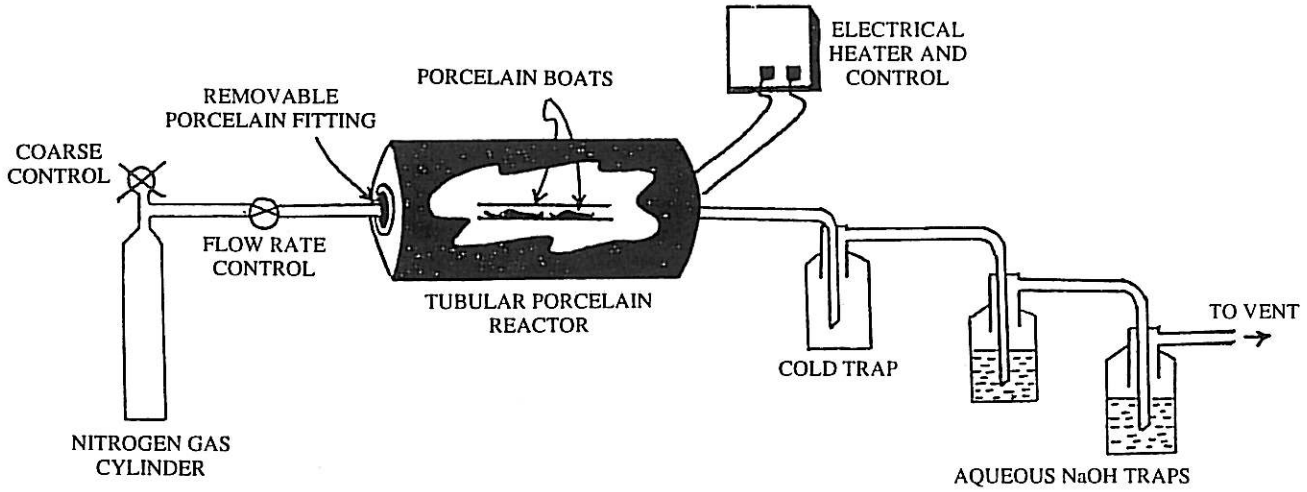


Fig. 3. Second stage carbonization and activation system.

7. Assessment of Carbon Activity by Iodine Adsorption from Aqueous Solution

0.1 g of dry AC was weighed into a stoppered 250 ml flask. 5 ml of 5% HC1 was added and the mixture was gently heated up to boiling point and was kept at this temperature for 30 min. Carbon was cooled to room temperature and 50 ml of 0.01 M I_2 aq. sol. was added. The mixture was well shaken, filtered and the first 5 ml. discarded. 20 ml of the filtrate was transferred to 100 ml conical flask and was titrated against 0.01 N sodium thio-sulfate ($Na_2S_2O_3$) aq. solution until the disappearance of the yellow color. At this point 1 ml starch solution was added and the titration was continued until blue colour disappeared.

8. Assessment of Carbon Activity by Removing Methylene Blue (MB) Dye from Aqueous Solution

Typically 0.1 g of powdered AC was added to 100 ml of MB (aq. sol.) containing 5 ppm of the dye. The solution was stirred, let settled and 5 ml quickly pipetted out, centrifuged 3 min at 2000 rpm and absorbance at 660 nm was measured. Stirring and repeating the measurements was continued at suitable intervals until colour is nearly completely removed.

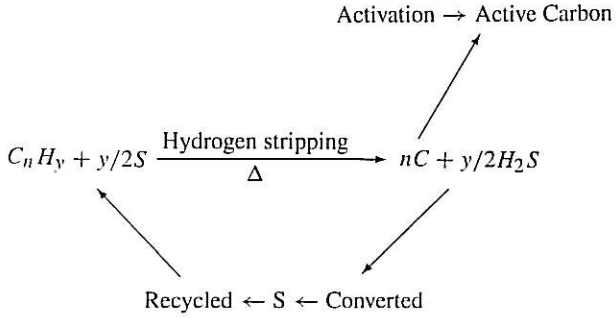
The concentration of un-adsorbed MB was determined from a calibration curve of a series of aq. sol. of MB of known concentrations and measured absorbancies as given in the following table.

Solution No	*MB conc. (ppm)*	*Absorbance (λ = 660 mm)*
1	1	0.189
2	2	0.386
3	4	0.724
4	5	0.898
5	7	1.376
6	10	1.865
7	12	2.254
8	15	2.473

RESULTS

1. Materials

The reaction is based on carbonizing a suitable organic material with elemental sulfur from an accessible source. The produced carbon can be activated by a variety of methods. The reaction also yields hydrogen sulfide (H_2S) as a by-product, which is converted to elemental sulfur and reused. The whole operation is generally presented as shown below.



It is proper to give short accounts on the carbon providing materials (Carbonaceous materials–CM) used in our work. We employed the following CM's:

(i) Vacuum residue (VR) 500^{+}°C supplied by the crude oil assessment department at P.R.C. It contained 8.5% hydrogen.

(ii) Asphaltenes separated from bituminous matter isolated from crude oil sludges (SA). Toluene is used to extract hydrocarbons and azeotrope water in one operation. A diagram of the operation is given in Fig. 1.

Asphaltenes were separated from sludge hydrocarbons (SHC) by precipitation with *n*-heptane (n-C_7: SHC 33:1). Asphaltenes constituted about 30% of SHC.

(iii) Waste rubber from used tyres (WR). Rubber from used tyres was crushed either by freezing in liquid - N_2, then crushing, or by an electrical blender. The crushed rubber was sieved and suitable particle size was isolated.

Activated carbon was also prepared from a blend of WR with SA in order to improve properties.

2. Measurement of Carbon Activity

2.1. *Adsorption of Acetic Acid (AA) from Aqueous Solution*

The results on the adsorption of 0.3 g AA dissolved in 50 ml water by different weights of granulated and powdered prepared activated carbons, are given in Table 1.

2.2. *Adsorption of Iodine from Aqueous Solution*

The term Iodine Number is defined as the number of milligrams of iodine adsorbed by 1g of activated

Table 1. Assessment of activity by adsorption of acetic acid from aqueous solution.

	Granulated Carbon				*Powdered Carbon*			
Carbon Sample Abbreviation	*carbon Experimental weight (g)*	*Actual Weight of acid* $\times 10^3$	*Weight of acid removed by 1 g*[1]	*%Acid removed*	*Carbon expt. w.t. (g)*	*Wt. of acid removed by 1g*	*%Acid removed preparation*	*Remarks on process of*
VR-AC_1	0.1005 0.1996 0.3052	6.0 12.0 14.0	0.060	20.0				VR:S[2]; 1:1 (250 C° → 900 C°)[3]
VR-AC_2	0.1010 0.1989 0.3016	12.0 14.0 18.0	0.071	23.7				VR:S; 1:1 (250 → 500 → 900 C°)
VR-AC_3	0.3000	7.7	0.039	13.0	0.1076	0.028	9.3	VR:S; 1:1.5 (250 → 350 → 500 → 900 C°)
VR-AC_{3a}	0.1015 0.2037 0.3099	2.4 6.0 24.0	0.077	25.8				VR:S; 1:1.5 Washed with CS_2 (250 → 500 C°)
WR-AC	0.1037 0.2023 0.3045	6.0 12.0 27.0	0.058	19.4	0.1012	0.049	16.3	WR:S; 1:1 250 → 500 → 900 C°
SA-AC	0.1016 0.2074 0.3060	12.0 24.0 30.0	0.118	39.4	0.1044	0.115	38.3	SA:S; 1:1 (250 → 500 → 900 C°)
AWR-AC					0.1018	0.088	29.3	AWR:S; 1:1 Refer to Exp. II.5
Commercial-AC					0.1054	0.086	28.7	obtained from MERK

[1] Calculated from corresponding experimental weights.

[2] Elemental sulfur.

[3] Values in brackets represent stages of treatment temperature.

Table 2. Volumetric determination of adsorbed iodine from aqueous solution

Carbon type	*ml*[1] $Na_2S_2O_3$ *(0.01 N)*	I_2 *Equivalence (g)*	*g* I_2 *Adsorbed by* 0.1 *g carbon*	*mg* I_2 *Adsorbed by* 1 *g carbon*
WR–AC	32	0.0406	0.0112	112
SA–AC	24	0.0305	0.0213	213
AWR–AC	28.6	0.0363	0.0155	155
VR–AC3	36.7	0.0466	0.0052	52
Commercial–AC	16.6	0.0217	0.0301	301

[1] 1 ml 1N $Na_2S_2O_3$ = 0.12691 g I.
[2]May also be termed: Iodine Number.

carbon. The measurement is usually done by contacting a specified weight of AC with a standard solution of I_2, under specified conditions of time, temperature and shaking. The amount of adsorbed iodine is calculated by back titration of unadsorbed I_2 with sodium thiosulfate ($Na_2S_2O_3$) using starch as indicator. The results are given in Table 2.

2.3. *Removal of Methylene-Blue (MB) Dye from Aqueous Solution*

The results of removing MB from aqueous solution as a function of time, using different types of prepared activated carbon are given in Table 3. The same table gives also the natural logarithms of the concentrations of unadsorbed MB remained in solution after each treatment time.

Figure 4 gives a plot of lnC Vs adsorption time (in seconds) of some of the activated carbons. The slopes of lines at certain adsorption time reflect the relative activity of carbon samples.

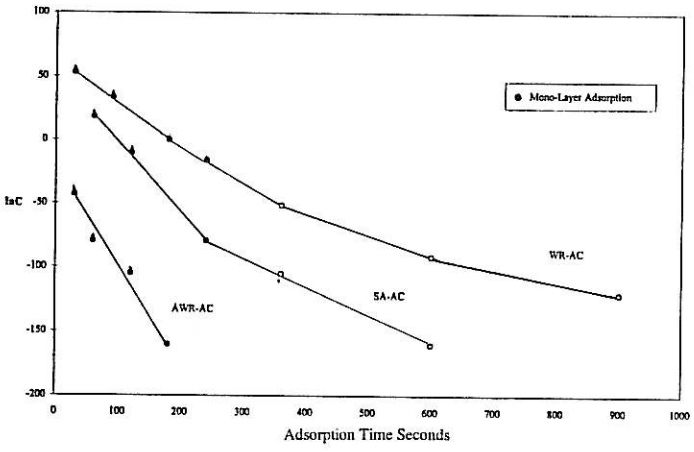


Fig. 4. Comparison of relative activity of prepared carbon.

DISCUSSION

Carbonaceous materials can be converted to carbon by a variety of methods capable of stripping hydrogen. These methods are usually thermal processes, therefore many unwanted constituents are also removed by the action of heat which effects a chain degradation of the carbonaceous material to carbon. Some of the carbon is lost during degradation and one usually looks for methods and conditions that minimize carbon loss.

For carbonaceous materials of petroleum origin, and the like, the use of elemental sulfur as a carbonizing agent has proved very effective [1, 2, 8, 9]. It is well established that elemental sulfur attacks hydrocarbons at a temperature as low as 100°C producing hydrogen sulfide [10].

$$\underset{\text{(Paraffin)}}{C_nH_{2n+2}} + S \xrightarrow{\Delta} \underset{\text{(Olefin)}}{C_nH_{2n}} + H_2S. \qquad (1)$$

However production of H_2S on a large scale as a by-product in any industrial operation is a big problem from the environmental point of view. This problem has been overcomed by the development of methods of conversion of H_2S to other useful materials such as elemental sulfur or to H_2SO_4. It is of interest here to mention that nearly 50% of total world-wide needs for sulfur is supplied by recovery from tail gases [11]. One of the most developed methods is the Claus Process or some of its modifications. Reactions involved in this process are:

$$H_2S_{(g)} + \tfrac{3}{2}O_2 \longrightarrow SO_{2(g)} + H_2O_{(g)}$$

$$\Delta H = -518.8\ KJ \qquad (2)$$

$$SO_{2(g)} + 2H_2S(g) \xrightarrow{(Fe_2O_3)} 3S_{(l)} + H_2O_{(g)}$$

$$\Delta H = 142.8\ KJ \qquad (3)$$

Table 3. Removal of methylene–blue dye from aqueous solution containing 5 ppm with activated carbon.

Carbon sample	*Wt.(g)*	*Time (sec)*	*A (660 nm)*	*M.B. remained (ppm)*	*M.B. removed (ppm)*	*% removed*	*ln C*	*normalized slope value*
VR-AC_1	0.1022	1800	0.639	3.40	1.60	32*	–	–
		5100	0.584	3.15	1.85	37	–	–
VR-AC_{3a}	0.1053	800	0.664	3.55	1.45	29*	–	–
		5100	0.629	3.35	1.65	33	–	–
WR-AC	0.1020	30	0.318	1.70	3.30	66	53.1	
		90	0.254	1.40	3.60	72	33.7	
		180	0.193	1.00	4.00	80	0.00	
		240	0.171	0.85	4.15	83	−16.3	0.40
		360	0.120	0.65	4.40	88	−51.1	
		600	0.078	0.40	4.60	92	−91.6	
		900	0.057	0.30	4.70	94	−120.4	
SA-AC	0.1018	60	0.227	1.20	3.80	76	18.2	
		120	0.174	0.90	4.10	82	−10.5	
		240	0.088	0.45	4.55	91	−79.9	0.68
		360	0.064	0.35	4.65	93	−105.0	
		600	0.035	0.20	4.80	96	−160.9	
AWR-AC	0.1012	30	0.126	0.65	4.35	87	−43.1	
		60	0.090	0.45	4.55	91	−79.9	1.00
		120	0.075	0.35	4.65	93	−105.0	
		180	0.043	0.20	4.80	96	−160.9	

(*) Carbon sample did not mix, with the solution and stayed floating even with vigorous stirring.

Versions of Claus units of variable capacities are available in the market of Chemical Process Industries.

The general equation for the carbonization reaction is:

$$C_nH_y + y/2S \xrightarrow[\Delta]{H_2-\text{Stripping}} nC + y/2H_2S \qquad (4)$$

C_nH_y = Carbonaceous material.

The value of y and thus the amount of elemental sulfur needed for the carbonization reaction is determined by the percentage of hydrogen in the feed.

Most of the petroleum heavy ends (and the like), when used as feeds for active carbon preparation, contain around 7–9% H.

If simple calculation is made taking into consideration the approximate average molecular weight of the feed material and that 2 g of H is needed to produce 34 g of H_2S, this will give a reasonable weight ratio of 1:1 of elemental sulfur to feed to effect a proper carbonization reaction.

Activation of C from reaction (4) by a suitable method to give AC (activated carbon) follows. The recovery of the carbonization agent (elemental sulfur) should be performed which is motivated by economical and environmental considerations when applying the process on an industrial scale.

Using vacuum residue (VR) from the distillation of crude oil, namely Sarir 500$^+$°C which contained about 8.5% H did produce a type of AC (VR–$AC_{1,2,3}$ and $_{3a}$) which showed moderate activity toward acetic acid adsorption from aqueous solution (Table 1). The conditions of carbonization are mentioned in the same table which indicated that increasing the ratio of sulfur to feed to 1.5:1 deteriorated the quality (VR–AC3). Some improvement did occur when washing the prepared carbon with CS_2 prior to activation at 900°C. Deterioration of quality in VR–AC_3 was also obvious when powdered carbon was assessed in terms of acetic acid adsorption (Table 1). It is worth mentioning here that activated carbon prepared from vac.resid (VR–AC_1 and VR–AC_{3a}) repelled an organic matter dissolved in water like methylene blue (MB) and these AC

stayed floating on the surface, thus effecting very little removal of MB (Table 3). On the other hand similar type of AC (VR–AC_3), mixed with solution with no problem when an inorganic matter, like I_2, was dissolved in water and some removal of I_2 from solution did occur (Table 2). This observation needs further investigation.

Asphaltenes are regarded as the heaviest constituents of crude oils, having molecular weights of 2000–5000 and unit layer sheets stacked on top of each other in a similar manner to graphite. Asphaltenes are therefore ready to form activated carbon with small needed modifications which are attained by proper carbonization conditions.

The main goal of our work is to employ refuse materials in obtaining valuable substances. Sludges from storage tanks on land or from carrier ships is a heavy burden on the oil industry and consequently on the environment. Sludges are expected to contain a high percentage of asphaltic materials. We have carried out some detailed investigations on the potentials of hydrocarbons in sludges (SHC) and at this stage we focused on separating this portion from water and inorganic fines. After we achieved that, using a laboratory scale system (Fig. 1), we proceeded further to separate the asphaltenes from SHC. The yield of n-C_7 asphaltenes from Hamada crude oil sludge was about 30%.

On the same theme of using refuse materials we proceeded to employ waste rubber (WR) in the preparation of active carbon. Even though the incorporation of WR in an industry like AC preparation will have a very minor contribution to solving the environmental problem from piling of e.g. rubber from used tires, nevertheless, from the economic point of view we have a free raw material to use.

Waste rubber from tires contains about 12% carbon black as a hardening agent, and about 1% elemental sulfur as a volcanization agent, in addition to natural and synthetic and reclaimed rubbers and other additives such as plasticisers, accelerators, antioxidants etc. Thus WR is a good feed for AC production, especially in terms of its contents of carbon black and sulfur.

Activated carbon prepared from carbonizing WR produced carbon of a medium activity compared to SA–AC. This is clear from Tables 1 and 2 in terms of acetic acid and iodine adsorption.

It was mentioned by Japanese workers in the field of carbonization that waste rubber; in a mixture with wood coal and a carboneceous binder [12], or in a mixture with high boiling (220–380°C) aromatic oils [8]; that the activated carbon produced possessed weak mechanical characteristics and adsorption properties tend to be weak. This in a way fits our findings. In an attempt to improve the physical properties and adsorption capability of WR-AC, it was coated with a petroleum binder prior to activation. Thus the carbonized matter at the 500°C stage obtained from WR was mixed with a 1:1 weight ratio of asphaltenes separated from Hamada Crude Oil sludge (SA) dissolved in benezene. After the evaporation of solvent, the SA–WR–AC mixture was further mixed with elemental sulfur in a 1:1 wt. ratio with respect to added asphaltene. The whole blend was carbonized in the usual two stages (250°C atmospheric followed by 500°C under N_2 atmosphere then activation at 900°C) was carried out to give the composite AWR-AC. The latter activated carbon showed a much improved mechanical properties as a first impression measurement when crushed by hands. Adsorption characteristics were very good with respect to acetic acid and iodine and excellent in terms of rate of removal of methylene blue from aqueous solution (Tables 1, 2 and 3 and Fig. 4).

The activity of carbon is not measured only by the amount of material adsorbed, but also by rate of adsorption (e.g. removal from solution) of the material. This rate is usually measured by the time in seconds needed to remove a certain concentration of methylene blue dye from aqueous solution. This determination required the construction of a calibration curve of MB in water, where measurements were carried out at λ660 nm.

The relative rates of removal of MB from aqueous solution by some types of AC prepared by us, are given in Table 3. Activated carbon prepared from vacuum residue. (VR-AC and VR-AC_{3a}) were excluded, since they resisted mixing with the MB solution.

A comparison is made between the slopes of the straight lines obtained for readings below 240 second (4 min.) of adsorption time and InC where C is the concentration of the remaining (unadsorbed) MB in solution. The results of this comparison study are given in Table 3 and plotted in Fig. 4. Calculated slopes normalized with respect to the slope of AWR-AC are given in the same table. It is obvious that regarding AWR-AC as a standard, the relative activities of SA-AC and WR-AC are 0.68 and 0.40 that of AWR-AC respectively.

Tentative explanation of the inflection point of the two straight lines in the plot of InC against adsorption times in WR-AC and SA-AC, is that: at this point monolayer adsorption is completed, and a slower multi-layer adsorption commenced. Higher

activity AWR-AC – i.e. greater surface area – does not show inflection point with the range of MB – concentration employed (5 ppm) thus a clear straight line is obtained.

CONCLUSIONS

The following conclusions may be drawn at the present stage of this study:

1. the study successfully yielded several types of activated carbons prepared from low value, or refuse materials.
2. Even though the activating medium was quite mild, represented by N_2-gas, the quality of some of the prepared activated carbon, especially AWR-AC and SA-AC was quite acceptable and these carbons possessed considerable adsorptive characteristics as measured by conventionally accepted standard methods.
3. A new method was proposed for expressing relative carbon activity. This is accomplished by normalizing the relative values of the slopes from InC against time plot of adsorption – where C is the concentration of unadsorbed coloured material in aqueous solution expressed in part per million and time in seconds.
4. The just mentioned plot in 3 above (i.e InC Vs time) may provide a way for estimating the point at which a mono-layer adsorption is completed. This is obtained at the inflection point of the two straight lines representing the rate of adsorption (Fig. 4). The amount of material adsorbed when a mono-layer is completed may help deriving a method for surface area determination of activated carbon.

REFERENCES

[1] Riley, H.L., 1947. *Quart. Rev.* **1**, 59.

[2] Mattson, J. and Harry, B. and Mark, J., 1977. Activated Carbon and Surface Chemistry, **9**.

[3] (a) Ali, L.H., and Saleem, F.F., 1982. Proceedings, First Arab Conference on the uses of sulfur in the Arab World. (Kuwait).
(b) Ali, L.H. and Saleem, F.F., 1985. Iraqi Patent No. 1805.

[4] Ali, L.H., and Dawood, I.H., 1990. Proceedings, carbon-90 Conference, Paris France, July 16–20.

[5] Murakawa, Sugiyama and Ijiri, 1975. Japan Kokai 75, 123, 095, *Chem. Abst.* **84** (6), 76740 W (1976).

[6] Bochlen, B. and Mucllor, R., 1977. Swiss 589, 007 (CI. COIB 37 108) *Chem. Abst.* **87**(8), 119952y).

[7] Pokonova *et al.*, 1989. *Fuel Sci. and Tech. Intern.* **7**, 951–967.

[8] Inone *et al.*, Japan Kokai 7698, 693. *Chem. Abst.* **87**(4) 581874 (1977).

[9] Hard, H.C., *et al.*, 1924. *J. Chem. Phys.* **28**, 1092.

[10] Hobson, G.D. and Pohl, W., 1975. *Modern Pet. Techn.* 4th Edition.

[11] Shreve, 1984. *Chemical Process Industries*, Fifth Edition Edited by Austin, G.T., Mcgraw Hill International Book Co.

[12] Watanle, Y. *et al.*, 1975. May 30, Appl. No. 582, 344 (Japan).

Petroleum Res.J. Vol. 9 (1997); P. 61-65, 3 FIGS.

Isolation and Characterization of Two Thermotolerant Methylotrophic Bacterial Strains

I.M. Misurati*, A.M. Suliman*, H.I. Ben Hussein* K.S. Baruni*

عزل وتعيين خصائص بعض سلالات البكتيريا المحُبّة للحرارة العالية والمؤكسدة لمادة الميثانول

عز الدين المصراتي، عبد الرحمن مسعود، هند بن حسين وخالد الباروني

أجريت عمليات عزل وتعيين خواص عدد من السلالات البكتيرية المحبة للحرارة العالية والمكونة للأبواغ من عينات تربة سطحية أظهرت الدراسة أن أحد هذه الأصناف والتي أطلق عليها إسم EM1 تنتمي إلى جنس العصويات وأخرى EM2 تنتمي إلى جنس الاكتينوميستات.

تمت اختبارات الكشف عن قدرة هذه العزلات على النمو في البيئات التي تتركب من بعض الأملاح المعدنية مذابة في الماء مع إضافة 50 ملي مول من مادة الميثانول كمصدر وحيد للكربون والطاقة. وقد تمت أيضاً دراسة بعض العوامل المؤثرة على النمو مثل تحديد درجة الحرارة المثلى لنمو البكتيريا وتأثير إضافة تراكيز مختلفة من مادة الميثانول وتحديد الرقم الهيدروجيني pH المثالي لنمو نفس البكتيريا.

وجد أن درجة الحرارة المثلى لنمو السلالتين تتراوح ما بين 50 إلى 55 درجة مئوية وباستخدام تقنيات المزرعة المستمرة تمت دراسة بعض العوامل المؤثرة الأخرى مثل استهلاك الميثانول وغاز الأكسجين وانتاج غاز ثاني أكسيد الكربون وحساب معدل النمو ونواتج عمليات الأيض الحيوي عن طريق الوزن الجاف للخلية والمحتوى البروتيني داخل الخلية.

Abstract *Two thermotolerant methylotrophic bacterial isolates* (EM_1, EM_2) *capable of growing in mineral salts medium, containing 50 mM methanol as the sole carbon and energy source, were studied. The maximum specific growth rates of* EM_1 *and* EM_2 *in batch culture were* $1.39\,h^{-1}$ *and* $0.8\,h^{-1}$ *respectively.*

Growth of the two tested microorganisms was influenced by different (growth conditions) methanol concentration, temperature and pH *values. They differed in their tolerance to methanol concentration. The optimum growth temperature of* EM_1 *and* EM_2 *were 50 and 55°C respectively. The highest specific growth rate* (μ_{max}) *of* EM_1 *and* EM_2 *were observed at the optimum* pH *7.4 and 8.0 respectively.*

In chemostat continuous culture of the isolate EM_1 *there was an increment in the different growth parameters: methanol concentration, oxygen consumption and* CO_2 *production. Moreover the metabolic and cell growth rate monitored as cell dry weight (mg/ml) and protein content in whole cells were also increased.*

INTRODUCTION

Methylotrophic bacteria play important roles in several biotechnological processes (Anthony 1982; Crawford and Hanson 1984; van Verseveld and Duine 1987). They are most interesting organisms particularly from an applied point of view since evidence has been published for the presence of methylotrophic bacterial strains in nature (Colby and Zatman 1975; Akiba *et al.*, 1970; Snedecor

*Petroleum Research Centre, P.O. Box 6431, Tripoli, G.S.P.L.A.J.

and Cooney 1974; Hitzman 1976), Consequently, these menthanol – utilizing thermotolerant bacterial strains may be of considerable industrial interest, both as single cell protein production (s.c.p.) and also for the transformation of methanol to useful metabolites. They have the ability to grow easily on this inexpensive carbon source. The use of microorganisms, capable of growing on petroleum derived fractions, such as methane and methanol, has been established.

The balance of mass – energy must be examined, thus, Yoshifumi *et al.*, (1983) found that there was an exponential increase of bacterial growth lag with the increase in methanol concentration.

Other growth conditions and regulation of methylotrophic bacteria were previously reported. (Dijkhuizen *et al.*, 1988). Methylotrophic bacteria are varied in their physiological behavior with respect to different growth conditions. Methanol utilizing bacteria are also classified according to their efficiency optima. The most important biotechnological factors for s.c.p. production are cell yield, growth rate, and crude protein content in whole cells of biomass (Lowry *et al.*, 1951).

Other parameters for biotechnological factors are substrate affinity, thermotolerance and the biological stability of the culture.

The objective of this work is to study two isolated local thermotolerant methylotropic bacteria and the effect of some environmental conditions on their growth.

MATERIALS AND METHODS

The bacterial strains were isolated on aerobic medium of the following composition (per litre of distilled water): $(NH_4)_2\ SO_4$ 1.5 g, K_2HPO, 4.65 g, $Na_2HPO_4.2H_2O$ 1.5 g $Mg\ SO_4.7H_2O$ 0.2 g, 2ml/litre of trace elements solution (Vishniac and Santer 1957) and 1.5% w/v of agar for isolates maintenance, was added to the same medium.

The medium was sterilized in autoclave at 121°C for 15 minutes. The microorganisms used throughout this study have recently been isolated in pure culture in our laboratory from soil samples, where one gram of each sample was introduced into 150 ml conical flask (in triplicates) containing 25 ml of the above medium. Appropriate amounts of (filter sterilized) methanol were added to each flask. The inoculated flasks were incubated in a horizontal shaker (80 rpm) at 55°C for three days. Culture suspensions of 72 h incubation were streaked out on methanol agar plates and incubated at 55°C for 48 h. Two types of colonies, designated as EM_1 and EM_2, producing good growth on methanol agar, were selected for subsequent experiments.

GROWTH EXPERIMENTS

Growth of the isolated bacterial strains on different methanol concentrations (25, 50, 100, 200, 300, 400, 500, 600 and 800 m mol) were examined in liquid medium. The effects of temperature and pH values on the growth of the isolated strains were carried out. Growth was monitored by measuring the optical density at 430 nm. Doubling time (Td) and the maximum specific growth rate (μ_{max}) of the two isolates (EM_1 and EM_2) were calculated according to the following equations:

$$Td = \frac{t_2 - t_1}{ldx(t_2) - ldx(t_1)} \quad (1)$$

$$\mu_{max} = \frac{In2}{Td} = \frac{0.693}{Td} \quad (2)$$

Continuous Culture Cultivation

The growth of strain EM_1, in continuous culture at 50°C and pH 7.4 was used to study the effect of various dilution rates. During continuous growth, methanol and oxygen consumption rates and CO_2 production were estimated as described by Brooke *et al.*, (1989). Dry weight was measured by gravimetry after drying overnight at 105°C, as previously conducted by Dijkhuizen *et al.*, (1988). Protein content in whole cells was estimated previously as stated by Duchards and Attwood, (1989) and Brooke *et al.*, (1989). Bovine serum albumin was used as standard protein.

RESULTS

The two isolated EM_1 and EM_2 were found to produce a good growth on agar medium containing 50 mM methanol, however these strains differed in several characteristics. EM_1 was gram positive, rod shaped cells of length up to 8.57–11.43 μm and spore forming bacilli. The other strain EM_2 was also gram positive but the cells showed filamentous shape non spore forming bacteria. Both strains do not utilize glucose as a carbon source and do not grow on nitrate, asparagine and methylamine HCI but they

can easily grow on glutamine as a nitrogen source other than ammonia.

Effect of Methanol Concentration on the Specific Growth Rate

The specific growth rate of the two tested bacterial strains was significantly affected by the high methanol concentration (Fig. 1). The highest specific growth rate (μ_{max}) 1.39 h^{-1} of the strain EM_1 was observed on methanol concentration range 0.1–0.2 mol. The specific growth rate (μ_{max}) suddenly decreased when the methanol concentration was more than 0.2 mol. The response of the strain EM_2 was different. This strain showed high sensitivity to the low methanol concentration. The specific growth rate (μ_{max}) of this strain was in the range of 0.8–0.84 h^{-1} in methanol concentration of up to 0.1–0.2 mol.

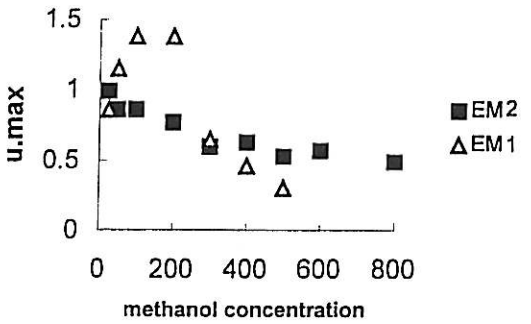


Fig. 1. Influence of different methanol concentration on the growth of two tested bacterial strains.

Effect of Temperature

The two bacterial strains were able to grow at a wide range of temperature 37–60°C (Fig. 2). The highest (μ_{max}) of the strain EM_1 1.3 h^{-1} was observed at 50°C and this value slowly decreased due to the increase of the growth temperature, however the highest (μ_{max}) value 1.0 h^{-1} of EM_2 was observed at 55°C.

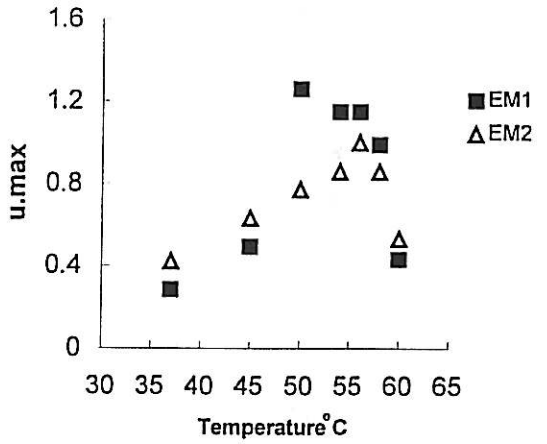


Fig. 2. Influence of the cultivation temperature on the growth of both strains.

Effect of pH

The results showed that the (μ_{max}) of the two bacterial strains were influenced by pH value (Fig. 3). The optimum pH values for the growth of EM_1 and EM_2 were 7.4, 8.0 respectively.

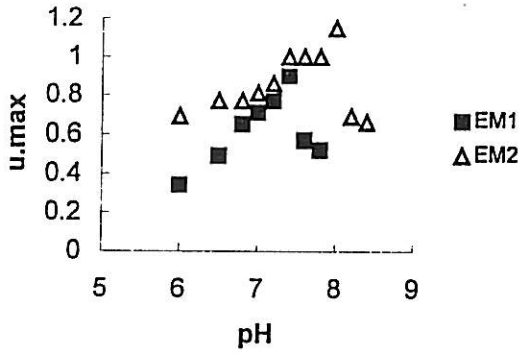


Fig. 3. Typical (μ_{max}) of different pH spectrum.

Effect of Dilution Rate on the Growth of the Bacillus Strain EM_1

As the above results revealed that the strain EM_1 was efficient to grow on methanol under optimal conditions, this strain was chosen for further investigations of the effect of dilution rate on the different parameters of continuous growth in chemostat culture. The results indicated that the increase of methanol dilution rate (D. rate) is associated

Table 1. Influence of growth rate on the kinetics of growth of bacillus strain EM1 in a carbon–limited chemostat culture (temp = 50.0°C, pH = 7.4, SR = 50.0 mM methanol.) Rates: [mM/h^{-1} (g dry weight/cells)$^{-1}$].

D. rate (h^{-1})	*q methanol*	*qo2*	*qco2*	*yield g/mol*	*dry wt mg/ml*	*protein %*
0.11	7.4	5.15	2.7	14.8	0.74	45.9
0.155	9.6	6.75	2.9	16.2	0.81	45.68
0.21	13.0	8.67	3.43	17.6	0.88	55.68
0.25	14.6	9.8	3.5	18.5	0.925	56.2
0.32	16.9	11.51	3.6	19.0	0.95	58.9

SR = concentration of methanol in the reservoir.
D = dilution.
q = consumption and/or production.

with an increase in the methanol and oxygen consumptión and CO_2 production. Influence of dilution rate on growth of the thermotolerant methylotrophic bacilli EM_1 in continuous culture at optimum temp 50°C, pH 7.4 and methanol concentration 50 mM is shown in Table 1. As the cultivation D. rate was increased the bacterial dry weight increased from 0.74–0.95 mg/ml at D. rate 0.11 h^{-1} to the maximum of 0.32 h^{-1}. The data indicated that the increase in protein content in whole cells is correlated with the D. rate and methanol consumption.

DISCUSSION

Microbial biomass production can be represented by different microbial growth parameters out of these is the maximum specific growth rate μ_{max}. From an economic point of view, the efficiency of an industrial growth process is increased with higher μ_{max} and in mixed culture the species with the greatest (μ_{max}) has the highest probability of survival Guthkre (1980). The results of this work revealed that μ_{max} of the tested bacterial strains EM_1 and EM_2 reached their highest values when the medium contained methanol in concentration range 50–200 mM. The influence of the methanol concentration on methanol utilizing bacteria growth and activity was not fully established. Girio and Attwood, (1991) found that the addition of 50 mM methanol as a carbon limited chemostat culture of methylobacterium species caused an acceleration of its metabolic rates. There is a relationship between methanol concentration and μ_{max} of Methylotrophic bacteria. Yoshifumi Amano *et al.*, (1983) found that the highest maximum specific growth rate was determined at methanol concentration lower than inhibition constant (ki) 40 g/l. The date indicated that the μ_{max} of the two bacterial strains was influenced by the growth temp. The results showed that the two isolates have the highest μ_{max} at temperature range 50–55°C which could strongly suggest that the two bacterial strains are methylotrophs thermotolerant bacteria. The thermophilic bacteria are classified with respect to pH into two major groups (Sonnleiter, 1983; Sundaram, 1986).

- Thermoacidophiles with pH optima in the range 1.5-4.0.
- Thermophilic neutrophiles with pH optima in the range 5.8-8.0.

Our bacterial strains have the highest μ_{max} value at the pH range 7.4–8.0. Thereby it could be suggested that these strains EM_1 and EM_2 are methylotrophic thermotolerant neutrophilic bacteria.

The resulting increase in the cell dry weight and protein content during continuous cultivation of the Bacillus efficient strain EM_1, the increase in methanol and oxygen consumption and the increase in D. rate, show a linear relationship.

Maintenance Energy Requirement

When q methanol is plotted against D. rate the resultant plot yield information regarding the maximum growth yield ($Y^{max}_{methanol}$) on methanol and maintenance energy requirement. Linear regression analysis of the date gave a $Y^{max}_{methanol}$ of 35.7 g cells. mol methanol.

The increment in cell dry weight and protein concentration suggested that there is polymer storage produced throughout the D. rate increment (Kjeldgaard and Kurland, 1963), whereas synthesis of their catabolic enzymes is not similarly adjusted (O'Brien *et al.*, 1980).

These anabolic, enzyme activities, and identification of some metabolic products, need further investigations.

REFERENCES

Akiba, T., Ueyamas, H., Yamauchi, Y., Seki, M. and Fukimbara, T. 1970. Utilization potency of lower alcohols by soil bacteria. *J Ferm Technol.* **48**, 323–328.

Anthony, C., 1978. The prediction of growth yields in methylotrophs. *J. Gen. Microbiol.* **104**, 91–104.

Anthony, C., 1982. *The Biochemistry of Methylotrophs*. London Academic Press.

Anthony, C., and Zatman, L.J., 1967. The microbial oxidation of methanol: purification and properties of the alcohol dehydrogenase of Pseudomonas sp. M 27. *Biochem J.* **104**, 953–959.

Brooke, A.G., Watling, G., Elizabeth., M., Attwood, M. M., and Tempest, D.W., 1989. Environmental control of metabolic fluxes in thermotolerant methylotrophic Bacillus strains. *Arch Microbiol* **151**, 268–273.

Brooke, A.G., Attwood, G., Margaret, M., and Tempest, D.W., 1990. Metabolic fluxes during the growth of thermotolerant methylotrophic Bacillus strain in methanol – sufficient chemostat culture Archives of microbiology **153**, 591–595, Department of Microbiology University of Sheffield, UK.

Colby, J. and Zatman, L.J., 1975. Enzymological aspects of the pathways for trimethylamine oxidation and C_1 assimilation in obligate methylotrophs and restricted facultative methylotrophs. *Biochem J.* **148**, 513–520.

Crawford, R.L., and Hanson, R.S. (eds), 1984. Proceedings of the 4th International Symposium Microbial growth on C_1 Compounds. Minneapolis, *Am. Soc. Microbiol.* Washington D.C.

Dijkhuizen, L. and Harder, W., 1975. Substrate inhibition in Pseudomonas oxalaticus OX1: a kinetic study of growth inhibition by oxalate and formate using extended cultures. Antonie van Leeuwenhock 7. *Microbiol Serol* **41**, 135–146.

Dijkhuizen, L., Arfman, N., Attwood, M.M., Brooke, A.G., Harder, W. and Walting, E.M., 1988. Isolation and initial characterisation of thermotolerant methylotrophic Bacillus strains. *FEMS Microbiol. Lett.* **52**, 209–214.

Duchards, M.G. and Attwood, M.M., 1989. The influence of C:N ratio in the growth medium on the cellular composition and regulation of enzyme activity in Hyphomicrobium X. *J. Gen. Microbiol.* **135**, 787–793.

Girio, M.F. and Attwood., Margaret. M., 1991. Metabolic aspects of the growth of a pink – pigmented facultative methylotroph in carbon – limited chemostat culture. *Applied Microbiol. Biotechnol.* **35**, 77–82, Department of Molecular biology and biotechnology, University of Sheffield, Sheffield, UK.

Guthkre, R., 1980. *Analysis and Modelling of Discontinuous Growth.* Manual for the UNEP/UNESCO ICRO training course on thioretical basis of kinetics of growth, metabolism and product formation. vol. 1.7.

Hitzman, D.O., 1976, United States Patent No. 3.981.774.

Kjeldgaard, N.O., and Kurland, C.G., 1963. The distribution of soluble and ribosomal RNA as a function of growth rate. *J. Mol. Biol.* **6**, 341–348.

Lowry, O.H., Rosebrough, N.J., Farr, A.L., and Randall, R.J., 1951. Protein measurement with the Folin phenol reagent. *J. Biol. Chem.* **193**, 265–275.

O'Brien, R.W., Neijssel, O.M. and Tempest, D.W., 1980. Glucose phosphoenol pyruvate phosphotransferase activity and glucose uptake rate of Klebsiella aerogenes growing in chemostat culture. *J. Gen. Microbiol*, **116**, 305–314.

Snedecor, B. and Cooney, C.L., 1974. Thermophilic mixed culture of bacteria using methanol for growth. *Appl. Microbiol.* **27**, 1112–1117.

Sonnleiter, B. 1983. Biotechnology of thermophilic bacteria-growth, products, and application. *Adv. Biochem. Bioeng.*, **28**, 69–138.

Sundaram, T.K., 1986. Physiology and growth of thermophilic bacteria. In: Brock, T.D. (ed) *Thermophiles, General Molecular and Applied Microbiology.* John Wiley and Sons. New York.

Yoshifumi, A., Nobuo, T., Hidekazu, S., Hideo, S., and Gyozo, T., 1983. Cultural Properties and Mass – Energy Balances in Methanol Fermentation by Metylomonas methanolovrans, Department of Fermentation Technology, Faculty of Engineering, Osaka University, Yamada – Kami, Suita-shi, Osaka **565**, Japan.

Van Verseveld, H.W., and Duine, J.A. (eds), 1987. *Proceedings of the 5th International Symposium*, Microbial Growth on C_1 compounds. Free University Press, Amsterdam Haren, The Netherlands.

Vishniac, W., and Santer, M. 1957. The Thiobacilli Bact. Rev. **21**, 95–213 Walker, J.F. 1964. Formaldehyde, 3rd ed. Reinhold publishing Crop. New York.

Petroleum Res.J. Vol. 9 (1997); P. 67–70, 3 FIGS.

Determination of Trace Amount of Lead in Potable Water by Flow Injection Flame Atomic Absorption Spectrometry Aided by a Pre-Concentration Micro Column

I.S. Bushina* H.M. Kut* and Seham S. Elmahmudi*

تحديد المقادير الضئيلة لعنصر الرصاص في مياه الشرب بواسطة جهاز لهب طيف الامتصاص الذرّي باستخدام طريقة التركيز المبدئي على العمود المصغر

إسماعيل بشينة، حسن كت و سهام المحمودي

لقد تم تحديد عنصر الرصاص لعينات مختارة من مياه الشرب بمدينة طرابلس وذلك باستخدام طريقة التركيز المباشر بواسطة عمود مبادل أيوني يحتوي على الألومينا المنشّطة.

حقنت المحاليل القياسية وكذلك العينات باستخدام منظومة الحقن المستمر بجهاز الامتصاص الذري. جمعت عينات المياه من مناطق مختلفة، حيث تم تعديل رقمها الهيدروجيني عند 4.5، وقيس تركيزها عند امرار محاليلها بمعدل 3.4 سم^3/دقيقة واستعمل حمض النيتريك (2M) لاخراج الرصاص.

وتشير النتائج إلى أن عينات المياه المدروسة تحتوي على 0.2–0.8 ميكروجرام/لتر، وكان الانحراف العياري النسبي 0.5%.

Abstract *Lead is determined by using on line pre-concentration micro column of activated alumina and a flow-injection atomic absorption spectrophotometer. Samples of groundwater were collected from different locations around Tripoli. Results were obtained for a flow rate of 3.4 ml/min. Nitric acid concentration for eluting lead was 2 M. Ammonia solution was used as a carrier at a concentration of 0.15 M. Samples and standards were injected at pH 4.5 using an injection loop of 1000 ul. Lead was determined at a range of 0.2–8.1 μg/l with RSD 0.5%.*

INTRODUCTION

The presence in water of toxic heavy metals such as lead, cadmium, and mercury has been of concern for many years. Major sources of lead pollution are industrial processes, such as lead smelting, and lead-containing industrial products, such as leaded motor gasoline, paints and water transporting pipes. Although the adverse health effects caused by lead have not been fully substantiated, most governments and environmental protection agencies around the world take precautionary measures against it, because it is believed that this element disrupts some of the normal reactions, occurring in the living body, when exceeding a certain level, causing damage of the nervous system and toxictiy [1]. Thus there is vital necessity for accurate lead determination.

Flame Atomic Absorption Spectrophotometry (FAAS) is the most commonly used technique for trace metal determination; it is easy to use and a lot of data base of information is now available. Although FAAS has been successfully used for lead determination, it has a limitation, that it is not sensitive enough for low level lead concentration.

Graphite furnace and hydride generation can offer this sensitivity but it needs skilled operators, it is of low precision and suffers from matrix inter-

*Petroleum Research Centre P.O. Box 6431 Tripoli, Libya, G.S.P.L.A.J.

ference [2]. Duel silica type atom trapping [3] can provide enough sensitivity at the level of μg/l for the determination of lead, but this technique requires a highly-skilled operators. Therefore the determination of trace elements below routine detection limit, using available equipment, becomes necessary.

Flow injection, flame atomic absorption analysis for trace elements has now been successfully developed for on line pre-concentration [4] procedure for many samples due to its improvement of sensitivity and reduction of analysis time. This technique, using a micro column of Chelex 100 ion exchanger, has been demonstrated by Olsen *et al.*, [5] in the determination of heavy metals in sea water. The potential of flow injection analysis (FIA) for rapid procedures using traditional ion exchangers have been studied for the determination of many elements [2, 6].

In this study on line pre-concentration by basic activated alumina in conjunction with flow anaylsis system was used for the evaluation of lead content in groundwater used for drinking purposes. The simplicity of the method and versatility of activated alumina in its basic form as on line pre-concentration column gives a well accepted system because it does not require major expenses for the determination of lead at trace level (μg/l), when a graphite furnace is not available.

EXPERIMENTAL

Sample Pre-treatment

Water samples, collected at the source, were immediately acidified with 2 M nitric acid and were then kept in polyethylene containers before conducting the analysis.

Materials and Reagents

All chemicals used were of high purity analytical grade. Nitric acid and ammonia solutions were obtained from (BDH) chemicals, Poole England. Standard solutions were prepared daily from stock standard solution supplied by VHG Lab. Tartaric acid (0.5 M), used as a complexing agent, was obtained from Chadwell Health, Essex, England. Aluminum oxide, activated, basic, 95+% (Aldrich Chemicals Co. Ltd.) and further activation [7] was made before it was used for packing the column. The PTFE (6 cm long, 3 mm i.d) mini column was packed with alumina (140 mesh). Water of high purity was used throughout the experimental work. Buffer solution (Ingold, Bestell. Nr. 9863) was used for calibration of pH metre.

Instrumentation and Apparatus

Atomic Absorption Spectrophotometer (Varian AA 1475) equipped with Epson printer, and lead hollow cathode lamp, was used in the determination of lead concentration. Knick Digital pH Meter 646 was used in our work for the adjustment of the pH at 4.5 Peristaltic pump, injection loop was calibrated at 1000 ul. PTFE syringes were used to inject the solutions.

Analytical Procedure

The acidified samples were kept for 24 h prior to analysis. The complexing agent (1 ml/100 ml of tartaric acid 0.5 M) was added.

Standards were adjusted to working pH using aqueous ammonia (2 M) and left 1 h. The alumina micro columns were prepared and flushed with the carrier solution (0.15 M NH_3). Water samples were pre-concentrated on the column prior to analysis. Three packed micro columns were used for every watere sample. When FAAS system is working using flame of air – acetylene the nebulizer tube was connected to the flow injection outlet system using a carrier flow rate of 3.4 ml/min. The micro column was connected to the system with injection loop of 1000 ul. Standards containing 10–1500 μg/l were first injected to the basic alumina column using ammonia as a carrier, then after 2 min. lead eluted using 1000 ul of 2 M HNO_3, the signal then recorded.

Micro column of activated alumina contained lead from water samples treated with identical procedure as that for standard solution. Lead was also eluted from the column using 1000 ul HNO_3 of 2 M to the FAAS system where signals were recorded.

RESULTS AND DISCUSSION

Lead II, 217 nm resonance line was used for the determination of lead by FAAS. The effects of various parameters, were determined. Acid concentration, flow rate, and pH were examined by using 1 μg/l ml^{-1} lead solution. The optimum conditions of the experimental work for lead determination in drinking water of Tripoli were thus established. Different concentrations of nitric acid solutions were prepared and were used for eluting lead content from activated alumina micro column. Fig. 1. represents the variation of the peak height response with nitric acid concentration.

Maximum absorbance of lead was obtained at a concentration of acid of 2 M, whereas below this concentration the absorbance is decreased by de-

creasing the concentration.

The maximum release of lead from the activated alumina surface being at acid concentration of 2 M may indicated either a shift to acid catalyzed alumina, which retains lead or a chemsorption between lead and alumina is taking place at acid concentration higher than 2 M. In both cases lead release will be reduced.

The effect of the flow rate of the carrier stream has been optimized. Fig. 2 depicts the flow rate of the carrier stream versus lead absorbance. Clearly the peak height response was found to increase very little when flow rate was extrapolated to 5 ml/min. The value of 3.4 ml/min. was thus selected as the operating flow rate for lead measurements.

0.15 M ammonia solution served as the carrier stream maintained the column basicity. Fig. 3. illustrates the dependence of absorbance on pH. It is evident that pH 4.5 is effective in accumulating lead on the alumina column. The calibration graph at the optimum conditions including flow rate, acid and ammonia concentrations showed a good linearity with the value of regression coefficient of 0.99963. The relative standard deviation ($n = 3$) at 100 ppb was found to be 0.5%.

Results of analyzed drinking groundwater samples from different localities in Tripoli area are summarised in Table 1.

It is quite clear from the table that the maximum amount of lead was found to be in Ghot ash Shaal area (8.13 μgl^{-1}). The value in that area is higher that the others probably because the water distribution pipe network is very old, extensively corroded and situated in a highly populated area of very heavy traffic. Contamination of water with polluted soil should not be ruled out.

Table 1. Present lead determination and associated standard deviation in drinking water from selected locations in Tripoli city

Sample name	*Lead concentration* (μgl^{-1})	*Sample name*	*Lead concentration* (μgl^{-1})
Hai 2 March	0.45 ± 0.03	Sidi El masry	0.75 ± 0.03
Zagouny	0.33 ± 0.02	Milk Factory*	0.60 ± 0.04
Petroleum Institute	0.80 ± 0.02	Zawit El mazy*	0.50 ± 0.02
Hai al Andalus*	0.60 ± 0.02	Mawashi Company*	2.10 ± 0.05
Ghot ash Shaal*	8.13 ± 0.04	Al Gasi mosque	2.50 ± 0.08

*No of replicate "n"= 4, otherwise No. $n = 3$

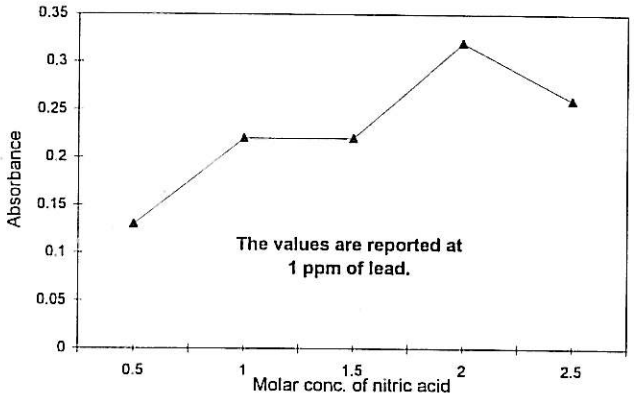


Fig. 1. Variation of absorbance with nitric acid concentration.

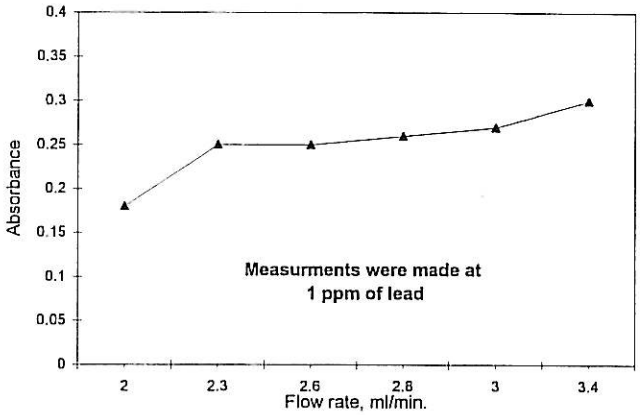


Fig. 2. Dependance of absorbance on flow rate.

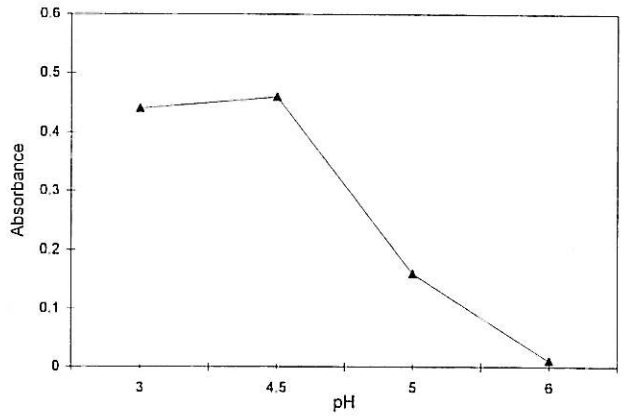


Fig. 3. Dependance of absorbance on pH.

ACKNOWLEDGEMENT

We thank Dr. E. El Hagy from the Chemisty department of Al fateh University for his useful discussions and assistance in alumina activation. We

are also very grateful to colleagues in the atomic absorption laboratory of PRC for their endless assistance. We express appreciation to Dr. L. H. Ali of PRC for his critical reading of the primary draft of this paper.

REFERENCES

[1] *Environment Chemistry*, Fourth Edition, Lewis Publication, Inc. 1990, p. 508.

[2] Yanan, Zhang, Riby, Philip, Cox, A. G. and McLeod, C. W., 1988. *Analyst.*, **113**, 125.

[3] Roberts, J.D. and Kahokola, K.V., 1989, *J. Anal. Atom. Spect.*, **4**, 185.

[4] Ruzicka, J. and Hansen, E.H., 1981. *Flow Injection Analysis* Wiley, Intersience. New York.

[5] Oslen, S., Pessenda, L.C., Ruzicka, J., and Hansen, E.H., 1983. *Analyst.*, **108**: 108–905.

[6] Cox, G. A., Cook, I. G. and McLeod, C. M., 1985. *Analyst.*, **110**, 331.

[7] Perrin, D.D., Armarego, L. F., and Perrin, D. R., 1980. *Purification of Laboratory Chemicals*. Pergamon Press Oxford, 26 p.